THE DESIGN OF A PROTOTYPE OTTO-ATKINSON ENGINE

AND EVALUATION OF THE PART LOAD FUEL EFFICIENCY.

Peter J van Binsbergen

1992

Thesis submitted to the Faculty of Engineering,
University of Cape Town, in fulfilment of the requirements
for the degree of Master of Science in Mechanical Engineering.

ABSTRACT

This thesis is an investigation into the application of the hybrid Otto-Atkinson cycle, as a means of improving the part load fuel efficiency of spark-ignition engines.

The primary objective of this thesis was to investigate the technical feasibility of the modified Atkinson cycle as a spark-ignition engine concept and thus to quantify the associated potential for greater fuel efficiency. The modified Atkinson cycle is a hybrid cycle which approximates the Otto cycle at full load but tends to emulate the Atkinson cycle at part load, and therefore it is referred to as the Otto-Atkinson cycle.

In order to fulfil this objective, a single cylinder engine which operated on the Otto-Atkinson cycle, was designed and constructed. This unusual cycle was achieved by a crank linkage which allowed the power output to be controlled by varying the inlet and compression strokes rather than by the more conventional method of throttling the induced fuel-air mixture. Thus the pumping losses associated with throttled part-load operation are eliminated. Furthermore, the expansion stroke is always greater than the compression stroke, the difference being greatest at part loads. This results in a cycle which approximates the Atkinson cycle for part-load operation.

A simplified thermodynamic simulation of the cycle was formulated. Theoretical predictions were made based on this simulation.

Tests were conducted on the engine to determine its fuel consumption at various loads. The objective of these tests was to establish the difference between the fuel consumption obtained using variable stroke operation and the fuel consumption observed for part throttle operation. The test engine was equiped to perform both cycles. Thus, experimentation was carried out at wide open throttle with load control by variable stroke, when testing the Otto-Atkinson cycle and at full stroke with load control by variable throttle, for comparison with the Otto-Atkinson results.

The results of specific fuel consumption as a function of torque, for part stroke operation, did not correlate well with the original theoretical expectations. The reason for this discrepancy was found to be that these theoretical predictions did not take into account the large burn angles that were found to be a feature of part-stroke operation. The large burn angles were a consequence of the lower flame speeds resulting from a reduction in turbulence. This reduction in turbulence was attributed to the reduction in piston speed associated with reduced strokes.

The thermodynamic simulation was modified to take the large burn angles into account. With this modification, the simulation showed a good correlation with the experimental results. For conventional burn angles the thermodynamic simulation predicted a 30% fuel saving for part-stroke operation at approximately one third of full power. It was therefore concluded that load control via variable intake and compression stroke had the potential for substantial fuel savings. However, these fuel savings can only be realised if the burn angle is kept to an acceptable magnitude.

As a result of balancing difficulties and the size and complexity of this engine it was also concluded, from a technical point of view, that the particular mechanism investigated in this study was not a viable means of achieving the Otto-Atkinson cycle.

Based on the findings of the experimental work and the predictions of the computer simulation, it is recommended that further research emphasis be placed on the reduction in burn angle requirements for part-stroke operation. It is also recommended that the research into the elimination of the throttle for part-load operation be continued.

ACKNOWLEDGEMENTS

I would like to express my thanks to the following people :

Dr A Yates for his guidance, advice and encouragement whilst supervising this project. His continuous interest and enthusiasm are greatly appreciated.

The staff of the Mechanical Workshop, all of whom contributed to this thesis.

Mr R Nates for his contribution to my understanding of various concepts related to this thesis.

The C.S.I.R Foundation for Research and Development for their financial support.

The Mechanical Engineering Department for funding the construction of the experimental engine.

Matla Power Station for granting me leave of absence to complete this study.

Huletts Aluminium for their donation of material.

TABLE OF CONTENTS

LIST OF FIGURES

LIST OF TABLES

NOMENCLATURE

SI	Spark Ignition
IC	Internal Combustion
V	Volume
PV	Pressure-Volume
T	Temperature
P	Pressure
VVC	Variable Valve Closure (also termed Variable Valve Timing VVT)
EIVC	Early Intake Valve Closure
LIVC	Late Intake Valve Closure
VCR	Variable Compression Ratio
CR	Compression Ratio
ER	Expansion Ratio
SFC	Specific Fuel Consumption (BSFC - Brake Specific Fuel Consumption)
MBT	Maximum Brake Torque
t	Time
rpm	Revolutions per Minute
ω	Radians per Second (2πrpm/60)
TDC	Top Dead Center
BTDC	Before Top Dead Center
ATDC	After Top Dead Center
η_i	Indicated Efficiency
ϕ	Air-Fuel Ratio
F/A	Fuel-Air Ratio
e_v	Volumetric Efficiency
Q	Calorific Value (kJ/kg)
IMEP	Indicated Mean Effective Pressure
BMEP	Brake Mean Effective Pressure
PMEP	Pumping Mean Effective Pressure
FMEP	Friction Mean Effective Pressure
T_i	Indicated Torque
$T_o=T_b$	Output (Brake) Torque
T_p	Pumping Torque
T_f	Friction Torque

CHAPTER ONE

INTRODUCTION

1.1 BACKGROUND

The four-stroke spark ignition (SI) engine is based on the Otto Cycle, consisting of isentropic compression (a), constant volume pressure rise (b), isentropic expansion (c) and constant volume pressure drop (d, fig 1). The overall efficiency of early four-stroke SI engines was in the region of 14% [1]. The four-stroke spark ignition engine has undergone many improvements in the 116 years since its invention. Notable improvements are in the areas of emission reduction, reduction in size and mass and an increase in usable engine speed, power output and efficiency. High octane fuels have allowed a considerable increase in the maximum usable compression ratio, this accounts for some of the increase in efficiency. Volumetric efficiency has been increased through a better understanding of fluid dynamics. Friction has been reduced through design improvements and advances in lubrication technology. This all results in an improvement in the overall efficiency.

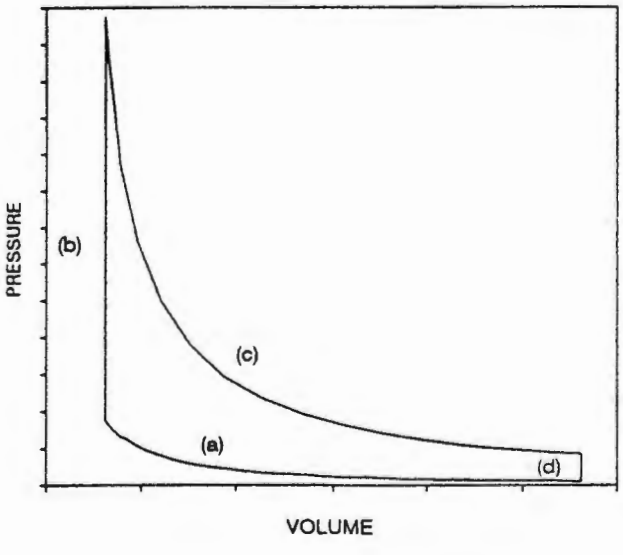

Figure 1. The Otto Cycle

An energy balance of the distribution of the fuel energy, in a modern engine at full load, figure 2 (a), shows that the fuel energy can be divided into approximately three equal parts; one third of the fuel energy is lost to the heat of the exhaust, one third is lost to the coolant and one third is obtained at the crankshaft as usable energy, a small portion of which is required to drive the accessories [2]. Thus the full load efficiency of the modern four-stroke engine is approximately 30%, more than double that of the engine of 1876.

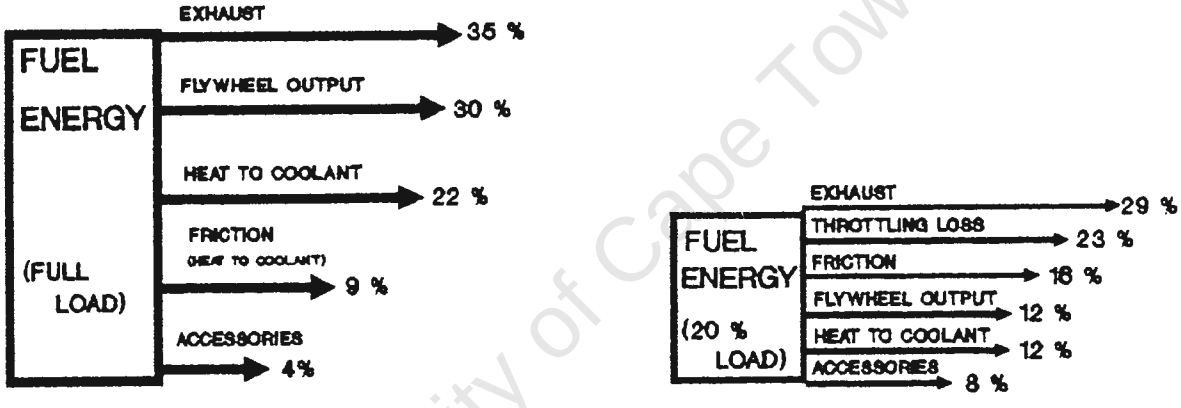

(a) Full load. (b) 20% of Full load.

Figure 2. Energy Balance

The part-load energy balance, figure 2(b), is quite different. With the engine producing 20% of the full load power, the exhaust and combustion (coolant) heat losses are reduced in approximate proportion to the reduction in fuel power whilst the mechanical friction and accessory losses remain approximately constant for constant engine speed. The part load situation introduces a new loss, namely the throttling loss, which accounts for approximately 23% of the fuel energy at this load condition, this is nearly double the flywheel output. Thus the part load efficiency is approximately 12%, more than a 50% reduction on the full load efficiency and lower than the maximum overall efficiency achieved by Otto in 1876.

Most research dealing with the performance of the internal combustion engine is done at full load conditions, although in practice these conditions are only encountered for short periods of time. The wind-drag on a motor vehicle is proportional to the square of the velocity. Thus, considering only the effects of wind drag, for a motor car to have a top speed of 180 km/h the maximum power must be 27 times greater than that required at 60 km/h. When a vehicle is operated at conditions other than top speed or hard acceleration, the power required is well below the maximum power available, "even on a heavy vehicle on a hilly route with frequent starts from rest , no more than 25% of the fuel is consumed at torques above 90% of full load" [3]. The increase in number of cars in the cities has resulted in a traffic situation where part load operation is the norm and the full power potential of the engine is seldom reached.

Depletion of the global oil reserves has resulted in the urgent need for an increase in the efficiency of the SI engine. New materials and technology are focused on a reduction in the heat lost to the exhaust and the coolant. Considering the energy balance (fig. 2) the first impression is that this would greatly improve the efficiency at both full and part load operation, however, the potential for improvement is not as great as it would seem.

Considering the heat lost to the coolant, a portion of this heat loss is due to heat transfer between the exhaust gasses and the coolant. If it were possible to totally eliminate the heat rejected to the coolant then the improvement in efficiency would be in the region of 25% with an increase in the heat rejected at the exhaust. Eliminating the rejection of heat to the coolant would result in an increase in the operating temperature of the engine, this has two drawbacks. (a) Increasing the operating temperature could result in abnormal combustion phenomenon. To prevent this a reduction in the compression ratio would be necessary, resulting in a reduction in the thermal efficiency. (b) Increased operating temperature would also result in an increase in the heat lost at the exhaust, further reducing the potential improvement in efficiency. Thus achieving a substantial improvment in efficiency by eliminating the heat rejected to the coolant is unlikely.

The heat rejection to the exhaust is a condition dictated by the second law of thermodynamics. However, a small improvement in efficiency is possible through utilisation of the waste heat to vaporise the fuel prior to induction. This results in an improvement in the region of 10% [4]. This 10% improvement was gained with methanol which has a high latent heat of vaporisation, the expected gains using gasoline are thus well below 10%.

An area which seems a rather obvious candidate for efficiency improvment is that of part-load operation, particularly the reduction or elimination of throttling losses. Two concepts which have the potential to achieve this are: (a) variable valve timing and (b) variable stroke engines. One variation of the latter has been proposed by Yates [5]. This concept elimates the throttle through a variable inlet and compression stroke whilst maintaining an approximately constant expansion and exhaust stroke. This is an unusual feature which results in a cycle that approximates the Atkinson cycle at part loads and the Otto cycle at full loads. For this reason the concept has been termed the Otto-Atkinson Cycle. Potential fuel savings of 15% to 25% have been predicted for the proposed mechanism.

As the concept proposed by Yates appears to have merit and has not been investigated, it was identified as a subject for research for this thesis. The theoretical motivation for this choice is discussed in more detail in chapter 2.

1.2 AIMS AND OBJECTIVES

The aim of this thesis is to build an engine based on the concept proposed by Yates [5]. The project includes a simple computer simulation of the engine as well as an experimental investigation to explore the validity of the model predictions. The latter part would entail the construction of a prototype engine based on the proposed mechanism.

The thesis objectives are as follows :

(i) To build the Otto-Atkinson engine.

(ii) To develop a computer model of the thermodynamic cycle of the engine.

(iii) To determine the fuel consumption characteristics based on dynamometer tests.

(iii) To compare the test results with predicted results based on the computer model.

(iv) To evaluate this concept of load control based on the following criteria :

(a) fuel efficiency

(b) flexibility of control - suitability for use in the motor industry, and

(c) identification of mass, size and friction penalties.

1.3 PROJECT OUTLINE

The project outline is shown in the following flow chart :

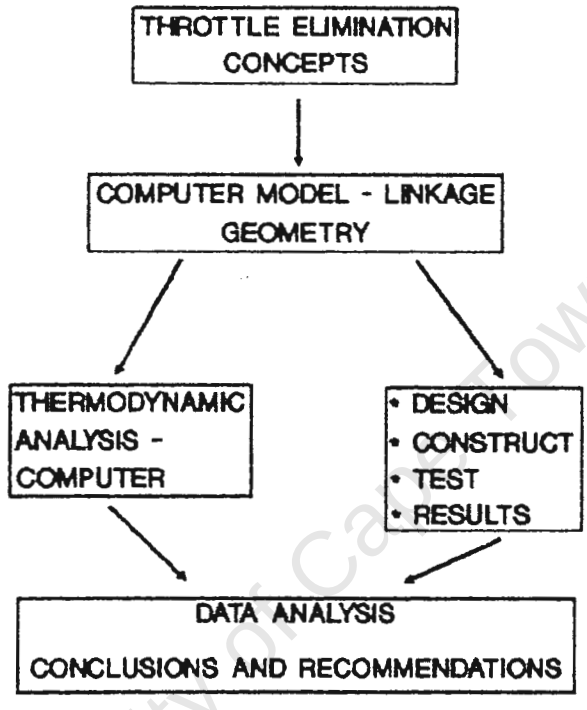

Figure 3. Project Outline Flowchart

The need for throttle elimination has been identified and one of the proposed solutions is the mechanism described by Yates [5]. To facilitate the design of an engine incorporating this mechanism a computer model was set up. This computer model served two functions; (a) to assist in the determination of geometric constraints of the mechanism, (b) to provide a prediction of the performance of the engine. Design and construction of the engine was followed by dynamometer testing and the results of these tests were compared with the computer model predictions. The analysis of these results is followed by discussion and conclusions.

CHAPTER TWO

THEORETICAL DEVELOPMENT

2.1 POWER REGULATION

The power output of an engine is a product of engine speed and torque. Controlling power output by means of engine speed is made possible by a concept known as continuously variable transmission. Continuously variable transmission allows operation at nominally constant torque, ie constant (full) throttle, whilst varying the engine speed to vary the power. This concept has been under development for many years, but due to technical difficulties it has not gained full acceptance by the automotive industry. Thus the control of power output must be achieved by torque regulation.

For satisfactory combustion the SI engine requires a fuel-air mixture at, or very near to, stoichiometric. The limits of combustion dictated by the fuel are in the region of 12 to 18 (air-fuel ratio) [1]. Thus to control the power output of the engine both the fuel flow and also the inlet air flow must be controlled, keeping the fuel and air in approximately the same proportion under all conditions. This function is performed by the carburettor or fuel injection system in conjunction with the simple throttle valve.

The ideal pressure-volume (PV) cycles for full throttle and part throttle operation are shown in figure 4. During the inlet stroke (1-2) the fuel-air mixture is drawn into the cylinder and, with the throttle fully open, there is little obstruction to the flow of the fuel-air mixture resulting in a negligible pressure drop. At part throttle, however, the throttle valve obstructs the flow of the incoming charge resulting in a considerable pressure drop during induction (1'-2'). The piston has to supply the work to pump the cylinder gasses from below atmospheric pressure during the intake stroke, to atmospheric pressure during the exhaust stroke. This results in a reduction of the usable energy at the flywheel, reducing the brake power and thus also the overall efficiency. The throttling loss is often termed pumping loss.

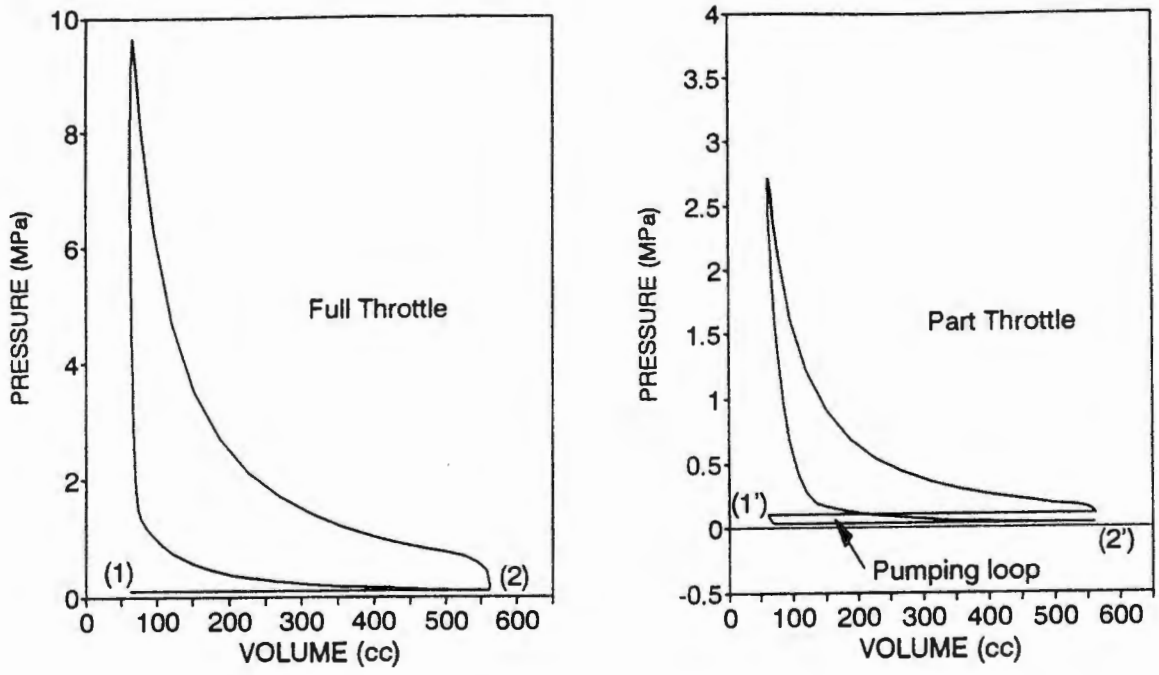

Figure 4. Full and Part Throttle Pressure-Volume Diagrams

Replacing the conventional throttle with an alternative form of torque control that eliminates this throttling loss, would result in an increase in efficiency and a potential fuel saving of up to 25% for urban driving conditions [5].

2.1.1 Literature Discussion

Some of the alternative forms of load control suggested by the literature are as follows :

(a) Variable valve closure (VVC) - The potential for elimination of the throttling losses was already identified by Ricardo, who proposed that the throttle be substituted by VVC [6]. In 1960 Saadawi proposed that elimination of the throttle by either early or late intake valve closure would result in an increase in efficiency of up to 20% [6].

(i) Early intake valve closure (EIVC) - once the required amount of fuel-air mix has entered the cylinder the inlet valve closes, the remainder of the inlet stroke involves expansion of the cylinder charge (figure. 5).

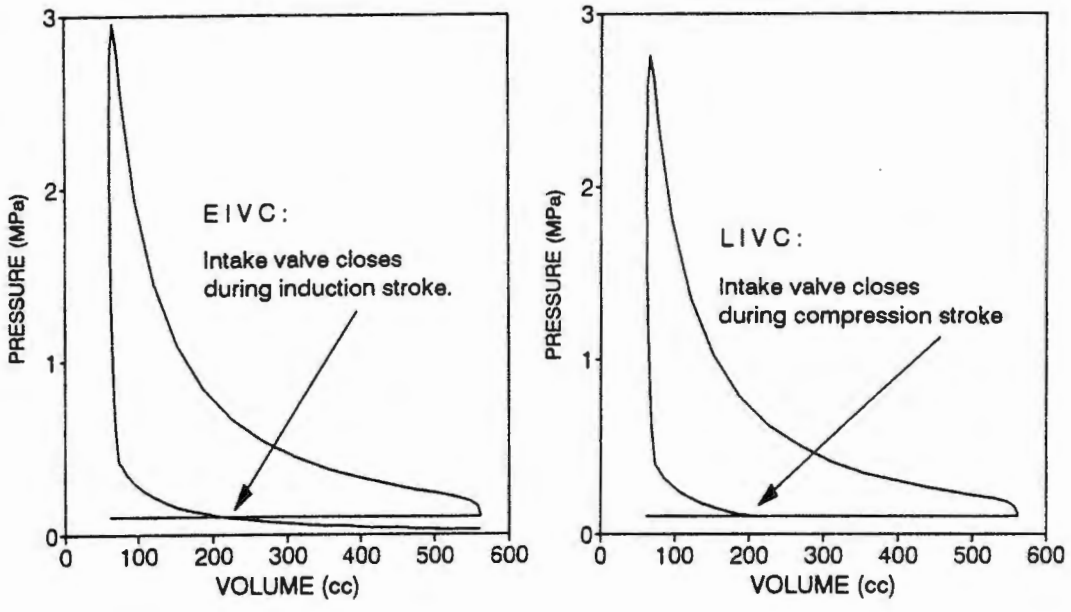

Figure 5. Early and Late Intake Valve Closure

(ii) Late intake valve closure (LIVC) - the inlet valve opening duration is lengthened such that a portion of the inlet charge is returned to the inlet manifold, with the required amount of fuel-air remaining in the cylinder (fig. 5).

(b) In multiple cylinder engines there is the possibility to cut the fuel supply to selected cylinders, thus reducing the effective engine capacity. This system is more suited to engines with many cylinders. Thiel experimented at part load by cutting out two cylinders in a four cylinder engine and found an improvement in brake specific fuel consumption of 10.4% at 40% of full torque and 14.4% at 26% of full torque. However, this concept has several drawbacks, namely; vibration, fuel distribution problems and fouling of the spark plugs in the non-active cylinders [3,7].

(c) Variable stroke - by varying the stroke the swept volume and thus the capacity is varied, this is, in effect, a variable capacity engine and is thus another approach to (b). The swash plate motor has potential for this concept as by varying the angle of the swash plate the stroke is varied. This concept has yet to find commercial acceptance [8]. Pouliot et al. built and tested a five cylinder variable displacement engine, data and analysis indicated the potential for a 25 to 40 percent improvement in efficiency under urban driving conditions [9].

(d) Variable inlet and compression stroke - this would in effect reduce the capacity of the engine, as in (c). However, by reducing only the inlet and compression strokes for part load, full expansion and exhaust strokes are maintained. This results in an engine cycle approaching the Atkinson cycle, which has been termed the Otto-Atkinson cycle [5].

Figure 6 is the pressure-volume diagram of the Otto-Atkinson cycle. As there is no pressure drop due to the throttling of the inlet mixture, the inlet stroke occurs at atmospheric pressure. At full load conditions the intake and compression strokes will equal the expansion and exhaust strokes, this follows the Otto cycle and has the normal exhaust blowdown at the end of the expansion stroke, figure 6(a). At part load conditions the inlet and compression strokes are reduced whilst maintaining a full expansion and exhaust stroke, figure 6(b). The decreased compression stroke results in a lower pressure P_{max}, allowing the greater expansion stroke to expand the burnt mixture more fully, approaching atmospheric pressure and reducing the magnitude of the exhaust blowdown. When the blowdown becomes negligible the cycle approaches the Atkinson cycle. Thus the cycle is a hybrid of the Otto cycle at full load conditions, approaching the Atkinson cycle at part load conditions.

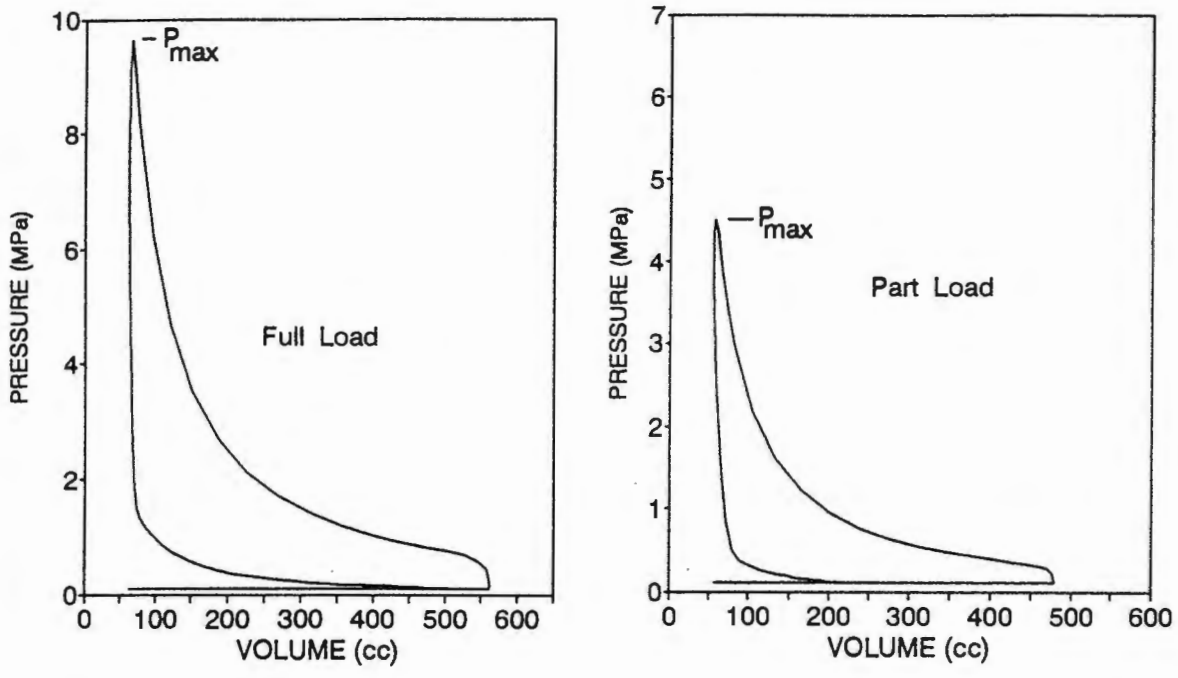

(a) Full load (b) Part load

Figure 6. Pressure-Volume Diagrams for the Otto-Atkinson Engine

2.1.2 Thesis Motivation

The concept of variable valve timing has received considerable research effort. This is chiefly due to the relative simplicity of the changes in design required to implement this form of load control. Late intake valve closure (LIVC) has greater advantages and has been selected as the most viable. There have been basically three approaches to this problem; Ma and Rajabu [10] used a computer simulation to investigate the viability of LIVC in engines with two or more intake valves, they suggested phase shifting the second intake valve with reference to the first. Saunders [11] also used a computer to simulate LIVC, a different cam profile was programmed for each load condition. Bruins suggested hydraulic tappets which can collapse (hydraulically) to allow variable valve timing. He outlined a design but gave no results and thus it can be assumed that his theory was not supported by experimental work [12].

Saadawi was one of the first to investigate variable valve timing experimentally [6], he used a series of seven cams to achieve different load conditions and achieved a 17.7% increase in efficiency at half load. Tuttle [13] investigated two conditions of EIVC by fitting modified camshafts and reported a maximum 40% reduction in pumping losses at part load. Saunders followed his computer simulation [11] with an experimental evaluation of the LIVC concept. Separate camshafts were used for each load condition [14]. An 11% improvement in efficiency was achieved which is almost 100% higher than the 6% predicted by his computer model.

The shortcoming of all these investigations is that none of them offer a flexible means of load control. Bruins offered a design of a concept which satisfies the requirement of flexible load control but gives no experimental support [12]. Yates [7] addresses this problem in a similar fashion as did Bruins ie hydraulic tappets which can collapse for variable valve timing. The experimental evidence from this investigation supports Bruins' theory, namely, that hydraulic tappets would only satisfy VVC requirements for low speed engines.

Both LIVC and EIVC only become really effective when coupled with variable compression ratio (VCR). In LIVC the effective compression stroke is shortened for part-load operation thus decreasing the effective compression ratio (fig. 5). Ma and Rajabu predicted an 8% improvement in fuel economy with LIVC alone and a 19% improvement with LIVC and variable compression ratio. The variable compression ratio piston has been suggested to achieve a variable compression ratio but due to the increased complexity, it has failed to gain acceptance [3,15]. In the case of EIVC, once the inlet valve closes the piston does work in expanding the cylinder contents below atmospheric pressure. As this process is not 100% reversible, not all the pumping losses are eliminated [5]. In fact, pumping losses are only reduced by 40% relative to the throttled engine [13]. Thus it would seem that at this stage variable valve timing does not offer a competitive solution to the throttling loss problem.

The Otto-Atkinson Engine: In a recent publication [5], Yates describes a mechanism which would theoretically eliminate the throttle (figure. 7). The engine would have a continuously variable load control, without the use of the conventional throttle arrangement. This would be accomplished by a continuously variable intake and compression stroke. Thus part-load operation would be achieved by having a short intake and compression stroke thereby decreasing the swept volume and so also the capacity of the engine. A salient feature of this engine is that the expansion stroke remains approximately constant, irrespective of the compression stroke. The direct result of this is that the engine follows the Otto cycle at full load but approaches the Atkinson cycle at part load, thus resulting in the Otto-Atkinson cycle (figure. 6). Although the compression ratio decreases at part load, as with LIVC, this does not have a major adverse effect on the thermal efficiency, this is due to the fact that the Atkinson cycle thermal efficiency is more dependent on the expansion ratio than the compression ratio. This concept appears to have merit and has not yet been investigated, thus it was selected as the topic of investigation for this thesis.

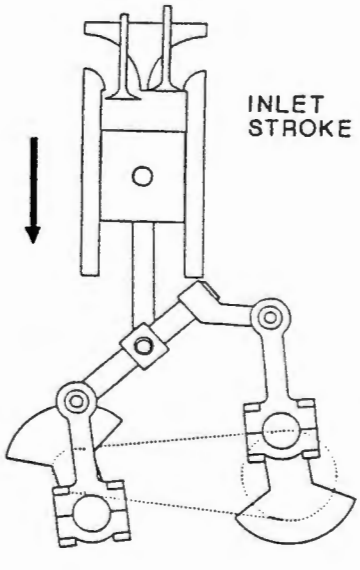

Figure 7. Diagram of the Variable Stroke Mechanism [5].

2.2 DEVELOPMENT OF THE OTTO-ATKINSON CONCEPT

The proposed motion of a variable intake and compression stroke, whilst retaining a full expansion and exhaust stroke, is based on the addition of the following two wave motions; cos(ωt) and sine(0.5ωt). Where ω is the angular speed of the primary crank and t the elapsed time. The proposed linkage, shown in figure 8, approximates this by using two crankshafts (1,2) which are linked by connecting rods (3,4) and a cross-link (5). The primary crankshaft (1) rotates at full engine speed and thus supplies the cos(ωt) motion. The auxiliary crankshaft (2) rotates at half engine speed and is ninety degrees out of phase when ωt equals $n\pi$ (n = 0, 2, 4 ...), this supplies the sine(0.5ωt) motion. The position of the slider (6) determines the magnitude of each component making up the final motion. It is necessary that the motion of the small end of one of the connecting rods (1,2) be constrained to motion in the vertical plane, the motion of the other is free to move within the constraints of the link (5) and its conrod.

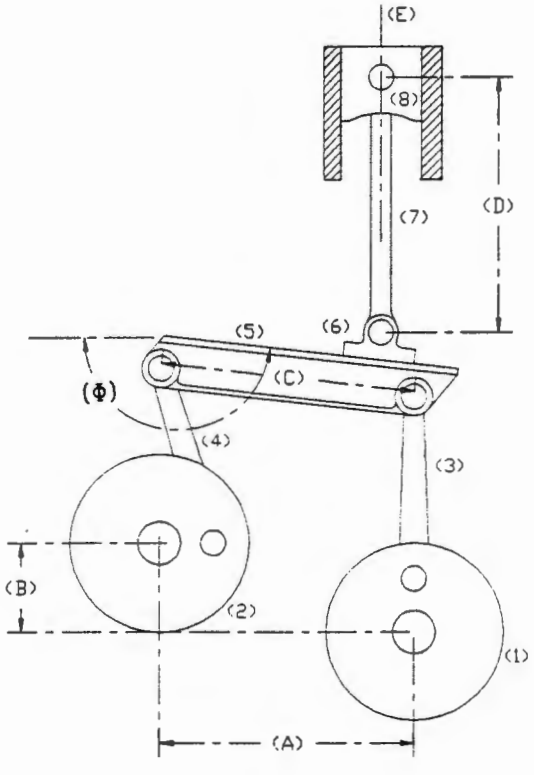

Figure 8. Diagram of the Otto-Atkinson linkage.

$$Y = (1-R)A\cos(\omega t) + A(R)\sin(0.5\omega t)$$

where: A = amplitude of motion of the conrod small ends.

R = ratio of the position of the slider over the maximum travel of the slider on the link.

Y = vertical displacement of the slider.

With the slider at the extreme right of the cross-link (fig.8) the motion would follow that of the primary crank ie normal full stroke motion. This represents full throttle operation. As the slider is moved towards the left of the cross-link a proportional amount of the auxiliary crank motion is added thus shortening the stroke for every alternate revolution of the primary crank. A point is reached where the amplitude of the short stroke becomes zero this represents the extreme of part-load operation. However, to overcome internal mechanical friction the minimum usable stroke will occur before this point is reached.

A cycle of this engine at approximately 30% inlet stroke is shown in Figure 9.

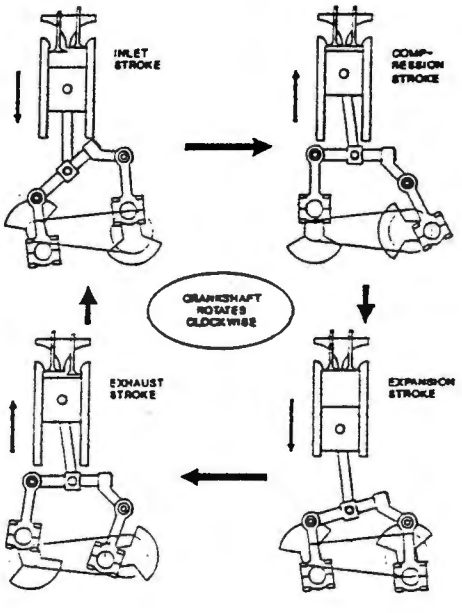

Figure 9. Otto-Atkinson Engine Cycle
30% Inlet Stroke [5].

2.3 COMPUTER SIMULATION

A computer model was used to calculate the locus of the crank linkage, and to determine the optimal configuration of the elements of the linkage. To simplify the design process a motor cycle engine was used to source the basic components. The discussion concerning the specific choice of engine is presented in chapter 4. The components sourced from the base engine were the two crankshafts (1,2), two conrods (3,4) and the piston (8), see figure 8. The following parameters remained flexible; centre distance between the primary and the auxiliary crankshafts (A), the vertical offset of the auxiliary crankshaft (B), the length of the link (C), the length of the piston rod (D) and the position of the line of motion of the piston, relative to the primary crankshaft centre (E). These parameters were defined as the variables in the computer model. The parameters were varied until optimal piston motion was achieved.

2.3.1 Compression ratio considerations

The position of the piston falls on the locus of an arc, the radius of which is defined by the piston rod. When the slider moves away from the piston centre-line, the piston rod is no longer in a vertical position at top dead centre. This results in an increase in the clearance volume. The intake and compression strokes are reduced for part-load operation. Combining the increase in clearance volume and the reduction in the compression stroke results in an undesirable decrease in the compression ratio at part load. To counter this effect the linkage had to be designed with the cross link slightly angled up towards the part load position (Φ in figure 8). This could either be achieved by using a longer connecting rod for the auxiliary crank or by giving the auxiliary crank a suitable vertical offset (B in figure 8).

The final configuration is tabulated below.

Centre distance	(A)	200 mm
Vertical offset	(B)	69.5 mm
Link length	(5)	200 mm
Piston - rod length	(7)	200 mm
Piston centre - line	(C)	25 mm
Link Angle	(Φ)	174 deg.

Table 1. Summary of the Final Configuration

The computer model was developed with the aid of a spreadsheet. The formulae used to determine the locus for the crank-linkage and finally the position of the piston relative to crank angle, were based on the geometrical, and thus trigonometrical, relations of the crank-linkage elements. Initially the model was over-simplified, but as the design took shape the model was updated to include the physical constraints set by the various components. Thus it was undergoing constant development.

Apart from assisting in determining the final configuration of the linkage, the computer model also rendered important information regarding the motion of the piston. This was used to make cycle predictions. The motion of the piston, with respect to the primary crankshaft, became of great importance during the design and construction of the engine.

CHAPTER THREE

CYCLE PREDICTIONS

The cycle predictions for the Otto-Atkinson engine were based on two computer models. The linkage simulation model was used for preliminary predictions, and secondly a thermodynamic model was developed to provide a detailed cycle prediction. A detailed discussion of the formulation of these models is covered in Appendix A.

3.1 LINKAGE SIMULATION MODEL - PISTON MOTION

The linkage model, which was used to determine the optimum linkage configuration, predicted the piston motion relative to primary crank angle. The piston motion for various slider positions could thus be determined. A graphical representation of the piston motion, as predicted by the computer model, is shown in figure 10. The following trends are identified from this figure.

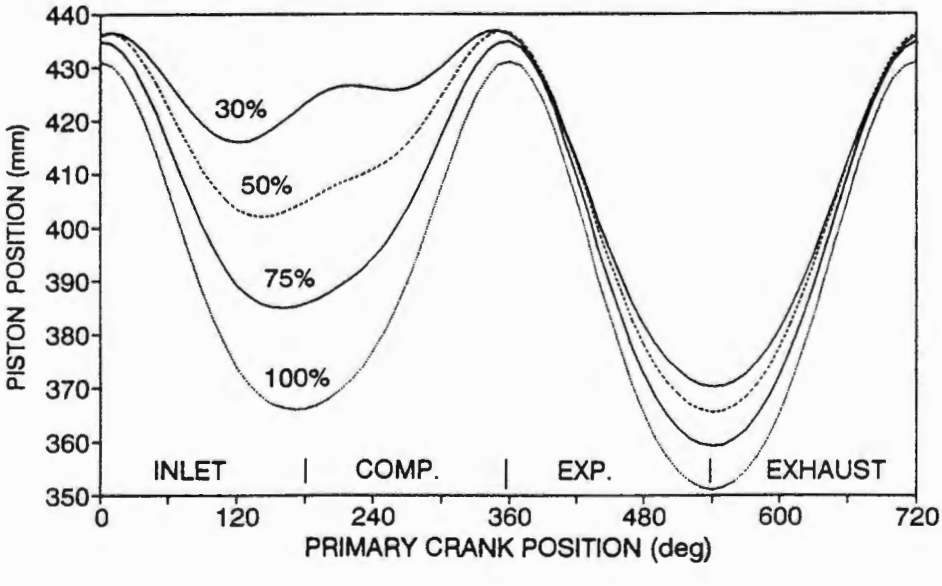

Figure 10. Piston Motion relative to Crank-Angle

(1) The crank-angle at which top dead centre occurs varies. The top dead centre with valves rocking is retarded relative to the primary crank top dead centre (0°, 360°). The top dead centre under compression is advanced with decreasing load.

(2) For the induction stroke the crank-angle at which bottom dead centre occurs varies. With reduced stroke the bottom dead centre is advanced relative to the primary crank bottom dead centre (180°).

(3) The piston position at top dead centre is not constant at all load conditions, this was an intention of the design.

(4) The expansion and exhaust stroke shortens with decreasing load.

These trends are of sufficient importance to warrant a more detailed discussion.

3.1.1 Varying top dead centre position with load variation

The phenomenon of a non-constant crank angle at which top dead centre occurs could result in serious difficulties in producing an engine which is functional over the full power range. For an engine to run efficiently the ignition timing is critical. Table 2 shows the shift in crank angle for various slider positions. It is evident that top dead centre, under compression, shifts by 16 degrees of primary crank shaft motion. Clearly a shift of 16 degrees requires an adjustment in ignition timing. For this reason it became evident that an ignition system which allowed a substantial shift in spark advance would have to be designed. It is also evident, from table 2, that the shift in top dead centre position is not linearly dependent on slider position. For commercial application this engine would require an ignition system which would automatically compensate for the shift in top dead centre position. However, for test conditions a manually adjustable system is preferable.

Slider Position ⟵ → % Stroke		Top Dead Centre Crank Angle	
		Compression	Valves Rocking
0	100	359	721
10	88	358	722
20	77	357	723
30	65	355	725
40	53	353	727
50	42	350	729
60	32	347	731
70	22	343	734

Table 2. TDC Crank-Angle for Various Slider Positions

	Open	Closed
Exhaust	76 BBDC	36 ATDC
Inlet	44 BTDC	68 ABDC

Table 3. Valve Timing for the Standard Engine

A shift in top dead centre position whilst the valves are rocking results in incorrect valve timing. The shift in top dead centre for valves rocking is also given in table 2; the valve timing for the standard motorcycle engine is given in table 3. When comparing these figures it is evident that the shift in top dead centre will have an adverse effect on the valve timing and thus also on the performance of the engine. Pouliot et al. found a similar problem with the valve timing of their five cylinder variable stroke engine. This they solved with a complex planetary gear mechanism [9]. The design of a

mechanism which could vary the valve timing as a function of slider position was considered. The mechanism would alter the length of the tension side of the timing chain and in so doing would also alter the valve timing. However, the valve timing affects the torque curve and also the maximum power. This thesis involves the improvement of efficiency, particularly at low load conditions. Efficiency at low loads is not affected by maximum power output, neither is maximum power output a consideration of the part-load operating regime. Thus it was decided that the increased complexity of variable valve timing was not warranted at this stage.

From table 2 it can be seen that the top dead centre position, with both valves rocking, is retarded for part load settings. This could result in the piston fouling the inlet valve. Provided fouling of the valves did not occur it was decided to leave the valve timing as for the standard motor.

3.1.2 Varying bottom dead centre during induction

As it was decided to leave the valve timing unchanged, the effects of an advanced bottom dead centre deserve mention. The valve timing is set relative to the primary crank, and so as the piston bottom dead centre varies the valve timing of the closure of the inlet valve is altered. In this case, as the stroke is reduced to decrease power output, the closure of the inlet valve relative to the piston bottom dead centre is retarded. This results in late intake valve closure, which is in itself a means of power reduction, (see section 2.1.1 in Chapter 2). The expected effect is thus a reduction in power from late intake valve closure, added to the desired reduction in power resulting from the reduced stroke. This may limit the minimum usable stroke to a somewhat greater stroke than was initially anticipated.

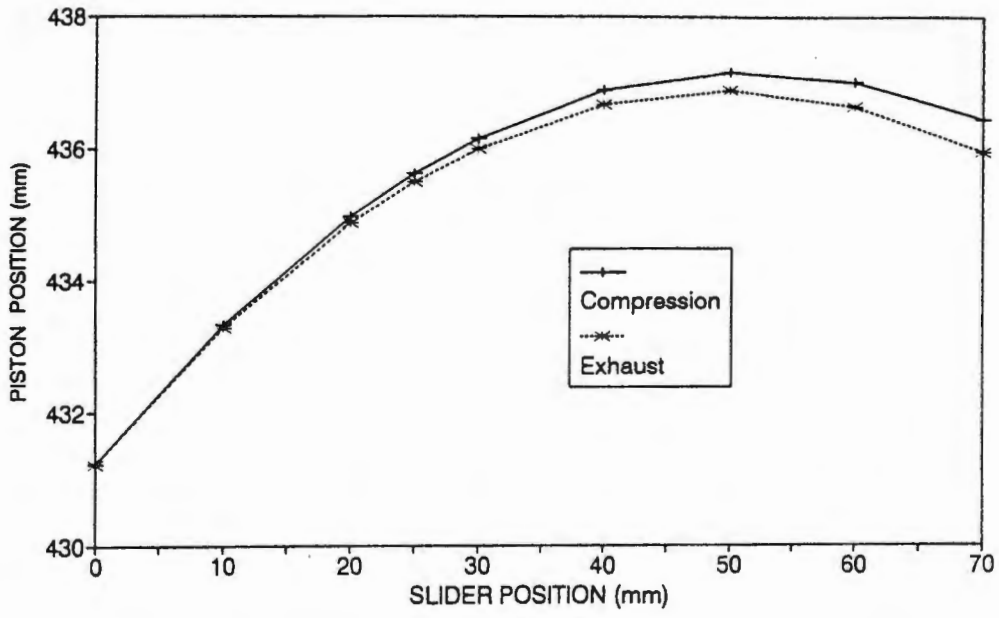

Figure 11. TDC Piston Position relative to Slider Position
(Slide at 0 gives maximum power)

3.1.3 Piston position varying at top dead centre

Figure 11 is a plot of top dead centre piston position relative to slider position. From this figure it is evident that the piston position at top dead centre varies with varying slider position. This is due to the geometry of the crank mechanism, as was discussed in the previous chapter. However, this trend has been utilised to increase piston height at low loads thus decreasing the clearance volume and somewhat countering the negative effect which the decreased swept volume has on the compression ratio. The converse applies at full load conditions, where the sharp drop off in piston height is partially offset by the increase in swept volume at this condition.

This trend was also of importance during the design of the crank case and cylinder block placement. To avoid fouling of the piston and head it was necessary to place the cylinder block such that the piston maintained sufficient clearance across the full load range. To allow for some adjustment of the clearance volume, brass shims were placed at the base of the cylinder block.

3.1.4 Decrease in expansion stroke at part load

Initially this crank linkage was described as a mechanism which allowed a variable intake and compression stroke whilst maintaining a full expansion and exhaust stroke. In practice this is not possible due to the physical constraints of the linkage. However, the trend of decreasing expansion and exhaust stroke at part-load conditions is advantageous. Maintaining a full expansion stroke for a decreasing compression stroke could result in expanding the burnt mixture below atmospheric pressure, before the exhaust valve opens. This would result in a negative work loop on the pressure-volume diagram which indicates a decrease in efficiency. In fact, there is no point in expanding the burnt mixture below the FMEP as the additional expansion would not even overcome the frictional work required for that expansion. Reducing the expansion and exhaust strokes along with decreasing inlet and compression strokes insures that this does not occur. However, the expansion and exhaust strokes are always greater than the inlet and compression strokes for any given load condition, thus allowing the mixture to expand more fully than in a conventional, equal stroke engine, and so further improving the efficiency by approaching the Atkinson Cycle.

These trends became of significant importance during the design of the crank case and the integration of the Otto-Atkinson linkage components and the sourced components.

3.2 LINKAGE SIMULATION MODEL - EFFICIENCY PREDICTIONS

Once the donor engine had been selected, the diameter of the cylinder bore and clearance volume were known. The piston motion and cylinder bore were then used to calculate the displaced volume for various slider positions. Figure 12 is a plot of the displaced volume during the compression and the expansion strokes for various slider positions. From this data, the compression and expansion ratios were calculated. These are plotted in figure 13 against percentage inlet stroke swept volume.

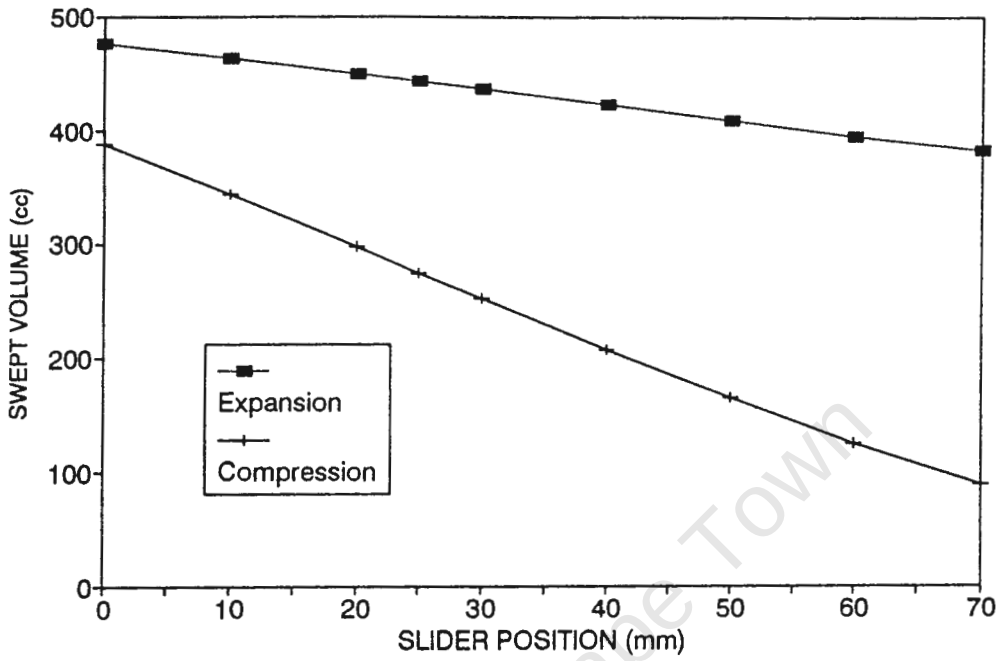

Figure 12. Displaced Volume against Slider Position

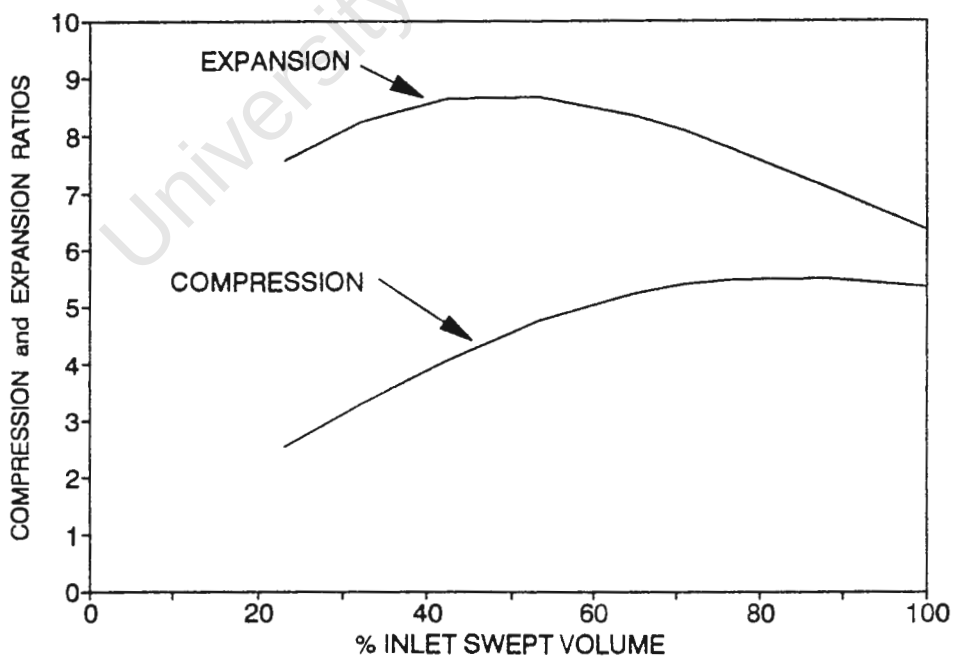

Figure 13. Compression and Expansion Ratio against Percentage Inlet Swept Volume

From these figures it is apparent that with decreased swept volume, the expansion stroke does not decrease at the same rate as the compression stroke. This results in the expansion ratio maintaining greater magnitudes over the full stroke range.

These initial predictions were used to determine the Otto and Atkinson thermal efficiency. The Otto efficiency is determined by the following formula:

$$\eta_{otto} = 1 - (CR)^{\gamma-1}$$

As the Otto Cycle defines equal compression and expansion ratios, this formula does not take the expansion ratio into account. Assuming a typical value of 1.4 for γ the Otto efficiency was calculated for various inlet strokes (compression ratios (CR) from fig. 13).

The Atkinson efficiency implies a different expansion ratio (ER) than compression ratio (CR) and therefore also takes account of the expansion ratio. The Atkinson cycle efficiency is determined by the following formula :

$$\eta_{atkinson} = 1 - \gamma \left[\frac{(ER-CR)}{(ER^{\gamma}-CR^{\gamma})} \right]$$

Assuming the same value for γ as for the Otto efficiency calculations, the Atkinson efficiency was calculated for various inlet strokes. The Otto and Atkinson efficiency are plotted against percentage inlet swept volume in figure. 14. From this figure it is evident that the Atkinson efficiency becomes progressively greater than the Otto efficiency as the inlet stroke is reduced. This is purely due to the over expansion resulting from the difference between the expansion and the compression strokes. It is also evident that the Atkinson efficiency remains virtually constant down to approximately 40% inlet stroke. The geometry of the linkage is such that even at full inlet stroke the expansion stroke exceeds the compression stroke. This results in the Atkinson efficiency exceeding the Otto efficiency across the full stroke range.

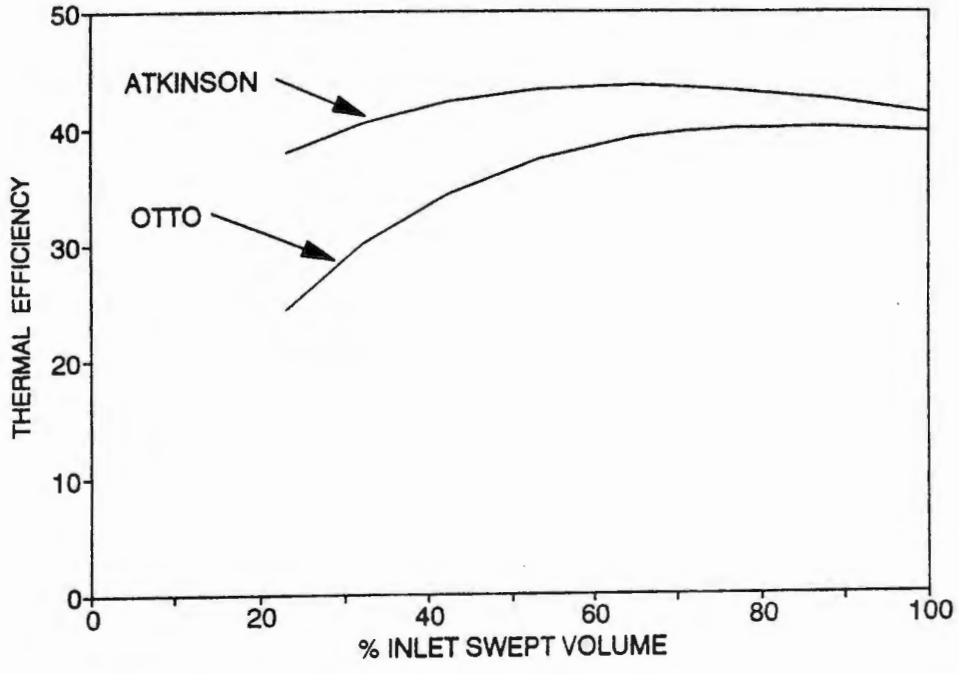

Figure 14. Otto and Atkinson Efficiency against Percentage Inlet Swept Volume

These initial cycle predictions only consider the thermal efficiency gains resulting from the over expansion of the hybrid Otto-Atkinson cycle. However, it was expected that the greatest efficiency gains would be as a result of the elimination of the pumping losses associated with throttled operation. For this reason a full cycle analysis that took pumping, frictional and heat losses into account was required.

3.3 THERMODYNAMIC CYCLE ANALYSIS

The piston motion relative to crank angle, determined by the linkage simulation, was used as the basis of this cycle analysis. The linkage simulation was customised to determine the piston position for primary crank angle at the following increments:

(1) Inlet and exhaust stroke - 20 degree increments.
(2) Compression and expansion stroke - 10 degree increments.
(3) Combustion - 5 degree increments.

An indepth thermodynamic cycle analysis involves calculations which are beyond the scope of this thesis. Thus some simplifying assumptions were necessary:

(a) Intake at wide open throttle occurred at atmospheric conditions. For part throttle intake it was assumed that manifold vacuum was reached within 15 degrees after top dead centre.

(b) Gas properties during compression and expansion were calculated in incremental steps, each step comprising two stages: first, an isentropic pressure change and secondly, a heat transfer calculation to determine the gas temperature.

(c) Combustion heat release was controlled by an arbitrary release model [16].

(d) Exhaust occurred at atmospheric pressure.

(e) Heat transfer was modelled using the convective heat transfer coefficient proposed by Sitkei [17].

Based on these assumtions a computer simulation was developed which would determine the pressure and temperature at the given increments of the primary crankshaft. A pressure volume diagram was plotted and the indicated work calculated. The indicated work was determined by multiplying the average pressure during each increment by the volume change occurring during that increment.

To simulate part stroke operation the piston motion for various slider positions was transported across from the linkage simulation, while manifold pressure was kept at atmospheric. As the inlet swept volume was reduced the mass of induced charge and thus fuel energy released decreased. This combined with a reduction in compression stroke resulted in lower pressures and therefore a reduction in indicated work. Part throttle operation was

simulated with the piston motion at full inlet stroke. To simulate different throttle positions various inlet manifold vacuums were considered. The reduced manifold pressure resulted in a reduction in the density and therefore the mass of the inlet charge. The pressure at the beginning of compression was also reduced. These combined effects resulted in a reduction in the indicated work.

At this point the cycle simulation was a general simulation for the Otto-Atkinson engine. In order to predict brake torque and brake specific fuel consumption (BSFC), the engine speed and associated frictional torque were required. These inputs were only determined once the engine had been constructed and friction tests carried out. Thus at this point predictions were made based on an assumed frictional torque of 15% of the indicated torque at full power. The following three figures are the predicted pressure-volume diagrams of the engine at full load, at 60% inlet stroke and at 0.4 Bar manifold vacuum. The latter two conditions produced approximately the same indicated work. From these figures it is evident that part-stroke operation does not suffer from the negative pumping loop characteristic of the throttled operation.

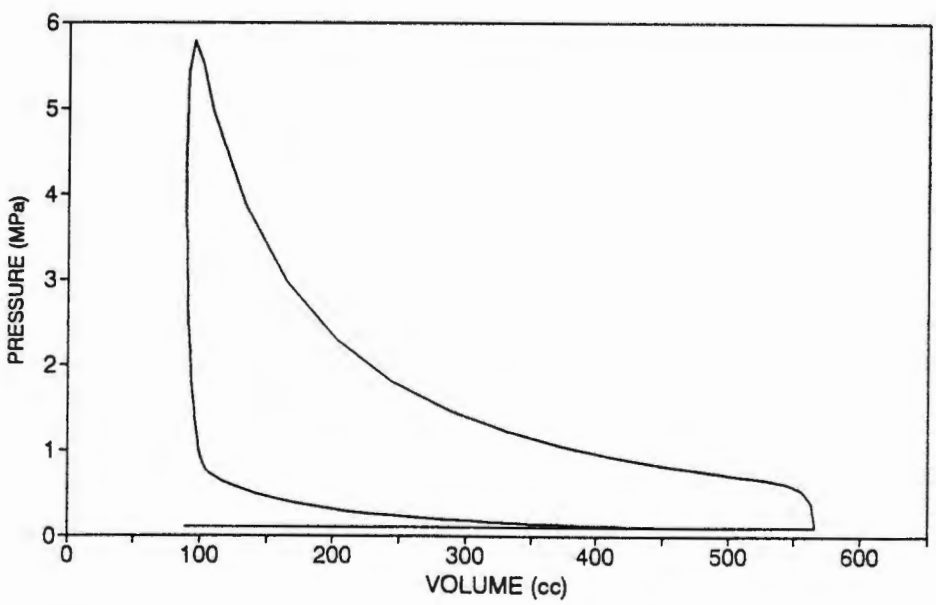

Figure 15. Predicted Pressure-Volume Diagram - Full load

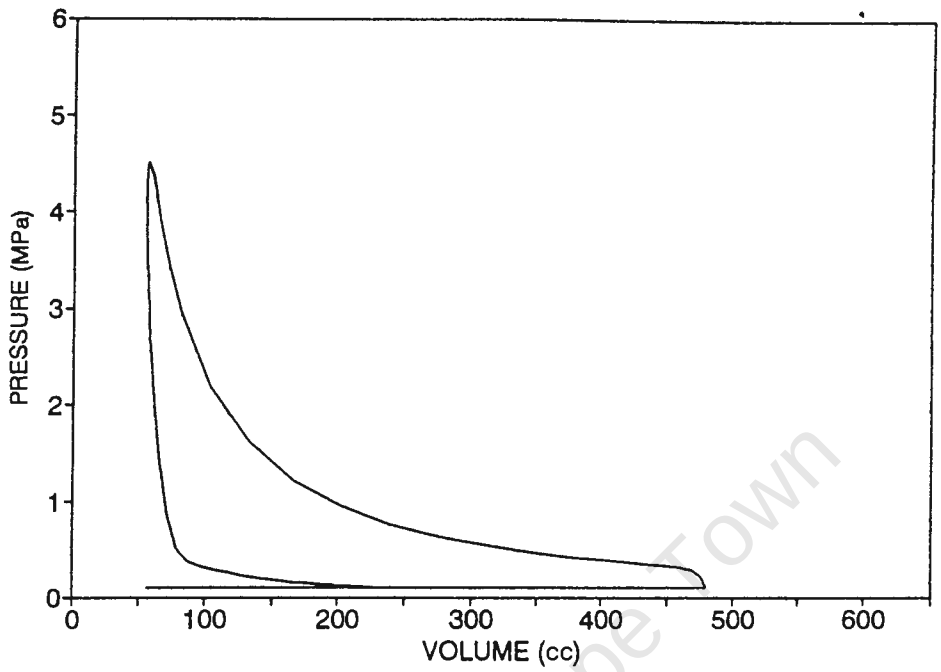

Figure 16. Predicted Pressure-Volume Diagram - 60% Stroke

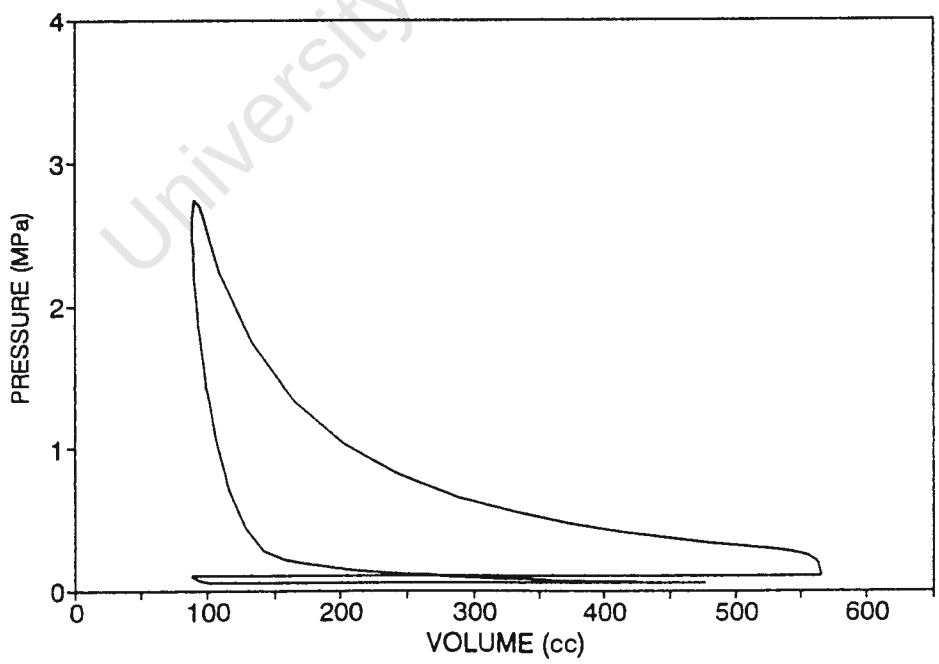

Figure 17. Predicted Pressure-Volume Diagram - 0.4 Bar Manifold Vacuum

In order to calculate the BSFC, an engine speed of 3000 rpm was selected. As discussed above, friction torque was taken as 15% of the indicated torque at full load. At these conditions the brake torque and brake power were calculated. The BSFC (g/kWhr) was then calculated from the brake power (kW) and the fuel consumption (g/hr) for various inlet strokes and manifold vacuums. Figure 18 is a plot of the predicted BSFC against brake torque. From this figure it is apparent that the variable stroke operation results in a substantial drop in BSFC and thus an improvement in efficiency. The part stroke curve falls below the part throttle curve across the full load range. This can be solely attributed to the means of load control. The mechanisms by which the efficiency is improved are as follows: (a) Primarily the absence of pumping losses, particularly in the low load range, (see figs. 16 and 17), and (b) the improvement in thermal efficiency associated with the tendency towards the Atkinson cycle (see fig. 14). The magnitude of the measured frictional torque will most likely be different from that assumed for these calculations. However, as the frictional torque is speed dependent, it is expected that the general trends exhibited in figure 18 will not change dramatically.

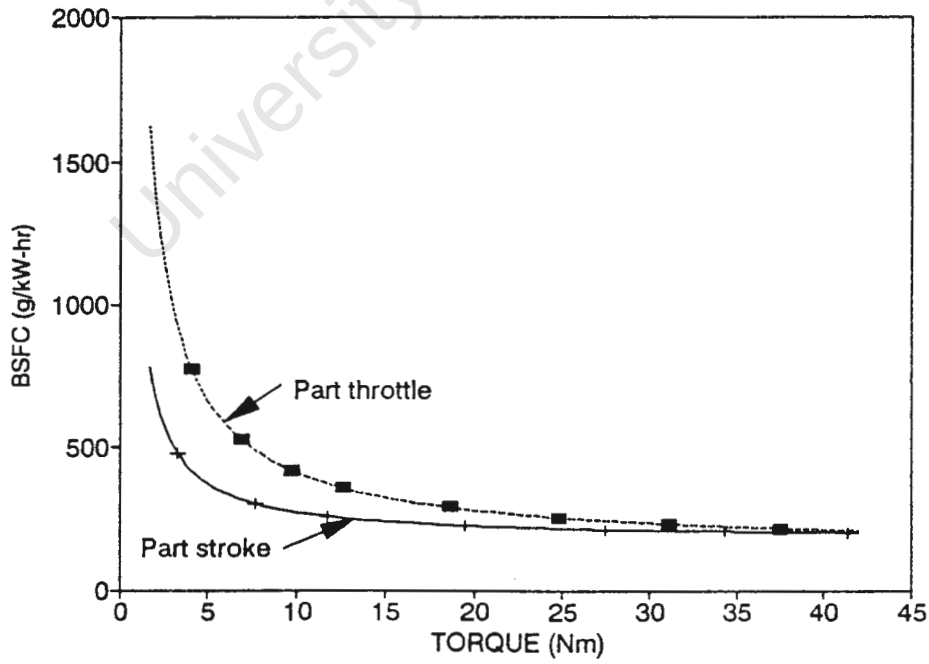

Figure 18. Predicted Brake Specific Fuel Consumption against Brake Torque

At this point it must be stressed that the friction of the Otto-Atkinson engine is expected to exceed that of a conventional four-stroke engine of similar capacity. However, as both the throttled and part stroke tests will be conducted on the Otto-Atkinson engine, the difference in BSFC will not reflect the friction penalty imposed by the Otto-Atkinson linkage. Thus for the sake of comparison the throttled BSFC will be predicted, using the frictional torque of the test engine and also using a typical frictional torque for a four-stroke engine of similar capacity. The former will predict the trend for the experimental work, the latter will exempt the part throttle operation from the friction penalty of the linkage and thus reflect the true advantage of the Otto-Atkinson engine. These predictions will be discussed along with the discussion of the experimental results.

CHAPTER FOUR

DESIGN OF A PROTOTYPE OTTO-ATKINSON ENGINE

Figure 8 is repeated here for convenience.

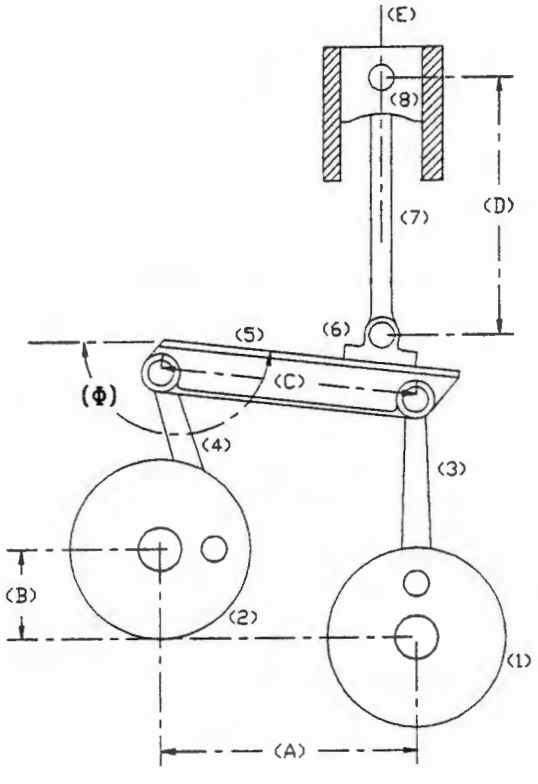

Figure 8. The Otto-Atkinson Linkage

In order to avoid unnecessary cost and excessive manufacturing time it was decided that the best approach was to begin with a base engine from which the standard components could be sourced. The engine selected was from a four-stroke Yamaha 500cc motor cycle. This selection was based on the following :

(a) A 500cc single cylinder engine represents the swept volume of one cylinder of a mid-range four cylinder motor car engine, (taken as 2 litre).

(b) This engine is a well proven, simple engine for which parts are easily obtainable.

This approach placed some limits on the flexibility of the design, however, as this was a prototype engine the cost of manufacturing an entire engine was not warranted.

The major components sourced from the donor engine were the two crankshafts (1,2), two conrods (3,4), the piston (8) and the cylinder and head. Many other minor components were sourced from the donor engine, these will be discussed later in this chapter.

4.1 LINKAGE COMPONENT DESIGN

The linkage components are exposed to two principal forces: gas pressure forces acting down on the piston, and inertia forces due to the acceleration of the reciprocating parts.

The gas pressure was estimated by modelling an idealized thermodynamic cycle for the engine [2]. A compression ratio of 9:1 was used, this was the compression ratio of the standard motor cycle engine. Heat losses during combustion were estimated as 10%. Calculations resulted in a peak pressure of 50 bar. With the area of the piston known, the peak gas pressure force on the piston was determined as 30 kN.

The inertia forces are dependent on the acceleration of the reciprocating parts. Due to the unusual motion of the linkage, the piston motion is not pure sinusoidal. For this reason the maximum acceleration was determined with the aid of the computer model. Time increments spanning one crank-angle degree before and after top dead centre were considered. The velocity change across the two time increments rendered the acceleration. The same procedure

was repeated for bottom dead centre. A maximum engine speed of 6000 rpm was considered and this resulted in a maximum acceleration of 23000 ms^{-2}, occurring at top dead centre. Having determined the maximum acceleration, the inertia forces in the linkage were calculated by multiplying the acceleration by the reciprocating mass under consideration.

With the maximum forces identified, the following components were designed: piston connecting rod (fig. 8 (7)), cross link (5), slider (6) and slider adjusting mechanism. Design detail is covered in Appendix B, design drawings can be found in Appendix E.

4.1.1 Piston connecting rod

The length of the connecting rod had been determined from the computer model. The upper boss had to satisfy the constraints set by the piston and gudgeon pin, the lower end was designed in conjunction with the slider. As the piston connecting rod adds to the reciprocating mass, size and mass constraints were also of importance. Material selection formed an important part of the design process.

4.1.2 Cross-link

The length of the cross-link had been determined from the computer model. The shape and cross-sectional dimensions were subject to the following design considerations:

(a) The link required freedom to tilt to a angle of 45°.

(b) As the link added to the reciprocating mass it was desirable to keep the mass at a minimum.

(c) The crankshaft bearing spacing and thus the width of the crankcase placed a restriction on the width of the link.

(d) A criterion of the design was that the slider be adjustable whilst the motor was operating. To satisfy this condition hydrodynamic lubrication had be maintained throughout the cycle, this placed a restriction on the minimum bearing surface area.

(e) The integration of the slider and the link had to allow motion along the link (d) but not in the plane perpendicular to it, thus a guide rail for the slider was required.

The configuration which satisfied all of these constraints was that of two parallel I-beam sections with the slider running on top. The two I-beam sections created a channel which restricted the slider to motion parallel to the link, see figure 19.

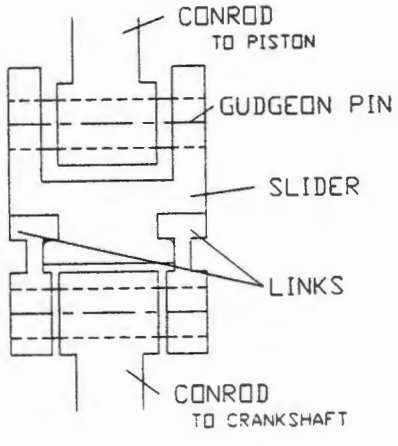

Figure 19. Cross Section of Links and Slider

The link is loaded in bending, with the extreme condition being that of a centrally placed load. The calculations showed that the greater of the two forces was the gas pressure force, acting down. Due to the inertial forces occurring at top dead centre, acting upwards, fatigue under cyclic loading had to be considered. This was also of importance in the material selection, as the material had to be as

light as possible, yet have the properties of high UTS and fatigue resistance. Working within the design constraints and taking the cyclic fatigue loading into consideration, an I-beam section of 45mm by 17mm with a 3mm webb was calculated.

4.1.3 Slider

The slider was designed in conjunction with the piston connecting rod and the cross-link, thus the slider was subjected to the design constraints of these two components. As the slider added to the reciprocating mass it was desirable to keep its mass at a minimum. Fatigue in the gudgeon pin lugs and load bearing parts had to be considered. To avoid excessive wear of the sliding surfaces, surface hardening was stipulated.

4.1.4 Adjusting mechanism

In order to satisfy the design criterion that the slider be adjustable under operating conditions it was necessary to design a mechanism to set and adjust the slider position.

The primary consideration was that the adjuster allow the position of the slider to be changed whilst the engine was running. The force required to move the slider under operating conditions also had to be considered. It was decided to use a nut and bolt type mechanism. With the bolt located in the crank case and the nut linked to the slider by control arms, rotation of the bolt resulted in motion of the nut and thus also the slider. The control arms added to the reciprocating mass and were exposed to high stresses, this had to be taken into consideration during the design and material selection.

The adjusting mechanism is shown below.

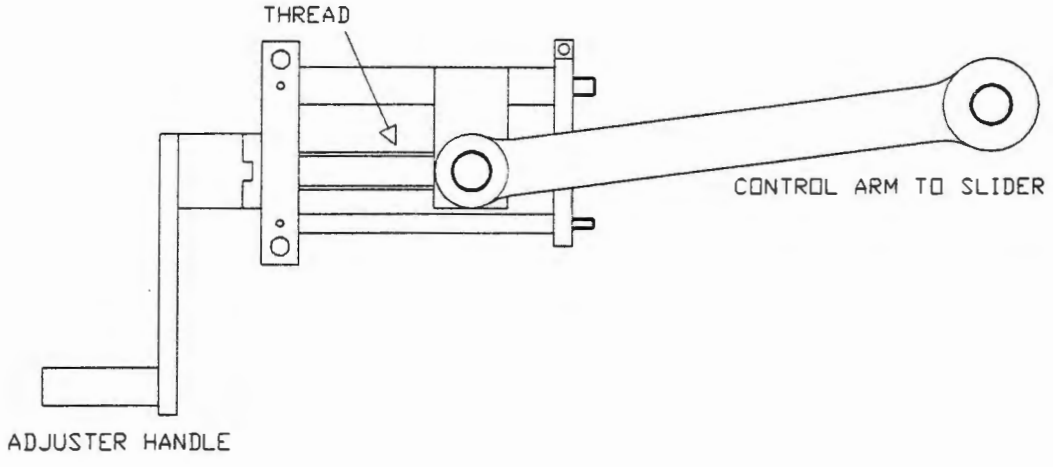

Figure 20. Slider Adjusting Mechanism

4.2 INTEGRATION OF THE ENGINE COMPONENTS

The following parts of the engine had to be designed and integrated with the Otto-Atkinson linkage and adjuster to form an integrated unit:

(1) Crankcase
(2) Power-out shaft
(3) Auxiliary crank drive
(4) Camshaft drive
(5) Points breaker drive and placing
(6) Oil pump drive and placing
(7) Lubricant distribution
(8) Piston, cylider and head
(9) Carburettor and exhaust

(1) Crankcase - The crankcase design took the form of two parallel plates, accurately spaced by three spacing blocks. A top deck was bolted to the top edges of these plates. Recesses for the bearings and primary crank small end guides were machined in the parallel plates. All auxiliaries were bolted to the outside surfaces of these plates. The complete crankcase assembly was then encapsulated in a sump which was bolted to the underside of the top deck.

(2) Power-out shaft - The power-out shaft was designed to similar dimensions as the primary shaft in the gearbox of the original motorcycle engine. This was to allow the original bearings and clutch housing to be used. The shaft was placed between the two crankshafts and was driven off the primary crankshaft using the orignal gear drive. The clutch housing ring gear was part of this gear drive, the clutch housing also served to counter balance the primary crankshaft flywheel.

(3) Auxiliary crank drive - The auxiliary crank was gear driven using the power-out shaft as an idler shaft. To produce half engine speed for the auxiliary crank a 2:1 gear ratio between the primary and auxiliary crank was used. The auxiliary crankshaft gear had to be manufactured.

(4) Camshaft drive - The camshaft was driven by the primary crankshaft using the original sprockets and an extended chain. Chain guides were added to prevent chain slap.

(5) Points breaker drive - The points breaker was gear driven using the original gear drive off the primary crank. A housing was designed to accommodate the points breaker base plate, cam spindle and mechanical advance in an oil-free environment. To allow adjustment of the ignition timing under operating conditions the base plate was modified so that it could be rotated whilst the engine was running.

(6,7) Lubrication system - The scavenging oil pump sourced from the original engine was used and gear driven off the points breaker drive. Oil was fed from the pump to the oil filter from which it went to the lubricant manifold for distribution.

(8) Cylinder and head - The cylinder block studs were mounted in the top deck of the crank case. Brass shims were included to allow the compression ratio to be adjusted. They were placed at the base of the cylinder block. To reduce the clearance volume the head was fitted without a head gasket.

(9) Carburettor and exhaust - The carburettor selected for this engine was a SU carburettor sourced from a Mini 850. The SU carburettor was selected as it satisfied the constraint of not requiring a manifold vacuum in order to supply fuel at low air velocities. The carburettor was fitted with an adapter plate. An exhaust was made up to fit the test cell configuration.

4.3 FABRICATION AND ASSEMBLY OF THE OTTO-ATKINSON ENGINE

Most of the components were fabricated in the workshop of the Mechanical Engineering department. The links and piston connecting rod were milled on a Computer Numeric Controlled (CNC) milling machine, this was also carried out in the department. These components and the slider were then liquid-nitrided before grinding of any critical surfaces was carried out. Finally gas tuff-riding was applied to insure good wear resistance. The control arms of the adjusting mechanism were also milled on the CNC milling machine. To insure that no flaws existed, which could lead to fatigue cracks, these components where hand finished and polished. All CNC programming and operation was carried out by the author. The lubrication system was fabricated during assembly.

Assembly began with the crankshafts and related components. The adjusting mechanism, control arms, slider, conrod and links were fitted together with the two crankshafts and located in one of the crankcase-plates, see figure 21. The second plate was then fitted, the spacing and parallelism of the two plates was insured by spacer blocks with locating dowels. The crankcase was then bolted together, the bolts passing through the spacing blocks. The gears were fitted to the primary and auxiliary cranks and the power-out shaft, the latter also served as an idler gear for the auxiliary crank. The motion of the crank-mechanism and adjuster could then be checked. This was found to be satisfactory thus assembly could continue.

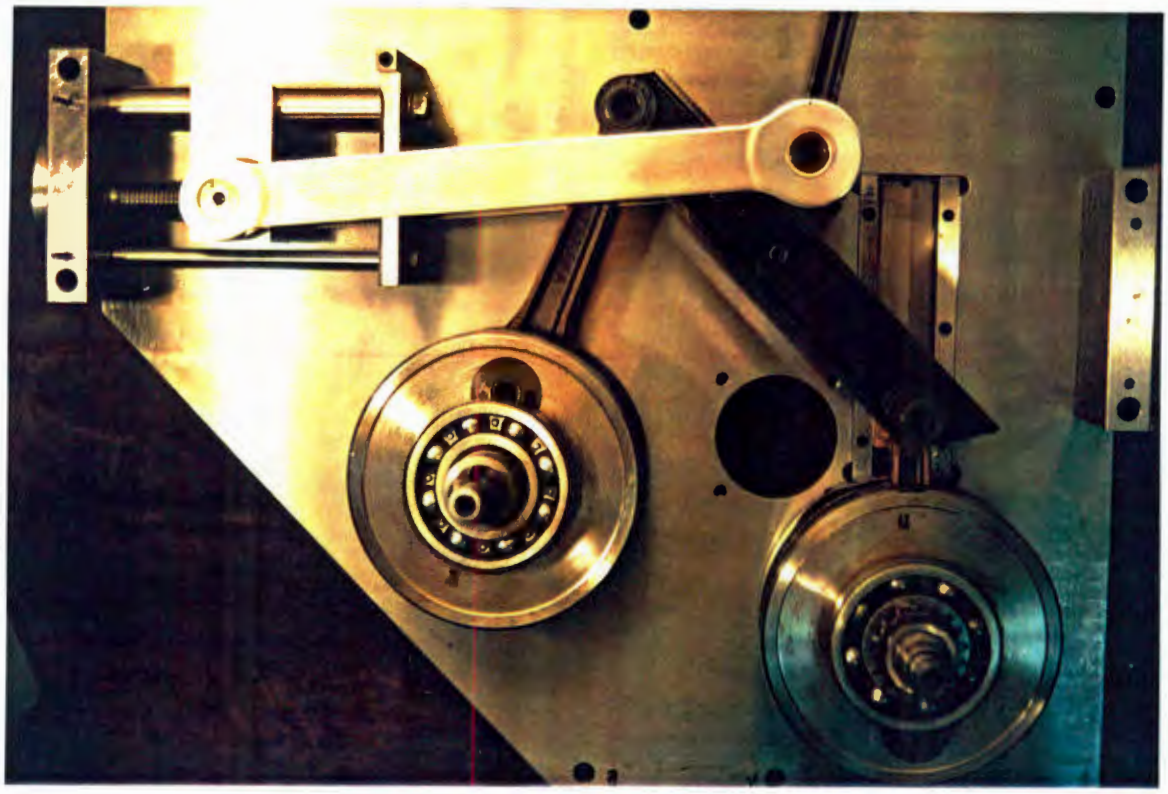

Figure 21. Photograph of the Assembled Linkage Components

4.3.1 Computer model verification

The top-plate was fitted to the crankcase-plates, the piston and cylinder block were then fitted. With the assembly at this point the motion of the piston relative to crank-angle was established. A protractor was fitted to the primary crankshaft so that with the aid of a pointer the crank angle at any given position of the piston could be found. A clock gauge was mounted on a magnetic base and positioned to register the height of the piston. The piston position relative to crank angle could then be found experimentally and compared with the computer model. These correlated favourably with the computer model. The computer model had indicated that the crank-angle at which top dead centre occurred, varied with slider position. This was also verified. Because of this phenomenon it was decided to set the slider at the position that coincided with the centre line of the cylinder and use this position for setting up the engine. A pointer was fitted and the gear on the auxiliary crank was marked for top dead centre.

4.3.2 Valve timing

The head and cam shaft drive chain were fitted and the valve timing was set by lining up the manufacturer's timing marks, (of the donor engine). The protractor and clock gauge were used to check the valve timing against the manufacturer's specifications.

Due to the shift in top dead centre with varying slider position it was necessary to check for the possibility of a valve fouling the piston. This was done by putting a layer plasticine on the crown of the piston, refitting the head and then rotating the engine, whilst adjusting the slider position from maximum to minimum load position. The head was then removed and a cross section of the plasticine was taken. The minimum clearance was found to be approximately 0.3mm, (at the inlet valve), which was not sufficient. To increase the clearance the piston was removed and the valve clearance pocket was deepened by approximately 1 mm. The piston, (with a layer of plasticine), and head were then refitted and the procedure repeated, the clearance was then found to be sufficient.

4.3.3 Lubrication system

The points drive and housing were fitted and checked for satisfactory operation. The oil pump (driven off the points drive) could then be fitted. With the oil pump in place the lubrication system was made up. 3/8" Bundi tubing was used for the oil pump intake, the feed line to the oil filter and the feed line from the filter to the lubricant manifold. 3/16" Bundi tubing was used to supply oil to the various components requiring lubrication. The two crankshafts had special caps made up which allowed oil to be fed into the centre of the crankshaft, as in the original motorcycle engine. Lubrication to the primary crankshaft small end guides was by drip feed and a spray feed was fitted for the underside of the piston and cylinder walls. The adjusting mechanism was also lubricated with a spray feed. Over and above the directed lubrication it was assumed that ample splash

lubrication would result from the rotating parts which were partially submerged in the sump oil. It was known that the original motorcycle engine had difficulties due to excessive exhaust valve temperatures. This was due to insufficient lubrication - the original design favoured the inlet valve rocker shaft. Sufficient lubrication to both rocker shafts was insured by a modification which gave each of the two rocker shafts an individual oil supply, fed down the centre. The lubrication system was then tested by driving the oil pump from an external source; it was found to function satisfactorily.

With the lubrication system fitted and tested final assembly and setting up of the engine could commmence. The sump was fitted and the engine was mounted on the engine stand which in turn was mounted on the dynamometer trolley. It was then coupled to the dynamometer via a flexible coupling. The carburettor was fitted and a throttle linkage to the dynamometer control system was made up; the exhaust was also fitted. Lubricant was topped up and a thermocouple to measure oil temperature was inserted through the dipstick aperture. A thermocouple was also fitted to register the temperature of a cooling fin in the vicinity of the exhaust port. The ignition electrics were connected up and the spark advance was set at 8 degrees before top dead centre, (the top dead centre mark was visible through a perspex spy-glass mounted in the sump wall). The draught created by the extractor fan was deemed sufficient cooling for preliminary testing, though for full testing a forced draught over the cooling fins would be supplied by a blower. The fuel system was then bled and the engine was motored to bleed the lubrication system.

At this stage the engine was ready for preliminary testing, these tests are discussed in Appendix C.

CHAPTER FIVE

EXPERIMENTAL APPARATUS AND PROCEDURE

The experimental work consisted of fuel consumption tests at constant speed and varying torque. The apparatus used for these tests was as follows :

5.1 EXPERIMENTAL APPARATUS

(a) Test engine

The engine used for testing was the Otto-Atkinson engine designed and built for this thesis. The load control was either by throttle adjustment or by stroke variation. The carburettor was of the SU type. The swept volume of the inlet process was variable from approximately 390 cubic centimetre to 90 cubic centimetre. The throttle and stroke control was effected manually from within the test cell. The ignition timing was dynamically variable, this was also manually adjusted from within the test cell.

(b) Dynamometer

The test cell was fitted with a fully instrumented eddy current dynamometer. The dynamometer provided the facility of either constant speed - varying torque or vise versa. The speed could thus be set at a desired level and the dynamometer would maintain this speed by adjusting the torque load.

(c) Fuel supply and metering system

The fuel was supplied by a 12 volt pump. Fuel metering was accomplished with a micro-oval fuel meter, from which fuel consumption could be measured with a precision of one millilitre. The time elapsed during each consumption test was measured with a digital stopwatch with a precision of 1/100th of a second.

(d) Ignition system

The test cell was supplied with a twelve volt power source which was used to power the ignition system. The ignition system was of the contact point breaker type.

(e) Cooling system

Cooling air was provided by a centrifugal fan. A maximum air speed of 100 km/h was measured directly in front of the engine. The test cell was also fitted with an extractor fan and ventilation which extracted the heated air and introduced fresh ambient air to the test cell.

(f) Instrumentation

Thermocouples were fitted to the cooling fins of the cylinder block. One thermocouple was clamped to a fin near the exhaust outlet. Another thermocouple was clamped to a cooling fin at the rear of the block. A thermocouple was also fitted at the airfilter inlet to measure the inlet air temperature. These thermocouples were connected to the test cell control panel. Initially a thermocouple was also placed in the sump to measure oil temperature. However, due to the large sump capacity (7 litres) it was found that once operating temperature was reached, the oil temperature did not fluctuate significantly. Recording of this data was thus discontinued.

The Dynamometer test panel was fitted with a digital torque readout with a precision of 0.1 Nm. Torque pulsations produced by the single cylinder engine and also possibly the vibrations caused the torque reading to fluctuate by an unsatisfactory amount. An analogue torque meter was therefore fitted and this had the advantage of internal damping which reduced the amplitude of the fluctuations. It was also established that the average torque value could be more accurately found with an analogue rather than a digital readout. The analogue meter registered amps but was calibrated to torque in newton metres.

(g) Exhaust gas sampling

Samples of exhaust gas were taken for each test condition. A take-off point was fitted to the exhaust to which the sample bags were attached. The gas samples were then analysed using an Orsatz Apparatus. As there were only three sample bags the tests were limited to three runs per test session.

5.2 EXPERIMENTAL PROCEDURE

Preliminary tests were run to check the engine for reliability and correct functioning. The results of these tests were used to facilitate design changes and establish an experimental procedure which would render satisfactory results. These tests are discussed in Appendix C. Friction tests were also conducted in order to compare the friction characteristics of the original engine with the Otto-Atkinson engine. These test are also discussed in Appendix C.

The aim of the experimental work was to obtain constant speed fuel consumption characteristics for the engine in the throttled form and at full throttle, using the stroke adjustment to vary the power. The full load condition was also investigated in order to produce a complete trend from full to part load in each operating mode.

5.2.1 Test parameters

The following parameters are summarised in table 4.

(a) Engine speed

The engine speed selected for all testing was 2800 rpm. This speed was selected for the following reasons: (a) This was the speed at which the vibrations reached a minimum. (b) This is a good mid-range engine speed. Due to difficulties which occurred during testing, other speeds were not investigated.

(b) Engine and inlet air temperature

The engine was warmed up until the rear cooling fin temperature reached 115 °C. This temperature stabilised at 115 +/- 4 °C. As the thermocouple fitted in the front cooling fin was directly in the blast of the cooling air it was found that it gave temperature data of little relevance. Therefore this data was neglected and emphasis was laid on the rear cooling fin. The inlet air was unavoidably heated by flowing over the engine, and with the engine at operating temperature, the inlet air temperature stabilised at 30 +/- 1 °C.

(c) Throttle and slider position

The positions of the throttle and slider were varied for different torque requirements. Recording the position of the throttle was not of importance. However, the position of the slider and thus the swept volume of the inlet stroke for each torque output was important. This was measured and recorded for each test condition.

(d) Ignition timing

Ignition timing was adjusted to give maximum brake torque. It was noted that for part stroke operation an excessively large ignition advance was required to produce maximum brake torque. The significant effect that this had on the test results is discussed in chapter 7.

(e) Torque output

The torque output was a dependent variable. This was registered on an analogue ammeter which had been calibrated to torque in newton metres.

(f) Fuel consumption

The fuel consumed for each test condition was also a dependent variable. The millilitres of fuel consumed over a time interval were recorded and the consumption in millilitres per second was calculated.

(1) Engine speed	2800 +/- 6 rpm
(2) Fin temperature	115 +/- 4 °C
Air inlet temperature	30 +/- 1 °C
(3) Throttle position	Variable
Slider position	Variable
(4) Ignition timing	Set at MBT
(5) Torque output	Dependent parameter
(6) Fuel consumption	Dependent parameter

Table 4. Summary of the Test Parameters

5.2.2 Test Procedure

The preliminary test work helped to establish a reliable test procedure. Figure 22 is a flow chart of the test procedure.

(a) Engine warm up

As the engine operating temperature and air inlet temperature can have a marked effect on the efficiency of the engine it was important that these parameters were controlled. It was found that the rear cooling fin temperature stabilised at approximately 115 °C, at which time the air inlet temperature also stablised, at approximately 30 °C. Prior to testing, the engine was allowed to warm up at wide open throttle with the slider at the full stroke position. When the fin temperature reached 70 °C the cooling fan was turned on and warming up continued until the fin temperature reached 115 °C. This took approximately eight minutes.

(b) Data capture

Once the engine had reached the desired operating temperature the testing could begin. The author remained in the test cell throughout the test in order to adjust the throttle or slider position and ignition advance. The fuel consumption data and exhaust gas capturing was also done from within the test cell. An assistant was present at the control panel in order to monitor the temperatures.

(1) Full throttle - full stroke : Some tests were run with the engine in the full power mode. The ignition timing was set for maximum torque. A fuel consumption reading was then taken. Finally an exhaust gas sample was taken at these operating conditions. A second fuel consumption reading was taken whilst the exhaust gasses were being collected.

(2) Part throttle : In this test mode the load was controlled by varying the throttle setting. The throttle was adjusted to produce the desired torque, the ignition timing was adjusted to give maximum torque at that throttle setting. If necessary the throttle was reset to the desired torque. A fuel consumption reading was then taken. Finally an exhaust gas sample was taken at these operating conditions. A second fuel consumption reading was taken whilst the exhaust gasses were being collected.

(3) Part stroke : This was done at wide open throttle. The swept volume of the inlet and compression stroke was controlled by adjusting the slider position. The stroke was adjusted to produce the desired torque and the position of the slider recorded. The ignition timing was adjusted to give maximum torque at that slider position. If necessary the slider position was reset to the desired torque and the change in slider position recorded. A fuel consumption reading was then taken. Finally an exhaust gas sample was taken at these operating conditions. A second fuel consumption reading was taken whilst the exhaust gasses were being collected.

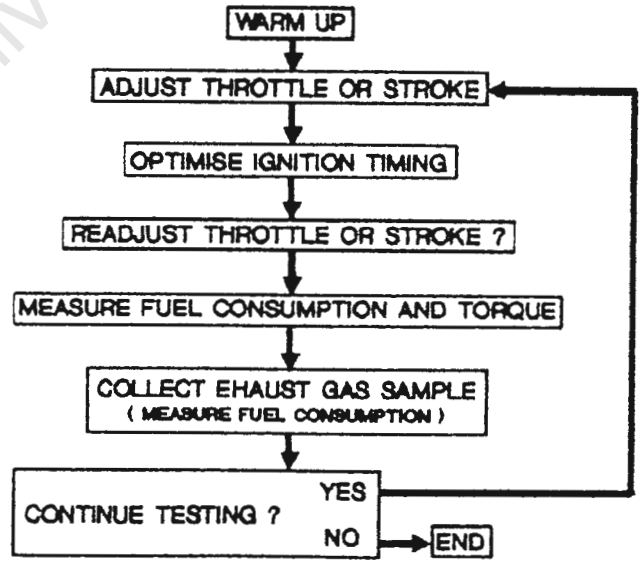

Figure 22. Test Procedure

The experimental work was fraught with difficulties which limited the extent of this investigation. The inertial imbalance caused by the reciprocating mass of the linkage resulted in excessive vibrations. An attempt was made to statically balance the crankshafts with counter weights, however, due to the characteristics of the mechanism this was only partially successful. These vibrations severely limited the testing to a speed at which they became the least obtrusive. The vibrations resulted in a fatigue failure of the exhaust system.

Torsional vibrations were set up between the two crankshafts and the power-output shaft. These vibrations occurred as a result of the auxiliary crankshaft alternately driving and being driven. A failure of the key in the auxiliary crankshaft drive gear resulted from these torsional vibrations. Torsional vibrations were also set up between the coupling of the power-output shaft and the dynamometer driven shaft. These vibrations were particularly noticeable whilst operating at very low torque outputs. At low torque output the torque pulsations characteristic of a single cylinder engine resulted in torsional vibrations occurring between the inertial masses of these two shafts. These torsional vibrations resulted in regular failure of the key in the power-output coupling, thus disrupting the test process.

The details of these failures and corrective action taken are discussed together with the preliminary tests in Appendix C.

CHAPTER SIX

EXPERIMENTAL RESULTS

The objective of the experimental work was to obtain fuel consumption figures for the Otto-Atkinson engine, operating in the part throttle - full stroke mode and operating in the full throttle - part stroke mode. In this way a comparison could be made between the two modes of load control. Any reduction in fuel consumption as a result of the reduced pumping losses, reduced friction and improvement in thermal efficiency of the Otto - Atkinson cycle could also be quantified. The test results are tabulated in appendix D.

For the sake of comparison the experimental results were reduced to specific fuel consumption (SFC). SFC is defined as the mass of fuel consumed per kilowatt hour (g/kW-hr). Since the fuel consumption was measured volumetrically, the density of the fuel was required; this was taken as 730 kg/m^3.

6.1 FUEL AIR RATIO CORRECTION

It is known that the fuel-air ratio has an effect on the efficiency and thus also the SFC. It was thought that the pulsations, to which the carburettor is exposed during wide open throttle operation, would have an effect on the fuel-air ratio and so also on the SFC. For this reason it was necessary to normalize the SFC results to stoichiometric fuel-air ratio. To do this the fuel-air ratio for each test condition was determined from the exhaust gas analysis and this was used to adjust the measured SFC.

6.1.1 Fuel-air ratio calculations

The Orsatz Apparatus rendered the dry volume fraction of CO, CO_2 and O_2. The following chemical equation defines the fuel-air mixture relationship to the combustion products (ϕ is the air-fuel ratio):

$$C_8H_{17.8} + \phi\,(O_2 + 3.76\,N_2) \longrightarrow a_1\,CO_2 + a_2\,H_2O + a_3\,N_2 + a_4\,CO + a_5\,O_2$$

Assuming zero O_2 under rich conditions and zero CO under lean conditions, the constants a_1 to a_5 were solved in terms of ϕ and related to the volume percentages. The results of these calculations are plotted in figure 23.

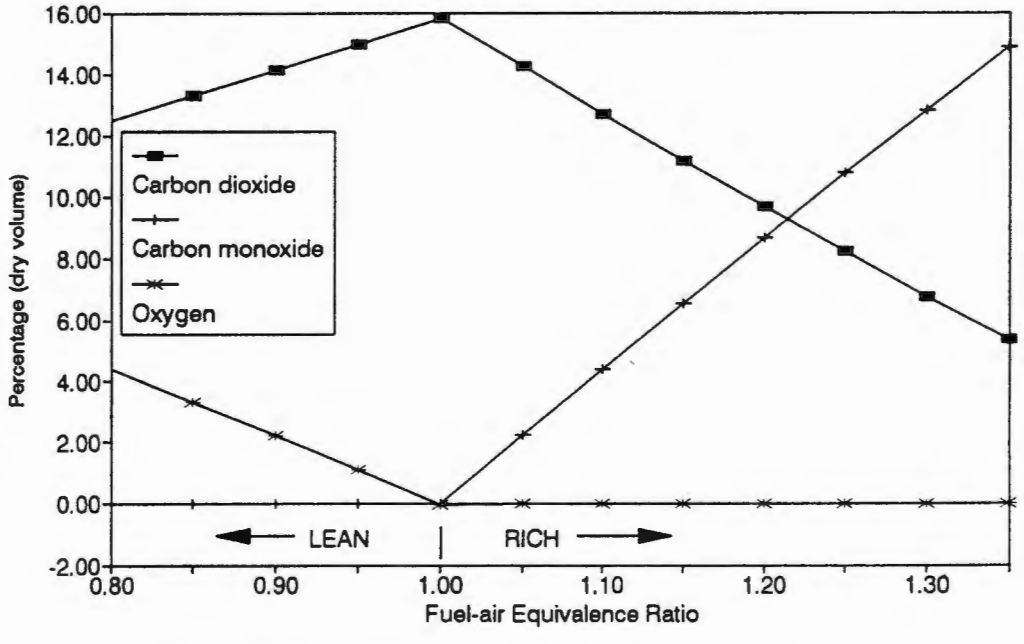

Figure 23. Determination of Fuel-Air Ratio from the Combustion Products

All of the experimental gas samples indicated that the carburettor was operating rich. The low percentage O_2 present was assumed to be due to incomplete combustion and possibly entrapment of ambient air in the Orsatz Apparatus. However, as the percentage O_2 remained relatively constant, it was ignored. The percentage CO and CO_2 were used independently to calculate the fuel-air ratio and the average of these two results was taken as the average fuel-air ratio for each sample.

6.1.2 SFC correction factor

The effect of fuel-air (F/A) ratio on efficiency is well documented in the literature. Data collected from several sources was plotted and a best fit curve of this data was made. Figure 24 is a plot of the efficiency correction factor, normalized for stoichiometric, against equivalence ratio (F/A ratio ÷ stoichiometric). From this curve, the SFC correction factor was established for each test result. This was used to correct all the SFC results to stoichiometric F/A ratio.

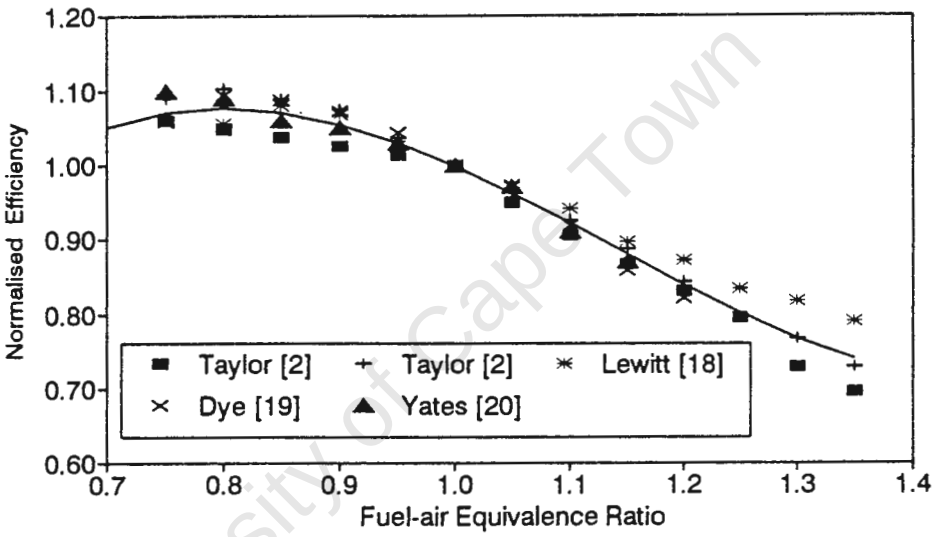

Figure 24. Efficiency Correction Factor against Equivalence Ratio

6.2 THEORETICAL FIT OF EXPERIMENTAL DATA

Figure 25 shows the corrected experimental data that was obtained from the tests. The difference between the trends of the part stroke and part throttle modes is not readily identifiable from figure 25. The clarity of this figure was improved by fitting curves to the experimental data. Due to difficulties experienced in operating at very light loads in the part stroke mode, no data below a torque of 5.5 Nm was available. To investigate engine performance at lighter loads it became necessary to extrapolate the test data trends to these torques. However, this practice only yields accurate results if the curve fitted to the data has the correct mathematical form.

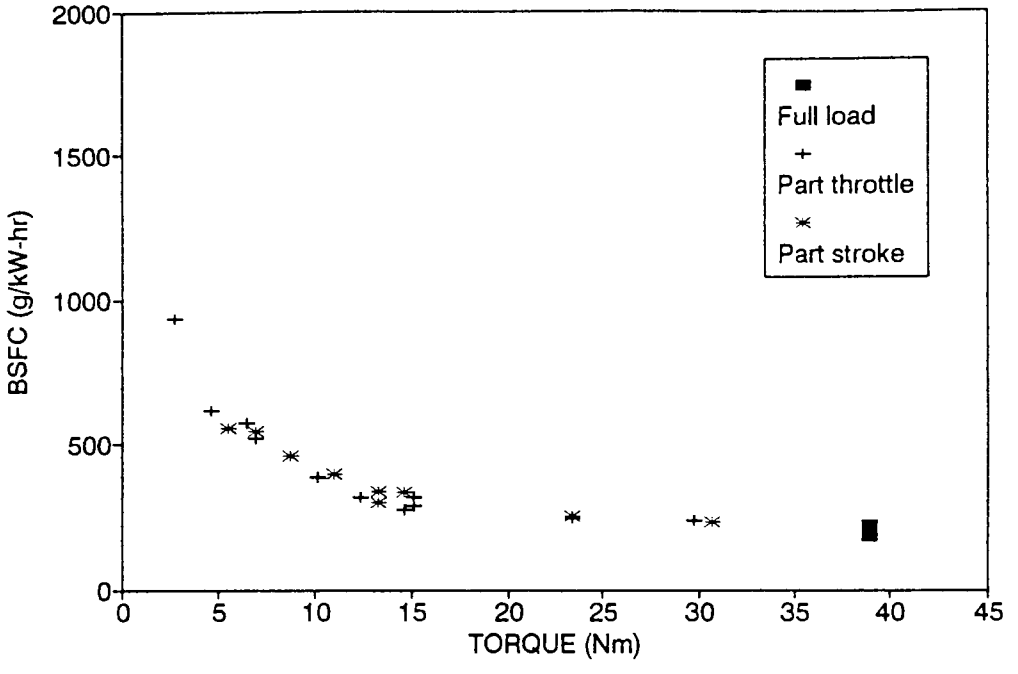

Figure 25. Measured Specific Fuel Consumption against Torque

6.2.1 Determination of the correct form for the regression curve

For the fit to be correct it was necessary that SFC be related to output torque, taking into consideration the effects of friction and pumping losses.

By definition, $$SFC \propto \frac{\text{fuel consumption}}{\text{output torque } (T_o)} \quad \text{(at constant speed)}$$

and $$\eta_i \propto \frac{\text{indicated torque } (T_i)}{\text{fuel consumption}} \quad \text{(at constant speed)}$$

therefore $$SFC \propto \frac{T_i}{T_o \, \eta_i}$$

But $T_i \propto IMEP = \rho_i . e_v . F/A . Q . \eta_i$ [2] ..... (1)

therefore $SFC \propto \frac{\rho_i . e_v . F/A . Q}{T_o}$ ..... (2)

e_v, F/A, and Q are all assumed constant

and due to manifold vacuum effects,

$$\rho_i = \text{constant} - f(T_p)$$

$$\propto 1 - k_1(T_p) \qquad \text{where } T_p = \text{pumping torque}$$

therefore Eq.(2) simplifies to,

$$SFC \propto \frac{1 - k_1(T_p)}{T_o} \qquad \text{..... (3)}$$

Also, it is known that η_i decreases with increasing pumping torque. As a first approximation the relationship was taken to be linear,

$$\eta_i = \text{constant} - f(T_p)$$

$$\propto 1 - k_2(T_p)$$

therefore Eq.(1) can be written as,

$$T_i \propto (1-k_1 . T_p) . e_v . F/A . Q . (1-k_2 . T_p)$$

or simply $T_i = AT_p^2 + BT_p + C$

also, by definition:

$$T_o = T_i - T_p - T_f$$

Assuming T_f constant at constant engine speeds and grouping terms:

$$T_o = AT_p^2 + B'T_p + C' \qquad \text{..... (4)}$$

where prime (') denotes redefined constants.

To a first approximation, the T_p^2 term can be considered the dominant term, thus Eq.(4) can be rewritten as:

$$T_p \cong A'\sqrt{T_o} + C' \qquad \text{..... (5)}$$

substituting Eq.(5) into Eq.(3) gives:

$$SFC \propto \frac{A'\sqrt{T_o} + C'}{T_o}$$

but $$\frac{\sqrt{T_o}}{T_o} = \sqrt{T_o}$$

therefore $$SFC = A'\sqrt{T_o} + \frac{C'}{T_o} \qquad \text{..... (6)}$$

Equation (6) gives the theoretically correct form of the regression for the SFC as a function of output torque.

Figure 26 shows the experimental results along with the regression of equation (6). From this figure the trends can clearly be seen. It is also evident that the regression was accurate.

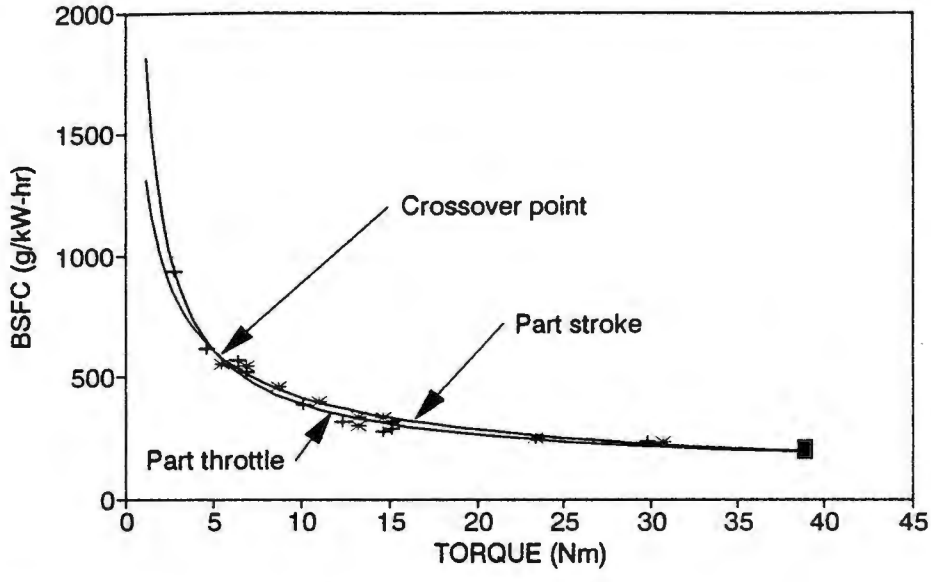

Figure 26. Measured Specific Fuel Consumption against Torque Theoretical Fit included

For ease of comparison figure 18 is repeated below. From these two figures it is apparent that the SFC against torque relationship predicted by the thermodynamic simulation is not reflected in the experimental results. The experimental results are discussed in the following chapter.

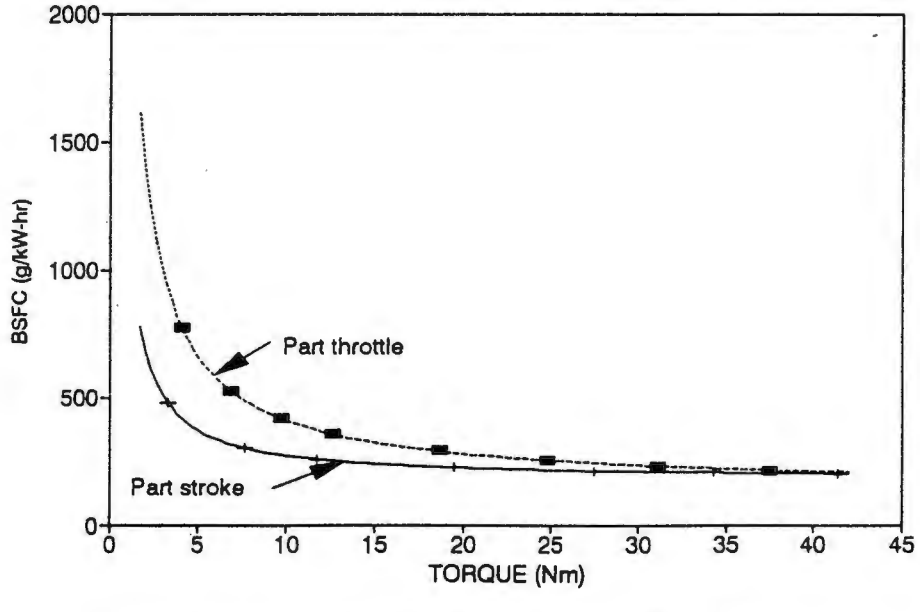

Figure 18. Predicted BSFC against Brake Torque

CHAPTER SEVEN

DISCUSSION OF EXPERIMENTAL RESULTS

The experimental results shown in figure 26 (pg.57) do not follow the theoretical expectations for the Otto-Atkinson engine.

It is known that the BSFC for spark ignition engines tends to rise as load is decreased. This trend is as a result of the pumping losses which occur at part load, and due to the increasing percentage of power being required to overcome mechanical friction. The results for throttled operation follow the general expected trends, see figure 18.

However, it was expected that the results for the variable stroke mode would, at worst, follow the throttled trend in the high torque region. This was anticipated as the reduction of friction and pumping losses were expected to be insignificant in this region. It was also expected that the absence of pumping losses, which cause the BSFC of the throttled tests to rise, would result in the part stroke curve remaining substantially lower than the throttled curve until light loads were approached where the BSFC rises as a result of the friction accounting for an increasing portion of the power produced. A reduction in stroke also results in a reduction in friction, further tending to counter a rise in BSFC in the mid range. This trend was also predicted by the thermodynamic simulation of the cycle, discussed in Chapter 3. From figure 26 it is apparent that the high and mid range operation is exposed to losses that were not anticipated. These losses are only overcome in the low torque range where the absence of pumping losses dominates. This results in the crossover of the two trends bringing the part stroke curve below the part throttle curve.

Below is a graphical representation of the difference between the SFC of the variable throttle operation and the variable stroke operation expressed as a percentage of variable throttle SFC. From this figure it is evident that the variable stroke operation only shows an advantage at a torque output below 5 newton metres, which is approximately 13 percent output. At a torque output

of 1.8 newton metres, which is approximately 5 percent output, the advantage is nearly 20 percent. This is in the region of the expected fuel efficiency gains, however, this gain was expected to occur at approximately 40 percent output. The possible causes of this unexpected trend are discussed below.

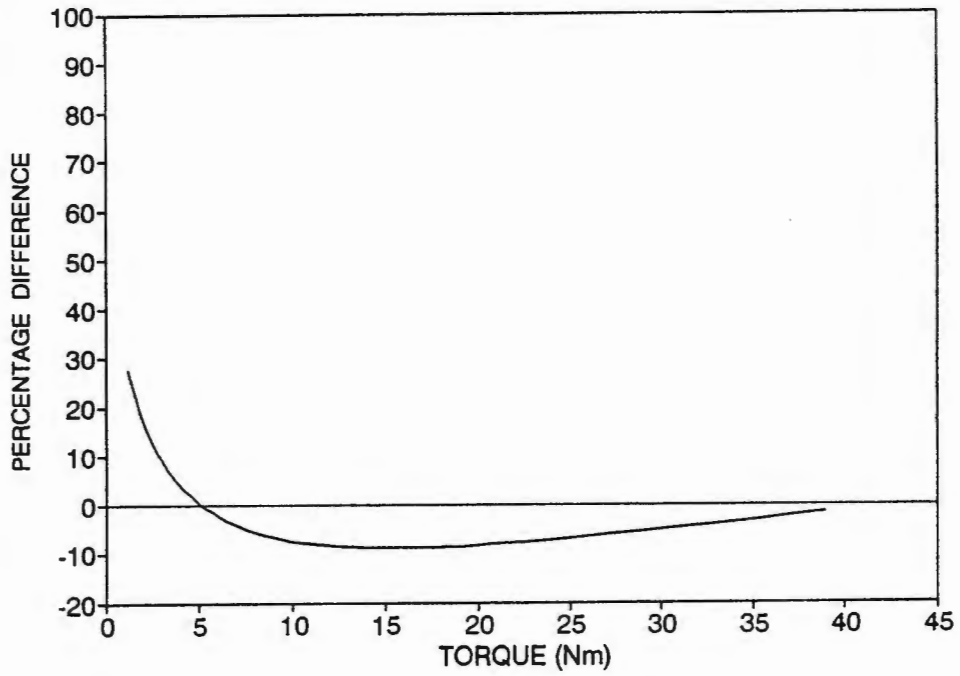

Figure 27. Percentage Difference in SFC
Variable Throttle minus Variable Stroke

7.1 FACTORS AFFECTING EFFICIENCY

7.1.1 Friction characteristics

Friction was considered as a possible cause for the dissapointing performance. The friction tests were run up to a speed of 1800 rpm. (due to equipment limitations). There is the possibility that the friction at the test speed of 2800 rpm no longer exhibits the trends determined at speeds below 1800 rpm. However, any changes would be exhibited in both the variable throttle and the variable stroke modes.

The likelihood of this characteristic changing under load was considered, but it was thought that any such change would be minimal. However, as there was no way of checking this theory it was not entirely ruled out.

7.1.2 Flame speed

During the experimental work it was noted that the ignition timing required excessive advance in order to reach maximum brake torque (MBT) during the variable stroke operation. This excessively large burn angle indicated very low flame speeds.

Flame speed is primarily dependent on piston speed, pressure and fuel-air ratio. Of these the effects of piston speed are by far the most significant [1]. Increasing turbulence results in a marked increase in flame speed, and since turbulence is directly proportional to piston speed, the flame speed increases significantly with increasing piston speed. It is for this reason that most spark igniton engines only require a relatively small ignition advance for typically up to a six fold increase in engine speed. However, if the stroke is reduced, at constant engine speed, the piston speed is seen to decrease. In the range of strokes at which the tests were run, the piston speed (inlet and compression stroke) was seen to vary from 7.5 $m.s^{-1}$ down to 2.9 $m.s^{-1}$. This decrease in piston speed clearly had a significant effect on the flame speed and so also the burn angle.

A reduction in compression ratio would result in a reduction in the pressure rise due to compression, and this would also have an adverse effect on the flame speed. However, the compression ratio, although lower than desired, was kept virtually constant across the test range. Thus it was thought that this effect was insignificant.

As the experimental results had been corrected for fuel-air ratio this factor was ignored.

A large burn angle coupled with a large spark advance results in a drop in the efficiency. The major mechanism of energy loss is through heat losses to the combustion chamber and cylinder walls. This is time dependent, thus a long burn duration allows more heat transfer with a resulting drop in the efficiency.

7.2 THERMODYNAMIC SIMULATION WITH OPTIMISED BURN ANGLE

The thermodynamic cycle simulation, discussed in Chapter 3 and Appendix A, was used to investigate the effects of burn angle on the performance of the Otto-Atkinson engine. The actual ignition advances, engine speed and friction, which were determined during the various engine tests, were substituted in the simulation. The full load point was used as a reference point in order to determine the correct dimensionless constant for the heat loss coefficient, (see discussion in Appendix A). With the simulation fitted to the full load point the BSFC against brake torque relationship was investigated for; (a) the varying throttle and (b) varying stroke regimes. Figure 28 is a graphical representation of this relationship. It is evident that the trends predicted by this simulation correlate well with the experimental results (fig. 26). The BSFC and brake torque magnitudes are clearly not the same as the experimental results, however the function of the simulation was primarily to theoretically predict the expected trends. From the good correlation it was assumed that the simulation was sufficiently correct to investigate the burn angle effects.

In order to isolate the burn angle effects, the ignition advance for varying stroke was modelled to match the actual ignition advance for varying throttle. Apart from this change, the simulation was left as discussed above. Figure 29 is a plot of BSFC against brake torque, the variable throttle results remain unchanged (a), the variable stroke results were determined using the same burn angle as for the throttled tests (b). Thus the change in trend for the variable stroke tests can be attributed solely to the effects of a reduced burn angle.

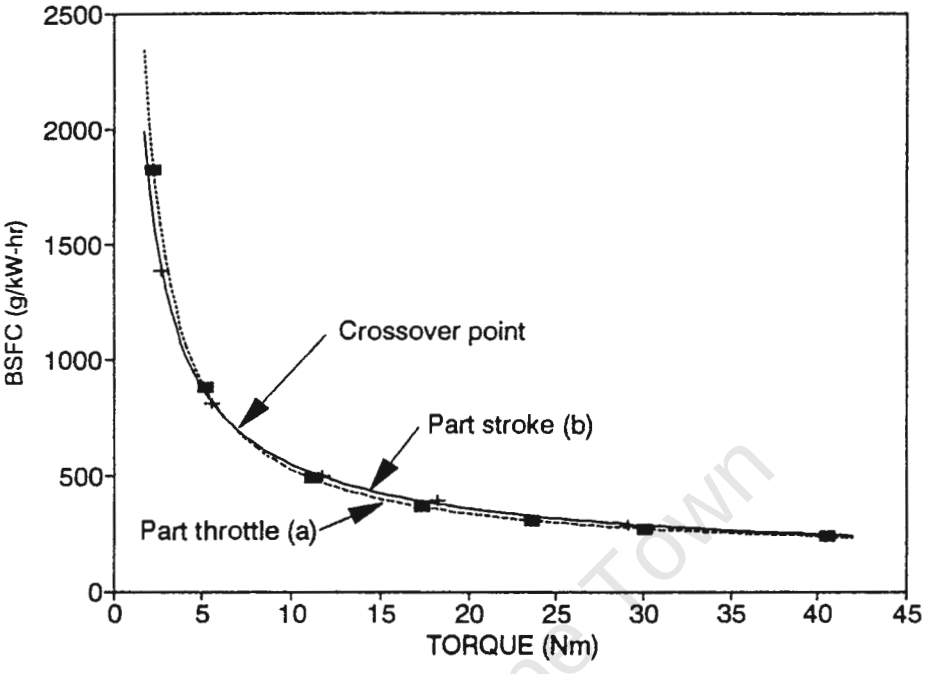

Figure 28. Predicted BSFC against Brake Torque - Actual Ignition Advance

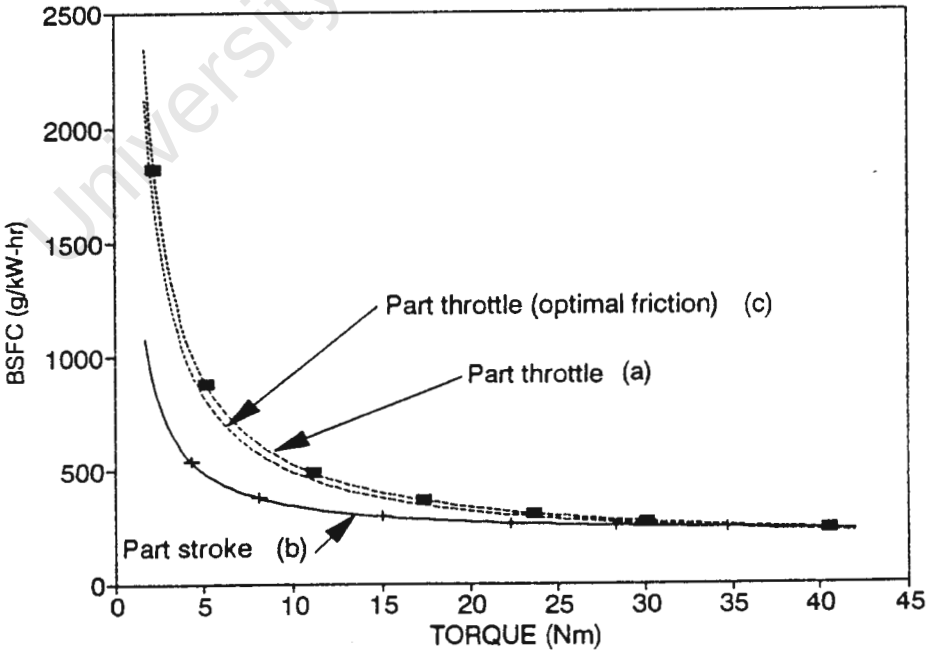

Figure 29. Predicted BSFC against Brake Torque - Ideal Ignition Advance

From the these figures, the magnitude of the burn angle effect on the efficiency of the spark ignition engine is clearly demonstrated. Accounting for the large burn angle resulted in BSFC trends that correlate well with the expected trends (fig. 18). For this reason it was concluded that the low burn speeds associated with part stroke operation were responsible for the deviation of the experimental results from the expected trends. Thus it could be assumed that any friction trends under motoring suitably reflected the friction under load.

The primary shortcoming of this variable stroke engine was thus identified as the large burn angles associated with reduced piston speed at part stroke. This difficulty associated with variable stroke engines has been reflected in the literature. Siegela recognised the need to maintain turbulence at short strokes, and it was suggested that this be could accomplished by inducing squish [8]. Pouliout et al. reported no sensitivity to ignition timing for their variable stroke engine [9]. They attributed this to the phenomenon of slow piston reversal at top dead centre, which was a feature of their mechanism. However, as their engine was not based on existing engine parts, the head and pistons were specially designed to induce maximum squish. As this thesis is the first investigation into the mechanism proposed by Yates [5], the capital outlay of designing and manufacturing a special piston and head was not warranted.

The thermodynamic model showed a significant increase in heat losses with reduced stroke. The heat losses increased from 28% at full load to 41% at 12% of full load. From these results it can be deduced that much of the drop in efficiency due to large burn angle results from to increased heat loss.

As was previously discussed, any advantage which the varying stroke results show over the throttled results are not a true reflection of the benefit of Otto-Atkinson engine over the conventional throttled four-stroke engine. This is as a result of the increased friction penalty of the Otto-Atkinson engine, which is not reflected in the comparative nature of the tests. To more realistically reflect the potential benefit of the Otto-Atkinson concept, the frictional torque measured for the original (donor) four-stroke engine, was substituted in the varying throttle mode of operation. This curve is also

plotted in figure 29, as curve (c). The true potential can thus be reflected as (c) minus (b). Figure 30 is a plot of the difference in BSFC of variable throttle operation (c) minus variable stroke operation (b) as a percentage of variable throttle operation (c).

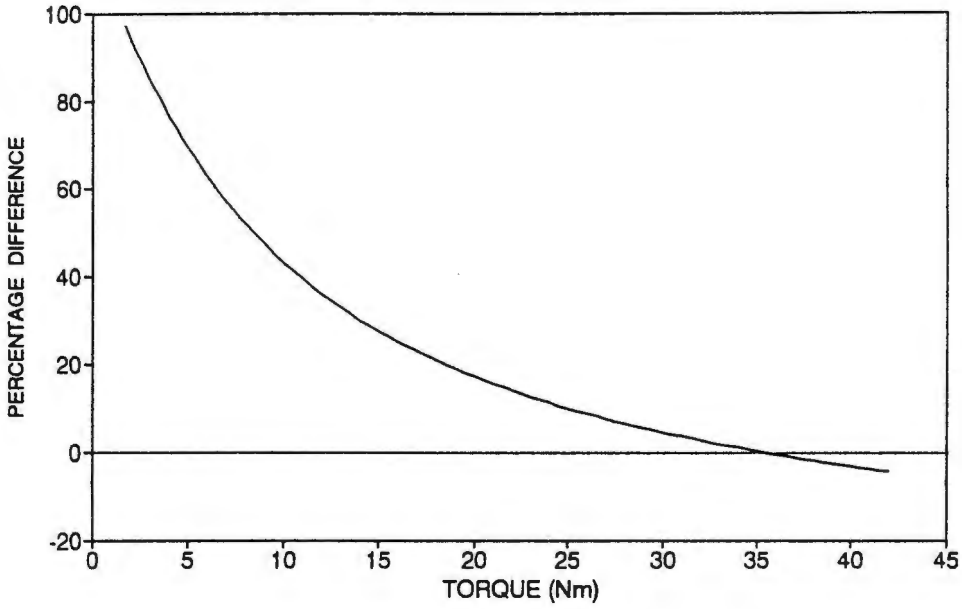

Figure 30. Percentage Difference in BSFC - (c) minus (b)

From figure 30 it is evident that the BSFC of the Otto-Atkinson engine suffers at full stroke, this is as a result of the higher friction associated with the Otto-Atkinson mechanism. As the stroke is reduced the following effects come into play:

(a) A reduction in friction with reduced stroke. This is the primary cause of the reduction in BSFC in the mid to high range.

(b) The increase in efficiency resulting from the greater expansion of the combustion gasses plays a part right through the load range, (see Chapter 3).

(c) As the output is reduced below 50% the real benefit of the variable stroke mechanism comes into play, namely, the absence of pumping losses. This results in fuel savings of approximately 30% at one third of full load.

Thus the fuel savings possible are in the region of 30% at approximately a third of full load, provided the burn angle is kept within the limits specified for efficient combustion [1]. As these savings were determined from the computer simulation it is expected that their magnitude is greater than realistically will be achieved. However, these predictions give a more representive reflection of the potential of the variable stroke method of load control than do the experimental results shown in figs. 26 and 27.

CHAPTER EIGHT

CONCLUSIONS

Based on the experimental observations, and the results and analysis thereof, the following conclusions may be drawn.

The difficulties experienced during testing, as a result of the inertial imbalance and torsional vibrations, indicate that this linkage is not a suitable means of attaining the Otto-Atkinson cycle. The inertial imbalance would require an extremely complex balancing system. The complexity and size of the linkage in its present form already severely limits any potential as a substitute for the conventional four-stroke engine and any further complexity would not be acceptable.

Testing at wide open throttle with a single cylinder engine should best be carried out with a fuel injection system rather than a carburettor. This would allow a more precise control of the fuel-air mixture. The selection of a SU carburettor was based on the need for a carburettor that would supply fuel at low air velocities without the requirement of a manifold vacuum, this requirement would be satisfied with a fuel injection system.

A factor which severely limits the potential of variable stroke engines is the extreme sensitivity of flame speed to decrease in piston speed. Turbulence could possibly be maintained by inducing squish. An advantageous side-effect of inducing squish would be that a suitable compression ratio would then also be maintained at part strokes. However, squish has the drawback of reducing efficiency due to fluid friction.

It would seem that the significant drop in burn speed and thus also efficiency with reduction in stroke has not been fully appreciated. This phenomenon requires investigation before further work is carried out in the field of variable stroke engines.

The experimental test results did not correlate well with the theoretical expectations. However, it was shown that this was due to the the large burn angles associated with the low piston speeds at part stroke operation. The thermodynamic simulation showed that the variable stroke concept has potential of fuel savings of up to 30% at a third of full load. This observation supports the theoretical expectations of fuel savings through eliminating pumping losses. Thus it can be concluded that the elimination of pumping losses still holds much potential for part load fuel savings. However, this potential can only be realised if the burn angle is kept within the limits set for maximum efficiency.

The thermodynamic simulation also showed that the drop in efficiency resulting from a large burn angle occurs primarily through an increase in the heat losses.

8.1 RECOMENDATIONS FOR FURTHER RESEARCH

This thesis has touched on some important points which warrant further research.

(a) The trends predicted by the thermodynamic simulation require experimental verification. The significant fuel savings predicted at part load are well worth investigating. Even though this prototype engine has the drawbacks of inertial imbalance and excessive size and complexity, it could still be used to further investigate burn angle effects. It is thus recommended that the piston and head be modified such that squish is induced with reducing stroke. Tests of a similar nature to the tests described in Chapter 5 should be carried out. However, it is recommended that the SU carburettor be replaced with a fuel injection system. Particular note should be taken of the ignition advance required to produce maximum brake torque. These results could then be compared with the predictions for optimal burn angle, discussed in Chapter 7.

(b) If the predicted savings are realised then further research into reducing burn angles with variable stroke engines would be warranted.

(c) Furthermore, if the predicted savings are realised then further research into alternatives to the throttle is recommended. Possibly other less complex methods of achieving a variable stroke should be considered, in particular a variable inlet stroke as this also results in gains in thermal efficiency.

(d) A final year Mechanical Engineering student at the University of Cape Town was set the task of investigating alternatives to the throttle with particular emphasis on multicylinder engines. A novel concept was recommended and deserves further investigation [22]. Bell suggested the following concept: a four-stroke engine of conventional arrangement (fixed swept volume) is fitted with a mechanism which consists of an induction cylinder through which the intake charge passes prior to entering the power producing cylinder. The stroke of the induction cylinder is varied to vary the mass of the induced charge. This would achieve the requirement of load control without a throttle. Furthermore, as the power cylinder is of fixed swept volume the burn angle problems experienced in this thesis would not feature. As the induction cylinder is only a pumping cylinder its design would not be constrained by the usual design constraints for the piston-cylinder arrangement. Thus the construction could be lightweight, unconventional materials could be used and bore/stroke ratios could be optimised for optimal size. The concept also has the added advantage of being a bolt-on mechanism which could possibly be driven off the fan belt. The potential of supercharging also exists. Preliminary analysis showed minimal friction penalties.

It is thus recommended that this concept be subjected to a full analysis. If this analysis shows the promised potential then construction and testing would be warranted.

REFERENCES

1. HAYWOOD J B, Internal Combustion Engine Fundamentals, McGraw-Hill, 1988.

2. TAYLOR C F, The Internal Combustion Engine in Theory and Practice, Volume 1, 2nd ed. M I T Press 1960, 1966 and 1985.

3. THIEL N W, "An investigation into the reduction of throttling losses in carburettor engines", The South African Mechanical Engineer, November 1968, p.101-104.

4. ROBINSON I M, "The Potential of Dissociated Methanol as a Fuel for Spark-Ignition Engines", M.Sc. Thesis, University of Cape Town, 1983.

5. YATES A D B, "The Atkinson cycle revisited for improved part-load fuel efficiency?", the South African Institution of Mechanical Engineers R&D Journal, April 1991, p.1-6.

6. SAADAWI M H, "Investigation of Cut-off and Throttle Governing of Petrol Engines", The Engineer, December 1960, p.1083-1092.

7. YATES A D B, "Throttling Loss Study", Report No INO 41/C, Energy Research Institute, April 1982.

8. SIEGLA D C and SIEWERT R M, "The Variable Stroke Engine - Problems and Promises", Society of Automotive Engineers Technical Paper Series, 780700, 1978.

9. POULIOT H N, DELAMETER W R and ROBINSON C W, "A Variable Displacement Spark-Ignition Engine", Society of Automotive Engineers Technical Paper Series, 770114, 1977.

10. MA T H and RAJABU H, "Computer simulation of an Otto-Atkinson cycle engine with variable timing multi-intake valves and variable compression ratio", Proc IMechE, Int.Conf: Combustion In Engines - Technology and Applications, May 1988, London.

11. SAUNDERS R J, "Atkinson cycle Spark-Ignition Engines", Int. J. of Vehicle Design, I A V D Congress on Vehicle Design and Components, 1984. Inderscience Enterprises Ltd. U.K. p.D1-D15.

12. BRUINS H J, "Variable Valve Timing for Cruise Efficiency", Automotive Design Engineering, January 1968, p.43-45.

13. TUTTLE J H, "Engine Load Control via Early Intake Valve Closing", Automotive Engineering, April 1982, p.51-55.

14. SAUNDERS R J and RABIA S M, "Part Load Efficiency in Gasoline Engines", p.55-82, (source unknown).

15. TAITEL Y and LURIA D, "The Otto-Atkinson Engine - A New Concept in Automotive Economy", Society of Automotive Engineers Technical Paper Series, 820352, 1982.

16. FERGUSON C R, Internal Combustion Engines - Applied Thermosciences, John Wiley and Sons Inc, 1986.

17. BORMAN G and NISHIWAKI K, "Internal-Combustion Engine Heat Transfer", Prog. Energy Combust. Sci., 1987, Volume 13, p.18.

18. LEWITT E H, Thermodynamics Applied to Heat Engines, Sixth Edition, Pitman Press, 1965.

19. DYE A, "Importance of Combustion-Chamber Turbulence shown in...New Approach to Combustion Analysis", Automotive Engineer, February/March 1985, p.32-35.

20. YATES A, "An Estimation of The Performance of Spark-Igniton Methanol Engines", M.Sc. Thesis, University of Cape Town, 1981.

21. DEN HARTOG J P, Mechanical Vibrations, Fourth Edition, McGraw-Hill Book Company, 1956.

22. BELL A J, "Atkinson Cycle Engine design", BSc. Thesis, UCT, 1991.

BIBLIOGRAPHY

1. STONE C R and KWAN E K M, "Variable Valve Timing for IC Engines", Automotive Engineer, August/September 1985, p.54-58.

2. ELROD A C and NELSON M T, "Development of a Variable Valve Timed Engine to Eliminate the Pumping Losses Associated with Throttled Operation", Society of Automotive Engineers Technical Paper Series, 860537, 1986.

3. DRESNER T L and BARKAN P, "The Application of a Two-Input Cam-Actuated Mechanism to Variable Valve Timing", Society of Automotive Engineers Technical Paper Series, 890676, 1989.

4. GRAY C, "A Review of Variable Engine Valve Timing", Society of Automotive Engineers Technical Paper Series, 880386, 1988.

5. BENSON RS and WHITEHOUSE N D, Internal Combustion Engines, Vols 1 and 2, Pergamon Press, 1979.

6. VAN WYLEN G J and SONNTAG R E, Fundamentals of Classical Thermodynamics, Third Edition, John Wiley and Sons Inc, 1985.

7. ROGERS G F C and MAYHEW Y R, Engineering Thermodynamics Work and Heat Treansfer, Second Edition, Longman Group Ltd, 1967.

8. SHIGLEY J E, Mechanical Engineering Design, First Metric Edition, McGraw-Hill Inc., 1986.

APPENDIX A

COMPUTER MODEL FORMULATION

A discussion of the computer models from the point of view of equation formation is covered in this appendix.

A-1 LINKAGE SIMULATION MODEL

This computer model was used to calculate the locus of the crank linkage and to determine the optimal configuration of the elements of the linkage. The computer model was developed with a spreadsheet package. A spreadsheet was selected as the best tool, as the model could be developed in stages with quick access to graphical representation of the data. The formulae used to determine the locus for the crank-linkage and finally the position of the piston relative to crank angle, were based on the geometrical, and thus trigonometrical, relations of the crank-linkage elements.

Initially the model was over-simplified; as the design took shape the model was updated to include the physical constraints set by the various components. Thus it was undergoing constant development. Expanding the spreadsheet to account for all the physical constraints, such that it would accurately predict the motion of the piston, resulted in some interesting and often complex geometrical relationships and equations.

The linkage was designed so that the piston motion relative to crank angle satisfied the following constraints:

(a) An inlet stroke variation from 100% down to 30% was required.

(b) The expansion stroke relative to inlet stroke may not result in expansion of the burnt gasses to a pressure below atmospheric as this would result in a negative work loop on the pressure-volume diagram.

(c) In order to maintain an acceptable compression ratio the top dead centre position of the piston must be such that the clearance volume decreases with decrease in stroke. The clearance volume constraints of the motorcycle engine head made it impossible to maintain the original compression ratio of 9:1; however, it was desirable to maintain a constant compression ratio.

This model yielded the piston motion relative to primary crank angle. It also provided predictions of the Otto and Atkinson thermal efficiency based on the compression and expansion ratios, these are discussed in Chapter 3.

In order to design the linkage components against failure due to inertial acceleration of the reciprocating parts, it was necessary to calculate the accelerations occurring at top and bottom dead centre. The linkage simulation was further developed to determine these accelerations. The distance travelled by the piston during one degree before and one degree after piston reversal was determined and this was divided by the time per degree to determine the velocity directly before and after piston reversal. The change in velocity with respect to time was then used to calculate the acceleration.

A-2 THERMODYNAMIC CYCLE MODEL

This model was used to predict the engine performance based on the thermodynamics of the internal combustion engine cycle. Of interest was the brake specific fuel consumption against brake torque relationship.

The piston motion relative to primary crank angle, produced by the linkage simulation, was used as a starting point for this model. It was desirable to divide each process into increments and consider each process incrementally. For this reason the linkage model was customised as follows: during the intake and exhaust process increments of 20 degrees were considered; to improve the accuracy during compression and expansion 10 degree increments were considered and during combustion 5 degree increments were considered.

A-2.1 Intake process

For the intake process at wide open throttle with varying stroke, it was assumed that induction occurred at atmospheric conditions. The piston motion for various slider positions was imported from the linkage model. With the piston diameter known the swept volume for the inlet stroke was calculated. Assuming ideal gas behaviour the mass of air induced was calculated with the following formula:

$$Mass_{air} = \frac{P \times V}{R \times T} \qquad \text{..... (1)}$$

The mass of fuel induced was then calculated from the fuel air ratio:

$$Mass_{fuel} = F/A_{ratio} \times Mass_{air} \qquad \text{..... (2)}$$

For part throttle simulation the piston motion for full inlet stroke was imported from the linkage model. Various manifold vacuums down to 0.55 Bar below atmospheric were investigated. It was assumed that manifold vacuum was attained by 15 degrees after piston top dead centre. The mass of air and thus the mass of fuel induced were calculated with Eqs.(1) and (2).

A-2.2 Compression process

Inlet valve closure occurs at 68 degrees after bottom dead centre of the primary crankshaft, however, it was assumed that the pressure and temperature of the trapped charge would begin to rise at approximately 30 degrees after bottom dead centre. During the inlet stroke the piston bottom dead centre advances with reduced stroke. The closing of the inlet valve at 68 degrees after bottom dead centre, relative to primary crankshaft, will thus result in some late intake valve closure as the stroke is reduced, further reducing the mass of the fuel-air charge induced.

Compression began thus at 210 degrees and the gas properties were calculated in two stages : first, an isentropic compression path expressed by the following two equations, and secondly, a heat transfer calculation, discussed in A-2.5.

$$T_2 = T_1 \times \left[\frac{V1}{V2}\right]^{\gamma-1} \qquad \text{..... (3)}$$

$$P_2 = P_1 \times \left[\frac{V1}{V2}\right]^{\gamma} \qquad \text{..... (4)}$$

T_1 and P_1 were taken as the final temperature and pressure of the previous increment. The ratio ($V1/V2$) was defined as the ratio of the volume at the previous increment to the volume at the current increment. The value for γ is based on the constant pressure specific heat (C_p) values of the cylinder contents, these are temperature dependent. Equations for C_p as a function of temperature were taken from thermodynamic tables.

A-2.3 Combustion

Combustion of the fuel-air charge begins before piston top dead centre and ideally ends between 10 and 15 degrees after piston top dead centre. The start of combustion is determined by the burn angle which is dependent on engine speed. For this reason the constant volume combustion of the Otto cycle is not an accurate assumption. A better combustion model is that of random heat release, referred to by Ferguson [16]. The portion of heat released at a given crank angle is determined by the following formula:

$$x = 0.5 \left[1 - \cos \left[\frac{\pi(\theta-\theta_2)}{\theta_B}\right] \right] \qquad \text{..... (5)}$$

A-2.5 Heat losses

To account for the heat losses to cylinder walls, a convective heat loss model proposed by Sitkei [17] was applied. This heat loss model was applied from the start of compression to the end of expansion, thus it served to partially correct the erroneous assumption of isentropic compression and expansion. The convective heat transfer coefficient was determined by the following formula:

$$h = 2.36 \times 10^{-4}(1-b)\frac{P^{0.7}C_m^{0.7}}{T^{0.2}d_e^{0.3}} \qquad \text{..... (8)}$$

where d_e is the equivalent diameter given by:

$$d_e = 4\ V/A$$

V = cylinder volume at current increment
A = heat absorbing area

The dimensionless constant **b** ranges from 0 to 0.35 depending on the type of combustion chamber, for this model a value of 0.2 was assumed. Once more data was available, **b** was altered to fit the data. Pressure (**P**) is in units of MPa, temperature (**T**) is in Kelvin and C_m is the mean piston speed in metres per second.

The heat transferred for a given increment (ΔQ_{hl}) was calculated with the convective heat transfer equation:

$$\Delta Q_{hl} = \Delta h A(T-T_w)(t) \qquad \text{..... (9)}$$

where **h** is determined from Eq.(8), **A** is the heat absorbing area, **T** is the gas temperature for the current increment, T_w is the wall temperature and **t** is the time duration of the current increment.

The change in temperature due to heat losses was calculated using the same formulae as for heat added during combustion. In fact, the heat transferred (ΔQ_{hl}) was added to the heat added during combustion (ΔQ_c) to give ΔQ_T. Eqs.(6) and (7) were then applied with ΔQ_T being substituted for ΔQ.

These processes modelled the complete cycle and thus rendered the final pressure relative to swept volume for each increment. This pressure-volume relation was then plotted on a pressure-volume (PV) diagram.

A-2.6 Performance calculations

The nett indicated work is equal to the area of the PV diagram. For sufficiently small increments this can be approximated by summing the incremental indicated work:

$$W_{ind} = \sum (P\delta V) \qquad \text{..... (10)}$$

where **P** is the average pressure for the given increment and **δV** is the change in volume occurring in that increment.

Taking **P** as absolute pressure, it will always be positive. During intake and expansion the δV term will be positive and therefore produce positive work. During compression and exhaust the δV term will be negative and will produce negative work.

The nett indicated work was divided by the time for one cycle, (two revolutions of the primary crankshaft), yielding the nett indicated power, from which the nett indicated torque was calculated (Power = Torque × ω). In order to predict the relationship of brake specific fuel consumtion (BSFC) to brake torque, the brake torque and power were required. The brake torque is related to the indicated torque by the following formula:

$$T_b = T_i - T_p - T_f \qquad \text{..... (11)}$$

where T_b is the brake torque, T_i the indicated torque, T_p the pumping torque and T_f the friction torque. However, nett indicated torque takes the pumping torque into account thus Eq.(11) is reduced to:

$$T_b = T_i - T_f \qquad \text{..... (12)}$$

Thus to calculate the brake torque the friction torque was required.

As the friction torque had to be determined from the test engine, this was not available until the engine was completed. At this point the cycle predictions were made based on an assumed frictional torque of 15% of indicated torque at full load. These are discussed in Chapter 3.

Once the engine had been constructed friction tests were run, which are discussed in Appendix C. From these tests a three dimensional relationship was developed with friction torque as a function of engine speed and slider position. The preliminary tests determined a suitable test speed. At this test speed the friction torque was calculated and the brake torque determined from Eq.(12). Figures of the predicted BSFC against brake torque were produced. A discussion and comparison of these predictions with the experimental engine performance are covered in Chapter 7.

APPENDIX B

COMPONENT DESIGN

The concept formation of the Otto-Atkinson engine is covered in Chapter 2. Discussion of the overall design is covered in Chapter 4. The design of the components of the linkage mechanism and accessories is detailed in this appendix. Design drawings for the various components can be found in Appendix E.

To minimise design and manufacturing costs a four-stroke 500 cubic centimetre motor cycle engine was purchased, from which many necessary components were sourced. As the Otto-Atkinson linkage requires two crankshafts, a second crankshaft and conrod were also purchased.

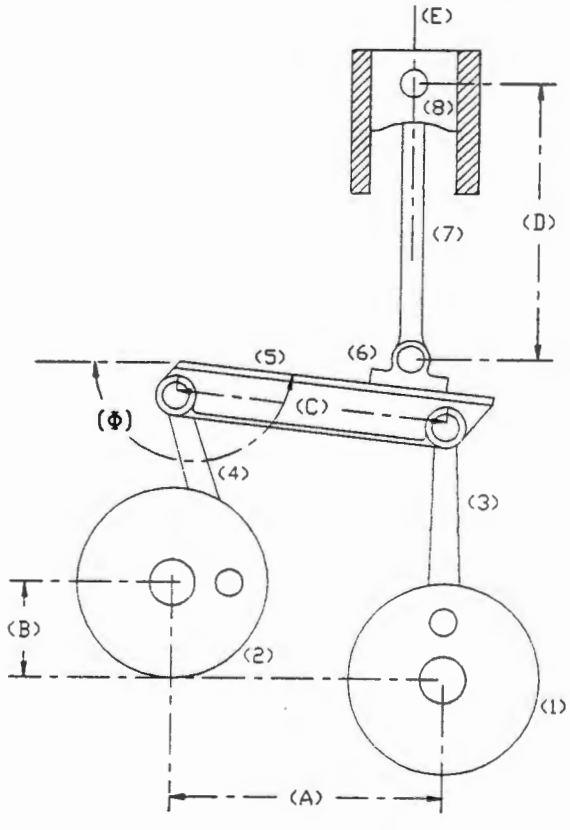

Figure B-1. The Otto-Atkinson Linkage

A computer model was set up to determine the optimal configuration of the elements of the linkage. The components sourced from the base engine were: the two crankshafts (1,2), two conrods (3,4), and the piston (8), see figure B-1. The following parameters were determined through the computer model: centre distance between the primary and auxiliary crankshafts (A), the vertical offset of the auxiliary crankshaft (B), the centre to centre length of the link (C), the offset angle of the link (Φ), the length of the piston rod (D), and the offset of the line of motion of the piston (E). The final configuration is tabulated in table B-1.

Centre distance	(A)	200 mm
Vertical offset	(B)	69.5 mm
Link length	(5)	200 mm
Piston - rod length	(7)	200 mm
Piston centre - line	(C)	25 mm
Link Angle	(Φ)	174 deg.

Table B-1. Summary of final configuration.

B-1 CALCULATION OF THE FORCES INVOLVED

The linkage components are exposed to two principal forces: gas pressure forces acting down on the piston and inertia forces due to the acceleration of the reciprocating parts.

The gas pressure was estimated by modelling an idealized thermodynamic cycle for the engine [2]. Initial pressure and temperature were taken as 1 bar and 20 $^{\circ}$C respectively. A compression ratio of 9:1 was used, this was the compression ratio of the standard motor cycle engine. Isentropic compression and constant volume heat release were assumed and combustion heat losses were estimated as 10%. The calculations resulted in a pressure of 50 bar. With the area of the piston known, the peak gas pressure force on the piston was determined as 30 kN.

The inertia forces are dependent on the acceleration of the reciprocating parts. For pure sinusoidal motion, the maximum acceleration occurs at the top and bottom dead centre positions and is determined by the following equation:

$$\text{inertial acceleration} = r(\omega)^2$$

where r = radial offset (m)

ω = radial velocity (rad/sec)

Due to the unusual motion of the linkage, the piston motion is not pure sinusoidal. For this reason the maximum acceleration had to be determined with the aid of the computer linkage model. Time increments spanning one crank-angle degree before and after piston reversal were considered and the velocity change across the two time increments rendered the acceleration. This procedure was repeated for top and bottom dead centre. A maximum engine speed of 6000 rpm was considered and this resulted in a maximum acceleration of 23000 ms^{-2}, occurring at top dead centre. With the maximum acceleration known, the relevant inertia forces in the linkage were calculated by multiplying the acceleration by the reciprocating mass under consideration.

These forces were used in the designing of the following components: piston connecting rod (fig. B-1(7)), cross link (5), slider (6) and slider adjusting mechanism.

B-2. MATERIAL SELECTION

Consideration of the forces to which these components would be exposed indicated that a material having the properties: high toughness, high UTS and good fatigue resistance would be required. Other factors to consider were possible distortion during machining and the effects of stress relieving and surface hardening. The material chosen for these components was a Bohler steel V155. This material has a UTS of 1200 Mpa, a yield stress of 800 Mpa and a Rockwell C hardness of 32, before surface hardening.

B-3 DESIGN OF THE LINKAGE COMPONENTS

B-3.1 Piston connecting rod

Design considerations : The length of the connecting rod had been determined by the computer model. The upper boss had to satisfy the constraints set by the piston and gudgeon pin, the lower end was designed in conjunction with the slider.

The most significant force acting on the conrod was the gas pressure force. At low engine speeds the countering inertia force would be negligible and thus it was evident that the piston connecting rod had to be designed against failure in buckling. An I-beam section was selected. Working within the design constraints and considering the buckling forces, an I-beam section of 20mm by 16mm with a webb of 6mm was calculated. The gudgeon pin bosses were designed to withstand failure in tension. For this the inertial forces were considered. The conrod was designed symetrically thus it was only necessary to consider the lower boss, which is exposed to the greater inertial mass and so also the greater inertial forces.

Phosphor-bronze bushes were press fitted into the bosses. These were toleranced to allow an easy running fit with the gudgeon pins. Lubrication passages were drilled through the boss to insure sufficiant lubrication of the gudgeon pin - bush interface.

B-3.2 Cross-link

Design considerations : The length of the cross-link had been determined from the computer model. The shape and cross-sectional dimensions were subject to the following design considerations:

(a) The link required freedom to tilt to a angle of 45 degrees.

(b) As the link added to the reciprocating mass it was desirable to keep the mass at a minimum.

(c) The crankshaft bearing spacing, and thus the width of the crankcase, placed a restriction on the width of the link.

(d) A criterion of the design is that the slider be adjustable whilst the motor is operating. To satisfy this condition hydrodynamic lubrication must be maintained throughout the cycle, which places a restriction on the minimum bearing surface area.

(e) The integration of the slider and the link had to allow motion along the link (d) but not allow motion in the plane perpendicular to the link, thus a guide rail for the slider was required.

Initially a circular section was considered for the link, see figure B-2. This introduced a serious difficulty as the condition could exist where the gas pressure forces tend to cause the slider to rotate about the link. This was clearly unacceptable. A rectangular cross-section was then considered as this solved the abovementioned difficulty. However, this did not fully satisfy the space and freedom of motion constraints (b,c). This led to the consideration of two parallel rectangular sections. The freedom of motion and space constraints were satisfied by this configuration. However, the rigidity to mass ratio was not optimised. The final configuration was that of two parallel I-beam sections with the slider running on top. The two I-beam sections created a channel which restricted the slider motion to motion parallel to the link, see figure B-2. This satisfied all the design considerations.

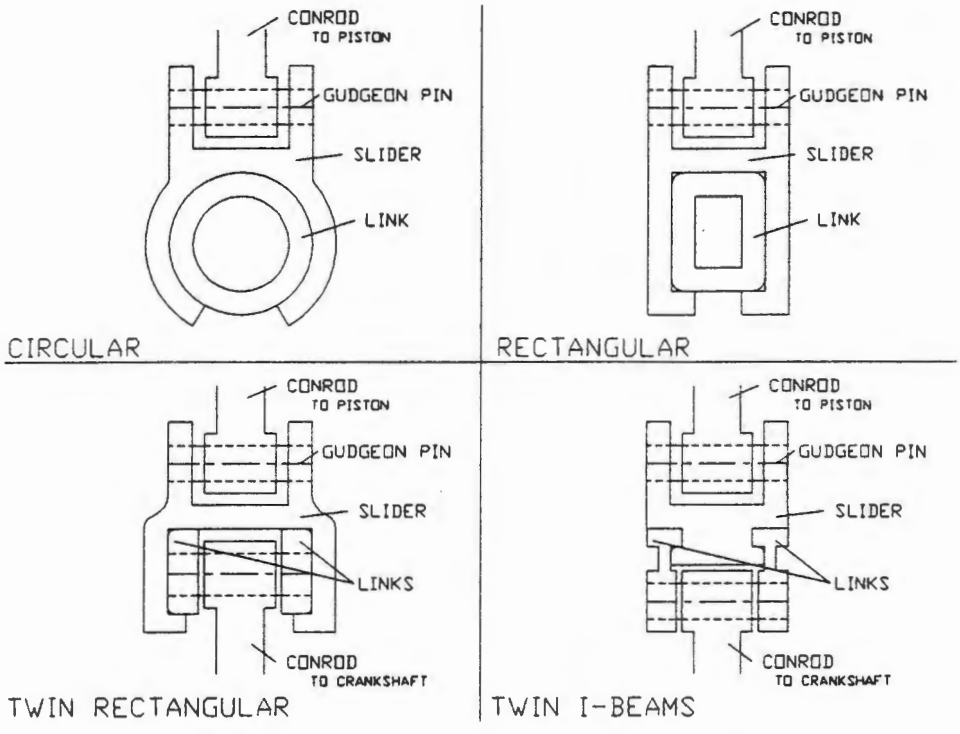

Figure B-2. Cross Section of Links and Slider

Accurate spacing and parallelism of the links was assured by a spacer block to which both links were fastened with cap screws. The gudgeon pin lugs were designed with a push fit for the gudgeon pins. As the conrods were bushed, this assured that the gudgeon pins would not rotate in the links and that rotation would occur between the conrods and the gudgeon pins. The gudgeon pin of the auxiliary crank was secured by circlips. An important consideration here was that the gudgeon pin did not extend beyond the outer edge of the links. This was to avoid fouling with the adjusting mechanism control arms. Thus the links were machined with a recess for the circlips. The gudgeon pin of the primary crank extended beyond the links to allow location in the small end guide slider blocks. The slider blocks were located in guides in the crank case and insured that the motion of the primary crank small end remained linear at all times. As the slider blocks were not bored right through, the gudgeon pin was effectively restricted from motion parallel to its axis.

The link is loaded in bending, with the extreme condition being that of a centrally placed load. The calculations showed that the greater of the two forces was the gas pressure force acting down on the link. Due to the inertial forces occurring at top dead centre, which act upwards, fatigue under cyclic loading had to be considered. The occurrence of failure in shear at the gudgeon pin boss was also considered. Working within the design constraints and taking the cyclic fatigue loading into consideration, an I-beam section of 45mm by 17mm with a 3mm webb was calculated.

To avoid stress concentrations and the resulting risk of fatigue failure, all corners were radiused. To minimise wear and friction on the sliding surfaces, surface hardening and grinding of these surfaces was stipulated.

B-3.3 Slider

Design considerations : The slider was designed in conjunction with the piston connecting rod and the cross-link, thus the slider was subjected to the design constraints of these two components. As the slider added to the reciprocating mass, it was desirable to keep its mass at a minimum. To avoid excessive wear of the sliding surfaces, surface hardening had to be considered.

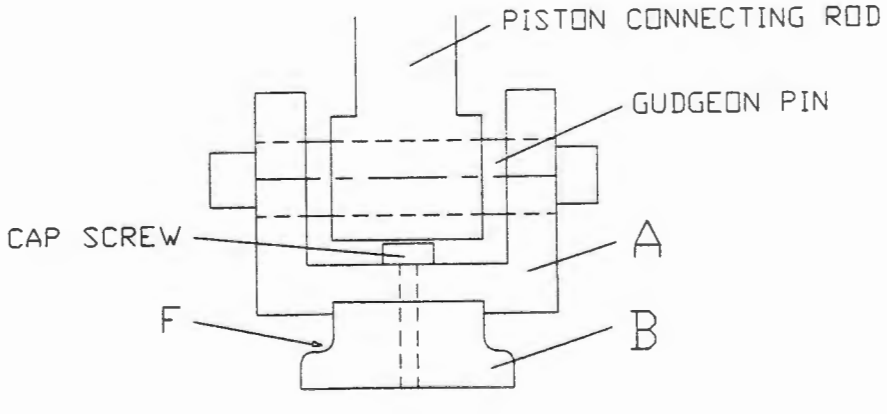

Figure B-3. Slider

Figure B-3 is a diagram of the slider. For machining purposes the slider was designed in two pieces (A) and (B). Accurate location of B in A was by a spigot. The two pieces were held together with M8 high tensile cap screws. The gudgeon pin lugs were designed with a press fit for the gudgeon pins. In this way the piston connecting rod would rotate on the gudgeon pin and not the gudgeon pin in the slider. The gudgeon pin was designed with extensions on which the control arms from the adjusting mechanism were located. The control arms were restricted from separating by the crank case walls. As the gudgeon pin was stepped, it in turn was held in place by the control arms.

The width of the slider was set by the width of the links; the length was sized to insure sufficient bearing area. The gudgeon pin lugs were designed to withstand the tensile forces resulting from the inertia of the piston, connecting rod, gudgeon pin and control arms. The T-piece (B) and cap screws were designed to withstand the additional inertial loading of part (A). Fatigue failure was also considered, particularly for the cap screws and the T-piece at the corner (F). This corner was radiused to reduce the likelihood of fatigue failure and also to reduce friction with the links.

B-3.4 Adjusting mechanism

In order to satisfy the design criterion that the slider be adjustable under operating conditions, it was necessary to design a mechanism to set and adjust the slider position.

Design considerations : The primary consideration was that the adjuster allow the position of the slider to be changed whilst the engine was running. The force required to move the slider under operating conditions also had to be considered.

It was decided to use a mechanism similar to a nut and bolt, with the bolt mounted and free to rotate in the crankcase and the nut free to move up and down the bolt, see figure B-4.

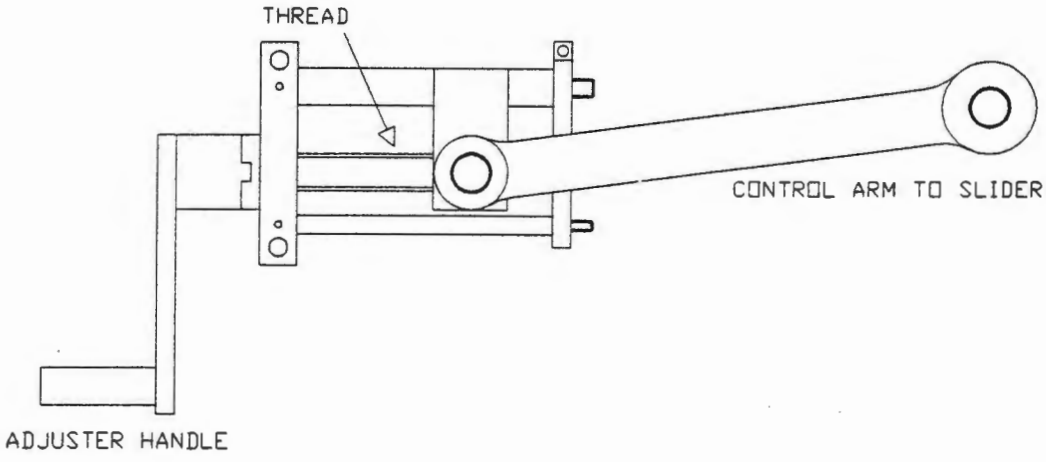

Figure B-4. Adjusting Mechanism

The adjuster block, represented by a nut, had pins on each side, on which the control arms were located. The control arms were also located on the gudgeon pin in the slider. Thus, as the bolt was rotated, the slider would be either pushed or pulled up and down the links. As the links are not always in a horizontal position, the control arms had to be able to withstand the inertial loading created by the cumulative mass of the piston, connecting rod, slider and gudgeon pin. These tensile or compressive forces had to be transmitted to the nut and thus also to the bolt by the control arms.

To insure that rotation of the threaded bar, represented by a bolt, could occur under axial loading, it was carried in thrust bearings. These bearings were located in plates which were mounted between the crank case side walls. A crank handle was fitted to the end of the bolt. The pitch of the thread was designed to withstand the above mentioned loading while a secondary consideration was a suitably fine pitch to allow accurate adjustment of the slider. A pitch of 2.5 mm

satisfied the design criteria. The position of the nut and therefore the position of the slider could be calculated from the number of turns of the crank. However, a hole was made in the adjusting mechanism which allowed a pin to be inserted to indicate slider position.

The control arms are exposed to pure tensile or compressive forces. As they add to the reciprocating mass, it was imperative to keep them as light as possible. For this reason steel was ruled out as a possible material. The size constraints were not as tight as for the links, thus aluminium alloys were considered. The material selected was an aircraft aluminium alloy (7075). This material has a relatively high UTS (565Mpa) and a low mass/volume ratio. However, being an aluminium alloy, it has bad fatigue properties, thus measures were taken to avoid fatigue failure. To insure that no surface flaws existed it was specified that the components be hand finished and polished.

Bronze bushes were press fitted in the bosses to allow free rotation of the links at the slider and adjuster block.

B-4 INTEGRATION OF THE ENGINE COMPONENTS

The following parts of the engine had to be integrated with the Otto-Atkinson linkage and adjuster to form an integrated unit:

(1) Crankcase
(2) Power-out shaft
(3) Auxiliary crank drive
(4) Cam shaft drive
(5) Points breaker drive and placing
(6) Oil pump drive and placing
(7) Lubricant distribution
(8) Cylinder and head
(9) Carburettor and exhaust

(1) Crankcase: A new crankcase had to be made to accommodate the Otto-Atkinson linkage and support the bearings of the two crankshafts and the power-out shaft. The crankcase took the form of two parallel mild steel plates of 19mm thickness, these plates were fixed accurately by three spacing blocks. A top deck of 19mm mild steel was bolted to the top edge of these two plates. Lugs for the engine mountings were made at each corner of the top deck, the crankcase was thus hung from the top deck. Recesses for the bearings and primary crank small end guides were machined in the parallel plates. To avoid wear of the crank case plates at the small end guides, gauge steel plates were fitted to line the guides. All auxiliaries were bolted on the outside surfaces of the plates. The complete crankcase assembly was then encapsulated in a sump, which was made of 3mm steel plate and was bolted to the underside of the top deck with a neopreen gasket to prevent oil leaks. The slider adjuster, the power-out shaft and the points had to be provided with access holes in the sump. To allow for these external inputs and outputs, special housings were made with oil seals and o-rings to prevent leakage.

(2) Power-out shaft: The power-out shaft was manufactured to similar dimensions as the primary shaft in the gearbox of the original engine. The material used was also V155. The power-out shaft was mounted in roller bearings, positioned between the two crankshafts and driven off the primary crankshaft using the orginal gear drive. The clutch cage was splined on the shaft. The clutch cage ring gear functioned as the driven gear. Power was transmitted via a flange which was keyed on the other end of the shaft.

(3) Auxiliary crank drive: The auxiliary crank was gear driven using the power-out shaft gear as an idler gear. A 2:1 ratio between the primary and the auxiliary crank satisfied the requirement of half engine speed for the auxiliary crank. To assure that the two cranks were perfectly in register the keyway in the auxiliary drive gear was calculated and accurately machined.

(4) Cam shaft drive: The cam shaft was chain driven off the primary crank using the original sprockets and an extended chain. Additional chain guides were added to prevent chain slap of the lengthened chain.

(5) Points breaker drive: The points breaker was gear driven using the original gear drive off the primary crank. A housing was designed to accommodate the points breaker base plate, cam spindle and mechanical advance in an oil-free environment. Because of the phenomenon of a varying top dead centre, it was necessary to have an ignition system which allowed easy adjustment of the spark advance. The plate on which the breaker points are mounted was modified, gear teeth were cut on a section of the circumference. These teeth were then mated with a spigot gear fitted on a spindle. Rotation of this spindle gave approximately 30 degrees rotation of the plate which equates to 60 degrees motion of the crankshaft. In this manner the spark advance could be varied whilst the engine was running.

(6,7) Lubrication system: The scavenging oil pump sourced from the original engine was used, and gear driven off the points breaker drive. This placed the oil pump in a fortunate position, as it was continually submerged in oil. This removed the need for priming and the risk of cavitation. A gauze mesh over the intake insured that no large particles could enter the pump. Oil was fed from the pump to the oil filter from which it went to the lubricant manifold for distribution. Oil was distributed to the two cranks and the cam shaft. The slider, adjusting mechanism and piston underside were lubricated via a spray feed. The primary crank small end guides were lubricated by a drip feed. The rest of the components were splash lubricated.

(8) Cylinder and head: The cylider block studs were mounted in the top deck of the crank case. At the base of the cylinder block copper shims were fitted; these were included to allow the compression ratio to be adjusted for testing purposes.

(9) Carburettor and exhaust: The carburettor was a SU carburettor sourced from a Mini 850cc. An SU carburettor was selected, as it satisfied the requirement of being able to supply fuel at low air velocities without a manifold vacuum being required. An adapter plate was made up to fit the carburettor to the motorcycle carburettor mounting. An original exhaust header of the motorcycle was available. This was brazed to a section of flexible steel tubing. A flange plate was brazed to the flexible tubing and bolted to the test cell exhaust system.

APPENDIX C

PRELIMINARY TESTING

Preliminary tests were run in order to check the engine for correct functioning. Failures which occurred during these tests resulted in some design changes and modifications. A reliable test procedure was established based on observations of the test parameters during these preliminary tests. Friction tests were also conducted.

C-1 INITIAL TESTING

The engine was fired up with the slider set at the maximum power setting (maximum swept volume). The carburettor and ignition settings were optimised to achieve relatively smooth operation. Vibration was immediately recognized as a major problem but this was expected as no attempts had been made to balance the increased reciprocating mass. The engine speed was varied using the throttle and for a short while a speed of 4000 rpm was investigated. The slider was then shifted towards the part-load setting (minimum swept volume), whilst the throttle was varied to maintain a constant engine speed. A position was reached where the engine was idling with the throttle fully open, this would indicate the minimum power setting of the slider. When the slider was shifted further back, (to decrease the inlet stroke further), the engine began to die, quick adjustment of the slider, (to increase the inlet stroke), kept the engine going. Thus the response to the slider position was deemed satisfactory. On returning to the full load condition the increased engine speed caused the failure of a component in the adjusting mechanism, it was thought to be a retaining circlip. The engine was immediately cut and removed from the test cell for a strip down and inspection of the failure. Due to the excessive vibrations it was also decided to balance the crankshafts before further testing could commence.

C-1.1 Failure and wear analysis

The entire engine was stripped down and inspected to ascertain the nature and cause of the failure; all parts were also inspected for wear.

The failure was, as expected, the retaining circlip in the adjusting mechanism. The inertial loading due to high engine speed with the slider at the full power setting had first dished the circlip and then popped it off. No damage was caused by either the circlip or the washer which came adrift, both items were found in the sump, intact. The auxiliary crankshaft nut was also found to have shaken loose, this was most likely due to torsional vibrations between the auxiliary crankshaft and the power-out shaft.

All surfaces exposed to wear were inspected and no signs of excessive wear were found, except for the small end of the piston connecting rod. As there was sufficient lubricant present it was thought that a piece of swarf had caused the damage. All moving parts were also inspected for sufficient lubrication and it was found to be satisfactory.

C-1.2 Damage correction and balancing

It was evident that the adjuster mechanism circlip could not withstand the inertial loading, a redesign of this item was thus required. The retaining function of the circlip was replaced by a thrust bearing. The thrust bearing was retained by a spigot and washer and an 8mm cap screw tapped into the centre of the threaded shaft of the adjusting mechanism. (See Appendix E for clarity).

To insure that the crankshaft nuts remained in place a washer with locking tabs was fitted to both crankshafts, a thread-locking compound was also applied.

A single cylinder reciprocating engine can never be fully balanced. The rotating mass component can be balanced by the fitting of counterbalance weights to the crankshaft, but the reciprocating component can not be balanced and will always result in a degree of imbalance [21]. However, to achieve an acceptable degree of balance, it is practice to add one half of the reciprocating out-of-balance-mass to the crankshaft counterbalance weights. This results in a 50% improvement in balance in the vertical plane but creates a 50% imbalance in the horizontal plane perpendicular to the crankshaft. The engine is thus left with an imbalance which is partially a reciprocating and partially a rotating mass imbalance.

Dynamic balancing of this engine, with its complex crank motion and shifting of mass from one crank to the other, as slider position is altered, would involve complexity which is beyond the scope of this thesis. It was therefore decided to attempt a static balance of the crankshafts as descibed above, in order to compensate for the increased reciprocating mass. Due to the shifting of the mass centre, with altered slider position, perfect static balance could not be attained for all conditions. The balancing was done with the slider at the *set-up* position, ie with the slider position corresponding to the cylinder centre line. As the crankshafts used in this engine had been balanced for the motorcycle engine in the standard configuration, it was necessary to take this into account when balancing the crankshafts for the additional reciprocating mass. Calculations showed that a mass of 0.545kg would have to be added to the primary crank and 0.1095kg to the auxiliary crank. This balance would result in a maximum static unbalanced mass of 0.1 kg at full power setting and 0.2 kg at minimum power setting. As these calculations were done for an engine speed of 6000 rpm, it can be expected that the minimum power imbalance would in fact be considerably lower than 0.2 kg.

Balancing masses were made up and the crankshafts were drilled and tapped; the masses were then bolted in place, see figure C-1 for clarity.

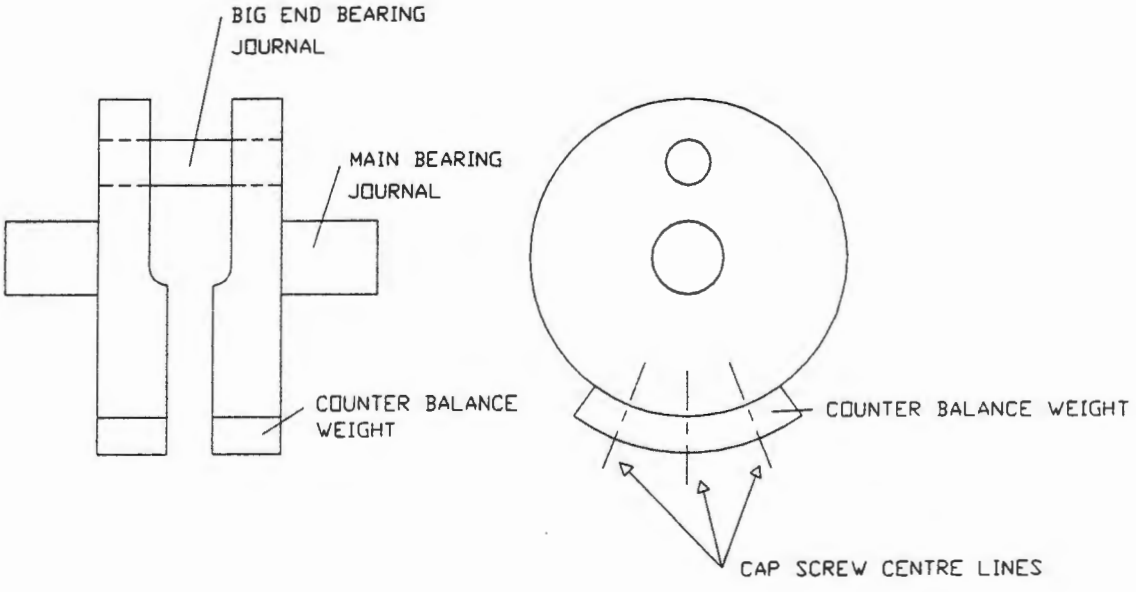

Figure C-1. Counter Balancing Masses.

C-2 SECOND PHASE TESTING

Once the engine had been reassembled the second phase of testing could begin. This began with friction tests which are discussed in section C-4 in this appendix. The engine was then refitted in the test cell.

The aim of this second phase testing was to obtain some preliminary results of the fuel consumption for varying torque. Engine speed was held constant at approximately 2800 rpm and the torque was varied first by throttle control, with the slider at the full stroke setting, then by altering the stroke by adjusting the slider position. This testing was interrupted by another failure. Although the engine continued to run, the increased noise indicated that all was not well.

The engine was removed from the test cell. As the noise was emitted from the vicinity of the adjusting mechanism, a full strip-down was necessary to ascertain the source of the noise and to analyse the failure.

C-2.1 Failure analysis

Stripping of the engine began with removal of the sump, at this point it could be seen that the adjuster mechanism was indeed the cause of the noise. The bronze insert carrying the thread had been dislodged. Further stripping required the removal of the cylinder head, barrel and piston. The piston showed signs of impact with the head and valves. As the motion of the piston had been checked prior to testing, this discovery pointed to a malfunction in the crank mechanism. Removal of the crankshaft nuts and lock washers led to the source of the problem. The tabs on the lock washers which locate in the keyway had broken off on both crankshafts. The nuts which secure the gears on the crankshafts were no longer at the desired torque. The key in the auxiliary crankshaft had sheared in half. This allowed the gear to rotate on the crankshaft, thus setting the two crankshafts out of register. This resulted in an undefined motion of the crank-linkage which caused the piston to hit the cylinder head. This motion of the crank-linkage could have resulted in inertial forces well above the design forces thus overstressing the adjusting mechanism which resulted in the failure of the bronze insert.

The mode of failure of the key, which was thought to be the cause of all the damage, was identified as fatigue. Due to the unusual motion of the two crankshafts torsional vibration occurs between the crankshaft drive gears and the power-out shaft gear. These torsional vibrations resulted in oscillating shock loading of the key which led to fatigue failure. The key under discussion was a stepped key, this step resulted in a stress concentration which would decrease the cycles to failure. Close inspection of the fragments of this key showed that the failure had indeed begun at the point identified. The key on the primary crankshaft was not stepped. Inspection of this key showed that although it had been subjected to high loads, failure of this key did not occur.

C-2.2 Damage correction

As it was felt that fault lay at the failure of the key, it was necessary to insure that a repeat failure would not occur. The torsional vibrations are a characteristic of the mechanism. They could possibly be reduced by decreasing the amount of backlash present in the gears, but this would require costly machining and time. A larger key was not possible due to size constraints of the existing crankshaft. Thus the components were redesigned to allow a standard key without a step, to be used. The lock washers were replaced with stronger ones.

For the above mentioned reason redesigning of the adjusting mechanism seemed unnecessary , thus a new bronze insert for the adjusting mechanism was manufactured. However, as a safety measure the thickness of the load-bearing lip was increased.

The piston was inspected and it was found that damage resulting from the impact with the head could be repaired by the workshop, replacement was therefore not necessary. The valves were tested and found to be leaking, this necessitated removal of the valves for straightening and regrinding of the seats.

C-3 THIRD PHASE TESTING

With the damage repaired testing continued. It was found that the ignition timing adjustment did not allow sufficient advance for maximum torque at light loads in the part stroke regime. The baseplate was removed and further teeth cut to allow rotation of 90 degrees of the baseplate, which results in 180 crank-angle degrees adjustment.

The preliminary fuel consumption results did not correlate well with the expected trends. When operating in the part stroke regime the throttle is kept fully open, this exposes the carburettor to pressure pulsations. As the stroke, and thus also piston speed, decrease, these pressure pulses will

become more apparent. The carburettor was of the SU type which would be sensitive to these pressure pulsations, resulting in fuel-air mixtures deviating from stoichiometric. This would clearly have an effect on the efficiency. Therefore it was decided to take gas samples for analysis in order to correct for changes in fuel-air ratio.

C-4 FRICTION TESTS

Prior to stripping the donor motorcycle engine friction tests were run in order to determine the relationship between friction and engine speed. These tests were then repeated for the completed Otto-Atkinson engine.

C-4.1 Test apparatus and procedure

The engine was driven by a D.C. motor. The power to this motor could be varied, thus providing variable speed. The D.C. power source was fitted with an ammeter and voltmeter registering field current and voltage. Power was transmitted by a Vee-belt and pulleys. The motorcycle engine had the driven pulley fitted to the starter shaft. On the Otto-Atkinson engine the driven pulley was fitted to the power-out flange. This drive would create some losses and the friction registered would thus include a component for the drive. However, as these tests were of a comparative nature and the same drive was used in both cases, this was not seen as a serious problem. The tests were run without inlet or outlet manifolds or the spark plug fitted. The movement of air through the spark plug aperture would also increase the power required to drive the engine. However, as mentioned above this would have little effect on the comparative results of these tests.

The motorcycle engine was motored at speeds varying from 350 to 1800 rpm. the limit on the maximum engine speed was imposed by the D.C. motor available for these tests. At each speed the field current and voltage were recorded. The test data was then used to calculate the

power required to drive the engine at each speed, the friction torque was then calculated. Figure C-2 is a plot of friction torque against engine speed. The Otto-Atkinson engine was tested for the same speed range. These tests were carried out with the slider set at the full stroke position as this condition provided similar piston motion to the motorcycle engine. The results of these tests are also plotted in figure C-2.

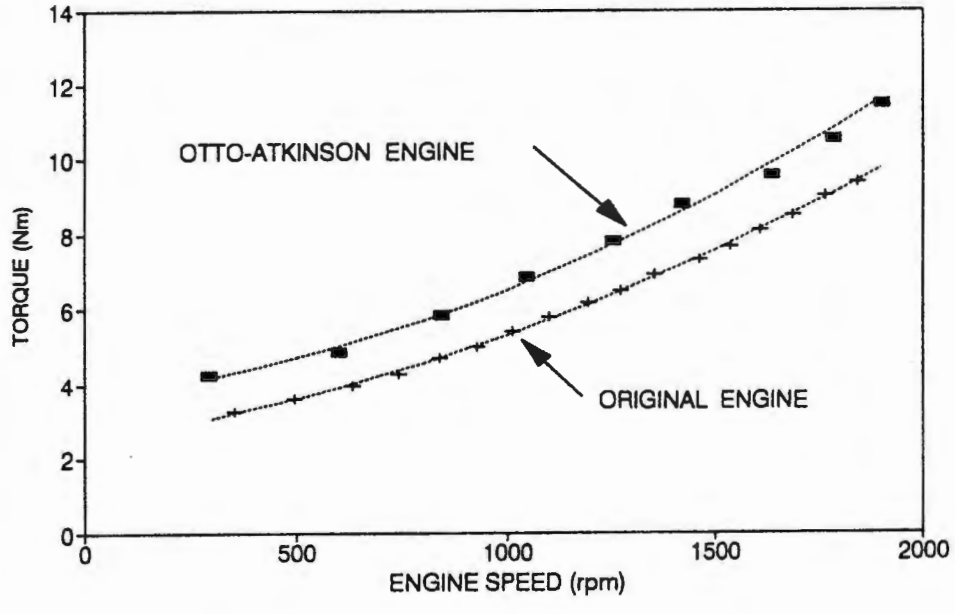

Figure C-2. Friction Torque for Varying Engine Speed

The reduction in inlet and compression stroke during part load operation of the Otto-Atkinson engine should result in a decrease in the friction. To investigate the relationship between length of stroke and friction, tests were carried out with varying strokes and the engine speed held at approximately 1500 rpm. Figure C-3 is a plot of friction torque against percentage stroke. From this figure it became apparent that the friction torque at the 65 percent stroke position was approximately equal to the friction torque of the motorcycle engine at 1500 rpm. To further investigate this observation additional tests were run on the Otto-Atkinson engine with the slider at the 65 percent stroke position and varying engine speeds.

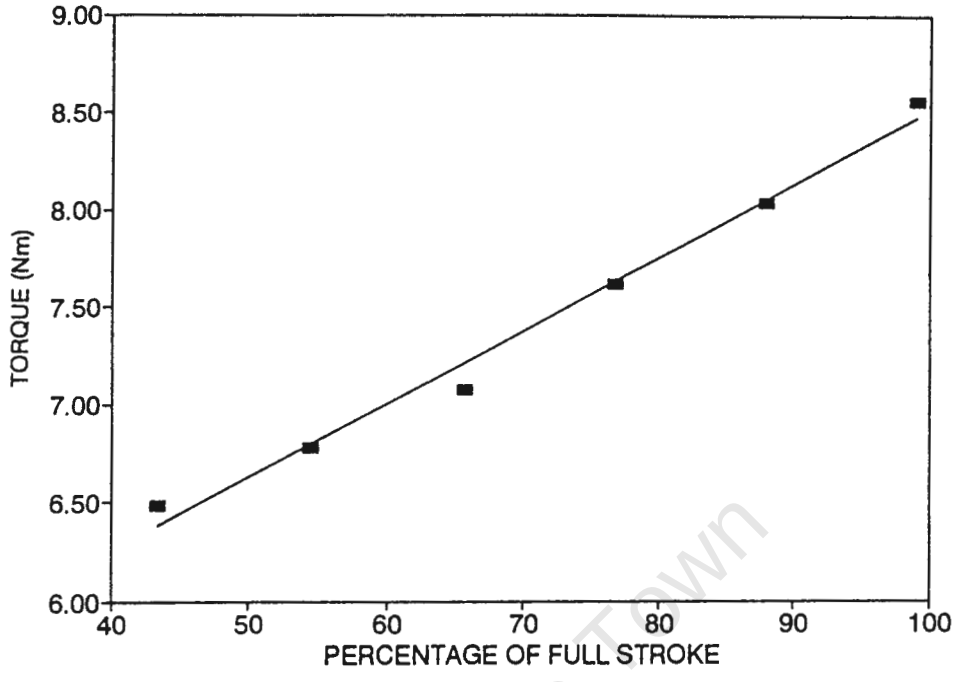

Figure C-3. Friction Torque for Various Strokes.
Otto-Atkinson Engine, speed +/- 1500 rpm.

These results were then plotted with the results of the motorcycle engine tests, see figure C-4.

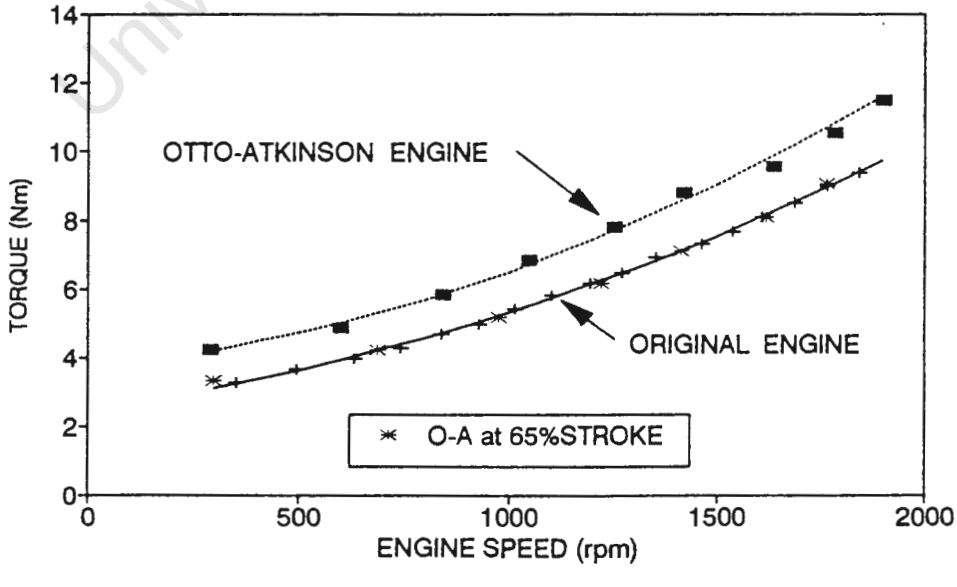

Figure C-4. Friction Torque for Varying Engine Speed.

From this figure it can be seen that the friction torque for the Otto-Atkinson engine with the slider at the 65 percent position correlates well with the friction torque for the motorcycle engine.

C-4.2 Discussion of test results

The friction torque of both engines was found to be somewhat higher than expected. This is most likely a result of losses in the D.C. motor, losses in the drive and the effort required to pump air through the spark plug aperture. However, as discussed previously these losses were approximately the same for both engines and have no real bearing to the comparative nature of these tests.

The friction torque of the Otto-Atkinson engine was higher over the full speed range, see figure C-2. This is to be expected as a result of the increase in the number of bearings, bushes and sliders making up the Otto-Atkinson linkage. However, the friction torque decreases with decrease in inlet stroke (figure C-3), and at the 65 percent position reaches similar magnitudes as the motorcycle engine, see figure C-4. It can also be deduced from these two figures that at less than 65 percent stroke the friction torque for the Otto-Atkinson engine will in fact be lower than the motorcycle engine. This is as a result of the decrease in piston ring to cylinder wall friction resulting from the decrease in stroke.

As it was the intention to test the engine at speeds exceeding 1800 rpm it was necessary to fit a curve to the friction test data and extrapolate to higher engine speeds. The percentage reduction in friction torque with reduced slider position was calculated from figure C-2. Thus at any engine speed or slider position the friction torque could be calculated.

APPENDIX D

EXPERIMENTAL DATA

The raw experimental data gathered during the fuel consumption tests is given in table D-1.

TEST CONDITION	TORQUE (Nm)	FUEL CONSUMED (ml)	TIME (s)	IGNITION ADVANCE (degrees BTDC)	FIN TEMP (°C)
Full load	38.9	93	82.6	15	119
	38.8	80	79.3	15	117
	38.6	30	25.6	15	115
	38.9	90	69.6	15	119
Part throttle	29.8	20	19.1	17	116
	23.4	20	23.8	:	117
	16.4	39	74.6	:	116
	15.1	43	69.1	:	115
	15.1	20	29.1	:	113
	14.7	44	76.1	:	115
	12.4	40	72.5	:	112
	10.1	40	72.9	:	117
	6.9	30	60.6	:	114
	4.6	20	57.4	:	113
	2.8	20	61.5	35	112
Part stroke	30.7	60	56.8	40	118
	23.4	42	42.1	55	115
	14.7	40	55.6	65	117
	13.3	39	59.2	65	114
	13.3	53	90.2	65	112
	11.0	10	15.5	70	116
	8.7	38	64.3	75	116
	6.9	10	18.4	75	113
	5.5	10	23.1	80	115

Table D-1. Experimental Data

Typical exhaust gas analysis results are given in table D-2.

Test condition	% CO_2	% O_2	% CO	Average F-A Equiv.
Full load	4.8	2.0	11.4	1.32
Part throttle	10.2	2.0	4.3	1.14
Part stroke	6.4	2.2	9.3	1.27

Table D-2. Typical Exhaust Gas Analysis Results

APPENDIX E

DESIGN DRAWINGS AND PHOTOGRAPHS

The design drawings of the components of the Otto-Atkinson linkage and specialised components are covered in this appendix. An assembly drawing of the linkage and adjusting mechanism is also included. Photographs of some of the components and of the engine in various stages of completion are included for clarity. Below follows a list of the drawings: (Please note, these drawings have been reduced and are thus no longer to scale.)

1. Connecting rod
2. Links
3. Slider
4. Adjusting mechanism
   - 4.1 Assembly
   - 4.2 Threaded and guide rods
   - 4.3 Mounting plate 1
   - 4.4 Adjuster block
   - 4.5 Mounting plate 2
   - 4.6 Control arms
5. Gudgeon pins
6. Primary crank small end guides
7. Power-out shaft
8. Points housing
9. Assembly of the Otto-Atkinson Linkage and slider adjusting mechanism

The following drawings are folded at the end of this appendix.

10. Crankcase plate 1(a)
11. Crankcase plate 1(b)
12. Crankcase plate 2(a)
13. Crankcase plate 2(b)
14. Crankcase top deck

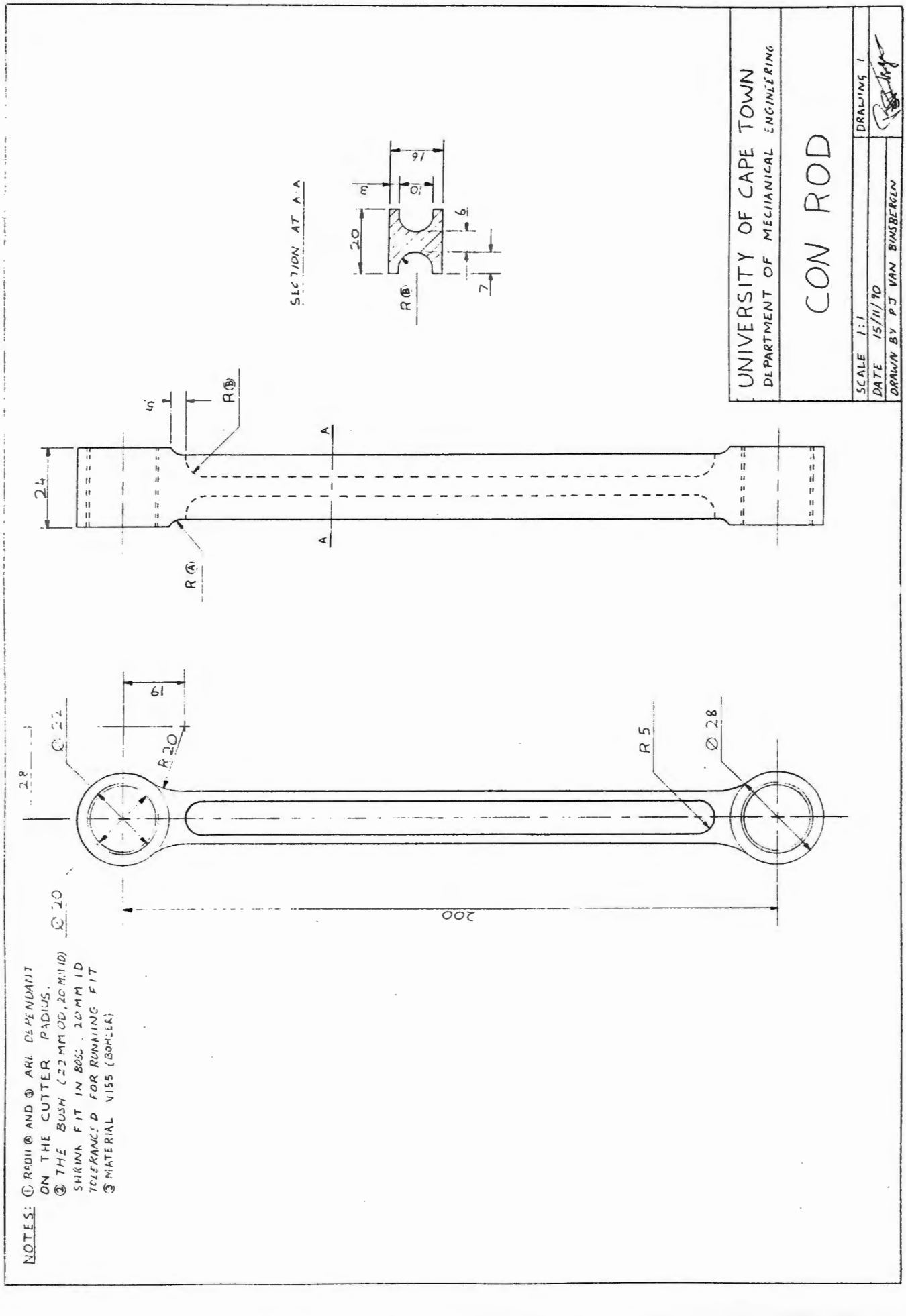
NOTES: ① RADII ® AND ® ARE DEPENDANT ON THE CUTTER RADIUS.
② THE BUSH (22 MM OD, 20 MM ID) SHRINK FIT IN BOSS. 20 MM ID TOLERANCED FOR RUNNING FIT
③ MATERIAL V155 (BOHLER)
UNIVERSITY OF CAPE TOWN
DEPARTMENT OF MECHANICAL ENGINEERING
CON ROD
SCALE 1:1
DRAWING 1
DATE 15/11/90
DRAWN BY PJ VAN BINSBERGEN
SECTION AT A-A
R®
R®
R®
A
A
24
28
Ø 22
Ø 20
19
R20
R5
Ø 28
200
91
20
6
7

NOTES: ① MATERIAL V155 (BOHLER)
② RADII Ⓐ ARE DEPENDANT ON THE CUTTER USED FOR THE SLIDE - SEE DRAWING 2
③ RADII Ⓑ ARE DEPENDANT ON THE CUTTER DIAMETER --ERE DRAWN AS 4MM RADII.

SIDE VIEW

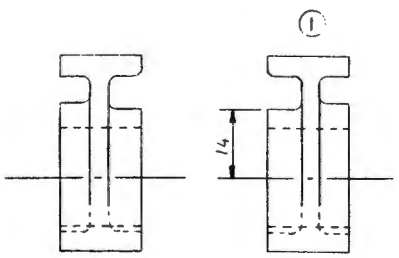

FRONT VIEW

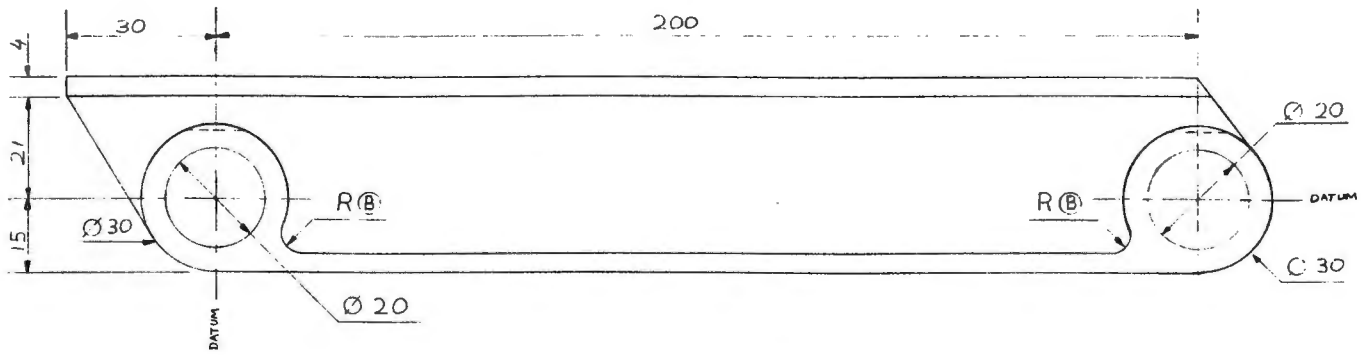

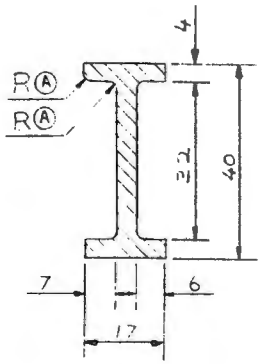

I-SECTION OF ①

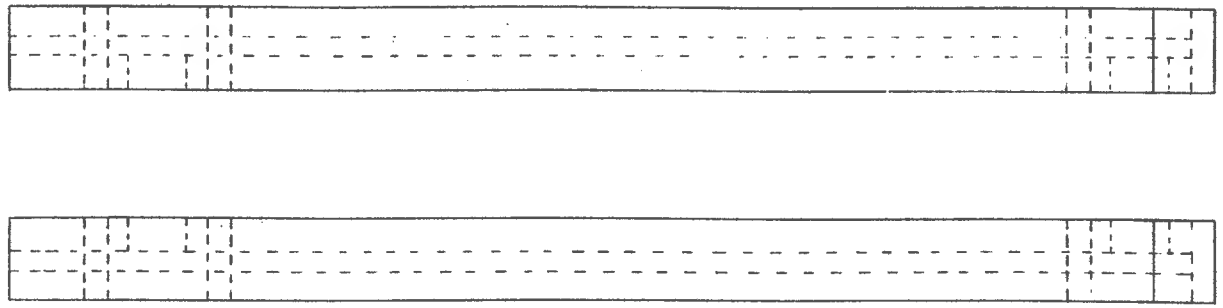

TOP VIEW

UNIVERSITY OF CAPE TOWN
DEPARTMENT OF MECHNICAL ENGINEERING

LINKS

SCALE 1:1	DRAWING 2
DATE 14/11/90	
DRAWN BY PJ VAN BINSBERGEN	

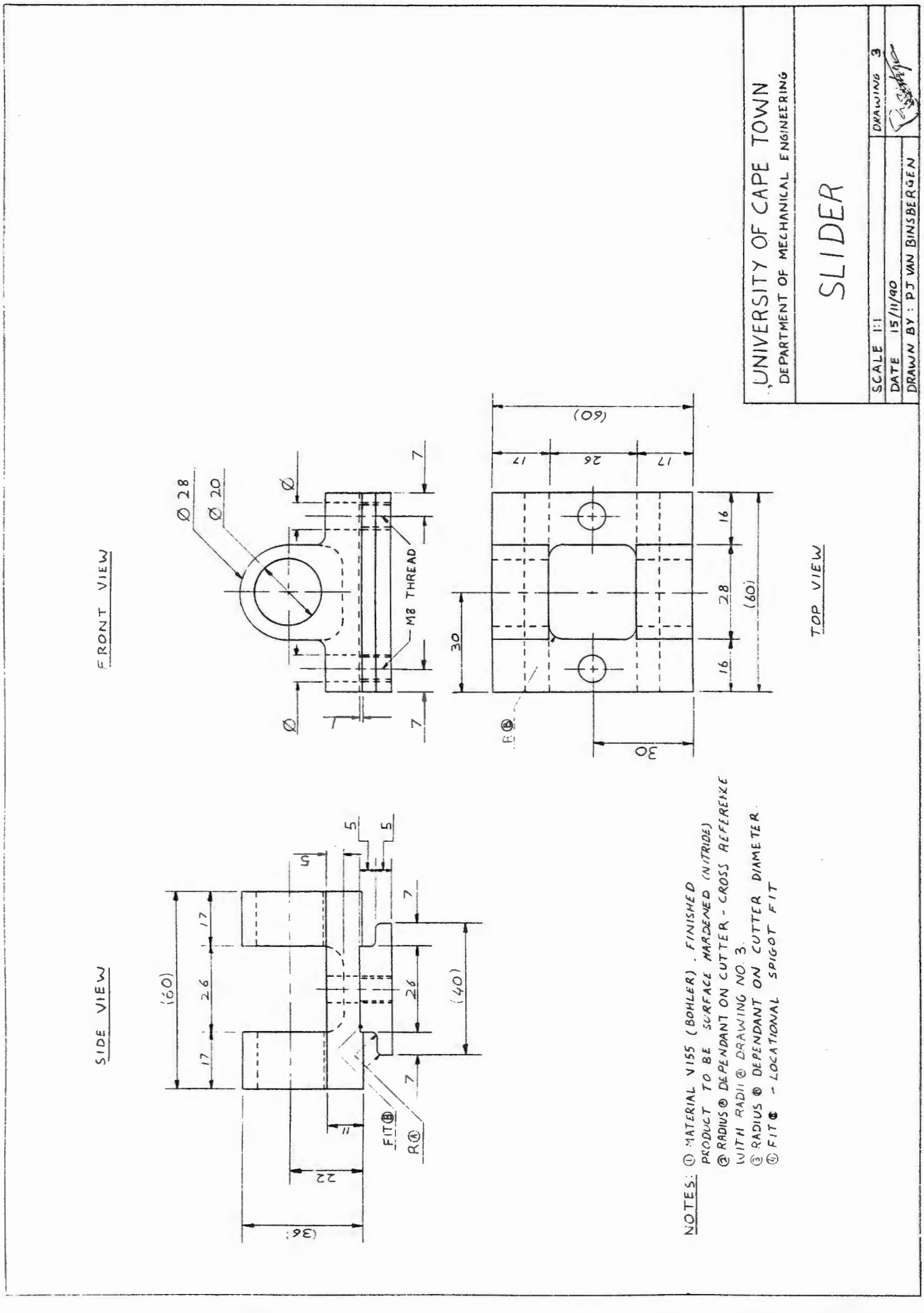
UNIVERSITY OF CAPE TOWN
DEPARTMENT OF MECHANICAL ENGINEERING
SLIDER
SCALE 1:1
DATE 15/11/90
DRAWN BY : PJ VAN BINSBERGEN
DRAWING 3
FRONT VIEW
SIDE VIEW
TOP VIEW
Ø 28
Ø 20
M8 THREAD
(60)
(40)
26
17
30
28
16
NOTES: ① MATERIAL V155 (BOHLER) . FINISHED
PRODUCT TO BE SURFACE HARDENED (NITRIDE)
② RADIUS ® DEPENDANT ON CUTTER - CROSS REFERENCE
WITH RADII ② DRAWING NO. 3.
③ RADIUS ® DEPENDANT ON CUTTER DIAMETER
④ FIT ⑤ - LOCATIONAL SPIGOT FIT

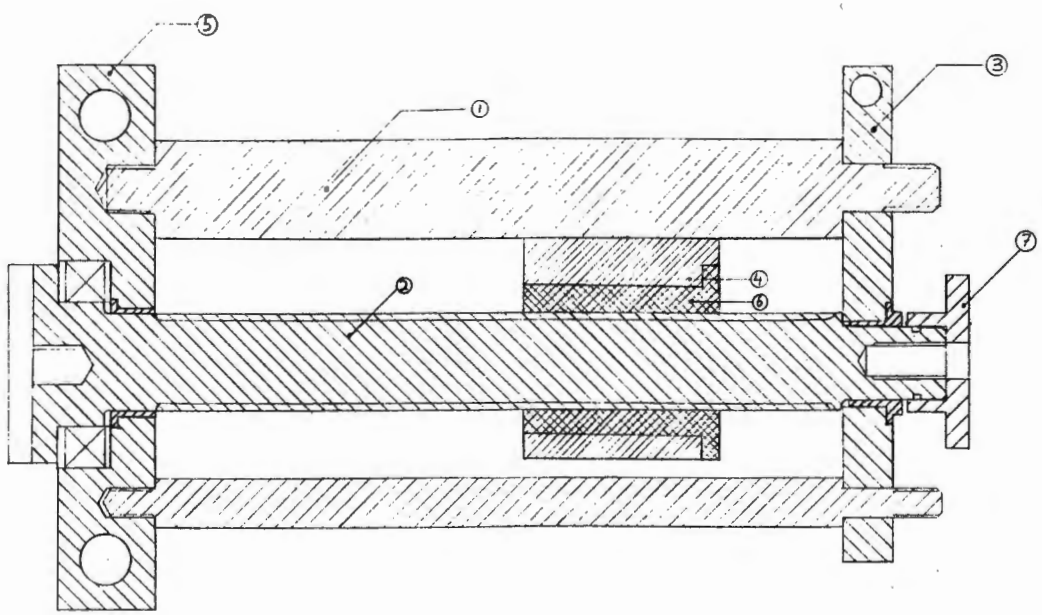

(NOTE: ORIGINALLY A CIRCLIP AND THRUST WASHER WERE USED IN PLACE OF THE THRUST BEARING FLANGE (7). THIS WAS ALTERRED DUE TO FAILURE OF THE CIRCLIP (APPENDIX C))

7	THRUST BEARING FLANGE
6	THREADED INSERT
5	MOUNTING PLATE 2
4	ADJUSTER BLOCK
3	MOUNTING PLATE 1
2	THREADED ROD
1	GUIDE ROD

UNIVERSITY OF CAPE TOWN

DEPARTMENT OF MECHANICAL ENGINEERING

ADJUSTER MECHANISM ASSEMBLY

SCALE – NOT TO SCALE	DRAWING 4.1
DATE 13-02-91	
DRAWN BY PJ VAN BINSBERGEN	

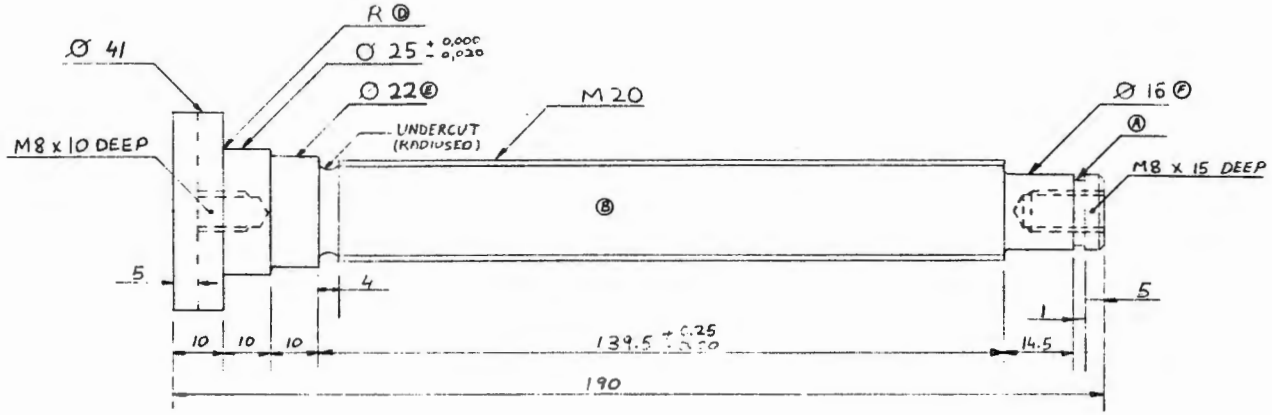

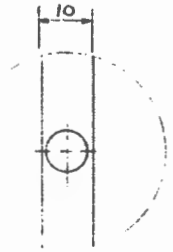

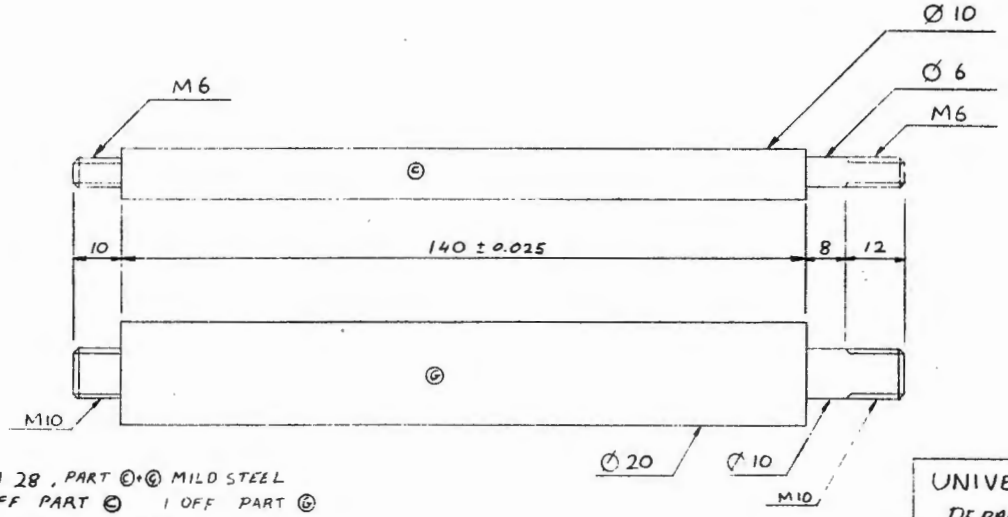

NOTES ① MATERIAL - PART B EN 28, PART C + G MILD STEEL
② 1 OFF PART B 1 OFF PART C 1 OFF PART G
③ CIRCLIP GROOVE A Ø 14.0 MIN. 14.5 MAX
④ ALL RADII 1 MM EXCEPT R④ 0.8 ± 0.2
⑤ D E + F TOLERANCED H7-e8 WITH BUSH [EASY RUNNING]
ALL DIAMETERS CONCENTRIC

UNIVERSITY OF CAPE TOWN
DEPARTMENT OF MECHANICAL ENGINEERING

THREADED AND GUIDE RODS

SCALE - 1:1	DRAWING 4.2
DATE 13-02-91	
DRAWN BY: PJ VAN BINSBERGEN	

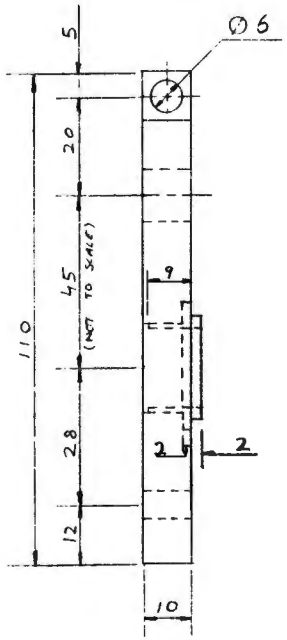

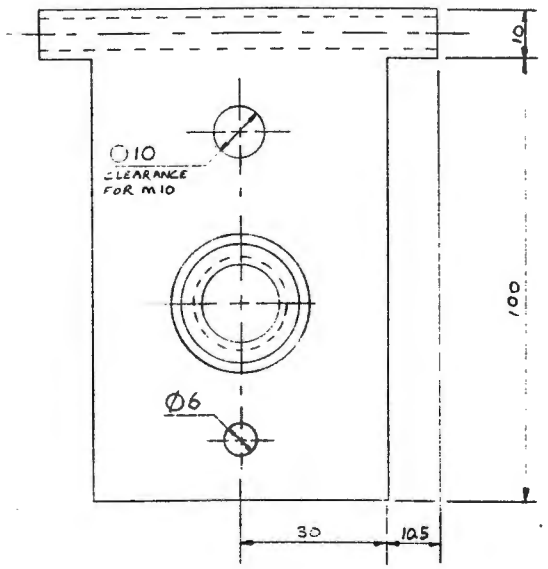

NOTES ① BUSH PRESS FIT IN Ø Ⓐ H7-r6 [Ø18]
② Ø Ⓐ RUNING FIT H7-f7 WITH Ø16 SHAFT
③ MATERIAL MILD STEEL
④ Ø6 HOLES CLEARANCE FOR 6MM THREAD
⑤ PLEASE REMOVE ALL BURRS AND SHARP EDGES

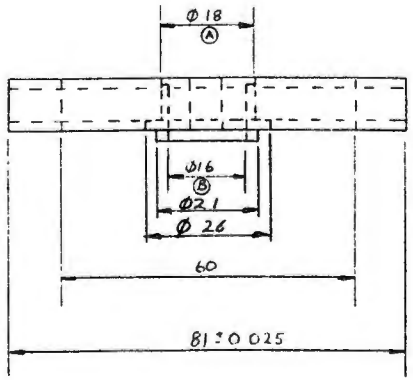

MOUNTING PLATE 1

DRAWING 4 SHEET 3

SCALE 1:1 P VAN BINSBERGEN

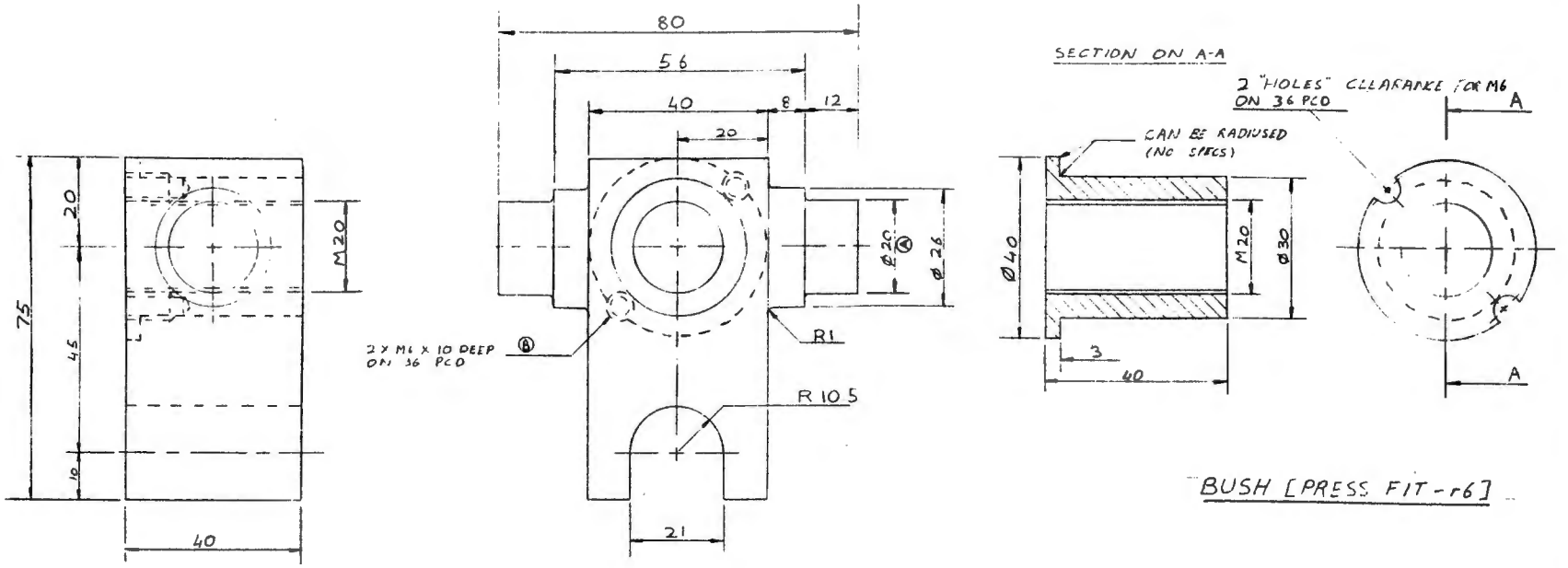

BUSH [PRESS FIT - r6]

NOTES ①MATERIAL V155
②ALL RADII 1MM
③ØA RUNNING FIT H7-F7
④ PLEASE REMOVE ALL BURRS AND SHARP EDGES
⑤ PLEASE DISCUSS HOLES ⑧ WITH ME

①MATERIAL : PHOSPHUR BRONZE

ADJUSTER BLOCK	
DRAWING 4 SHEET 4	
SCALE 1:1	P.VAN BINSBERGEN

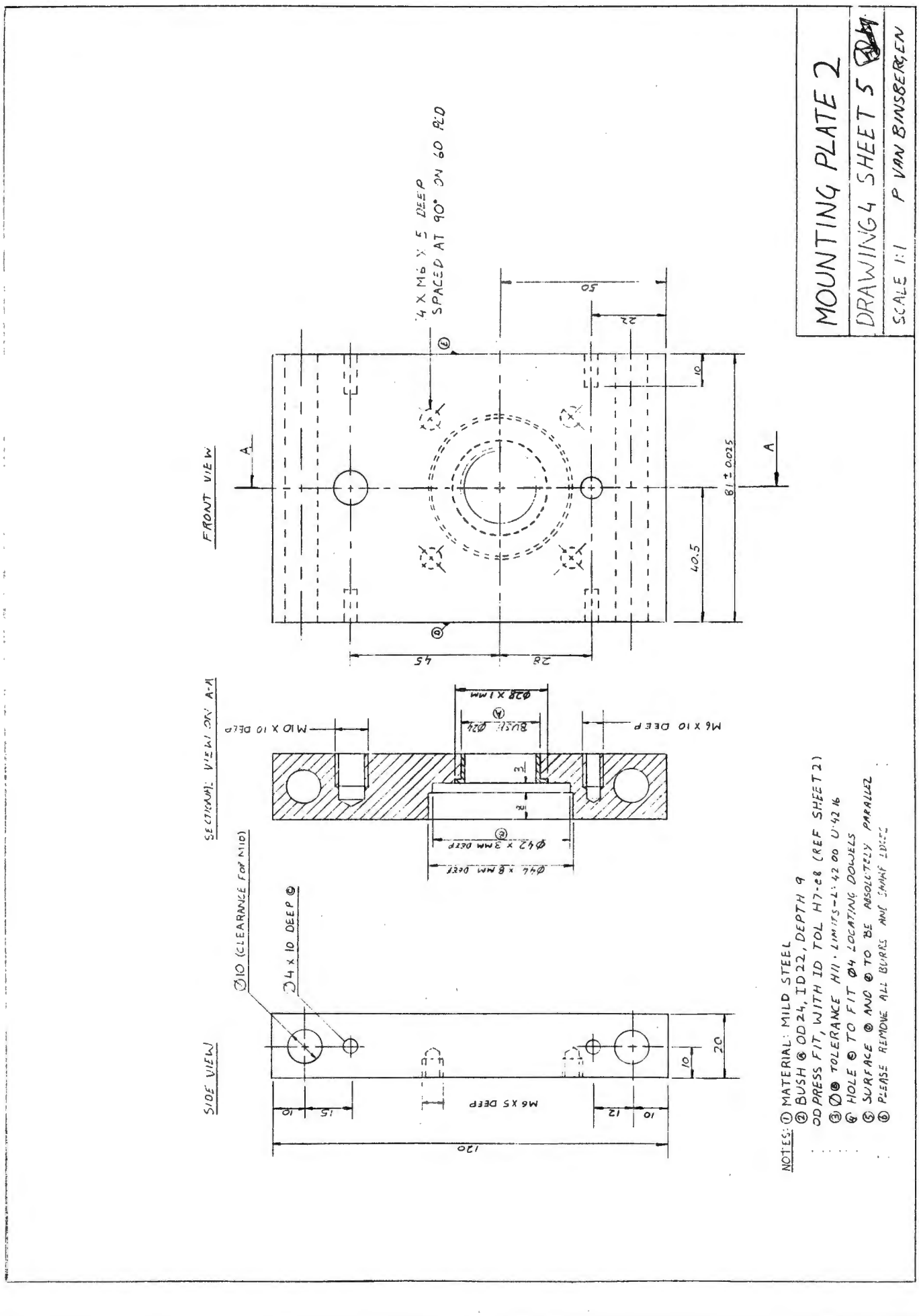
MOUNTING PLATE 2
DRAWING 4 SHEET 5
SCALE 1:1 P VAN BINSBERGEN
FRONT VIEW
4 X M6 X 5 DEEP
SPACED AT 90° ON 60 P.C.D
81 ± 0.025
40.5
45
28
50
22
10
SECTIONAL VIEW ON A-A
M10 X 10 DEEP
M6 X 10 DEEP
Ø28 X 1MM
Ø24 BUSH
Ø42 x 3MM DEEP
Ø44 x 8 MM DEEP
SIDE VIEW
Ø10 (CLEARANCE FOR M10)
Ø4 X 10 DEEP
M6 X5 DEEP
120
20
15
12
NOTES: ① MATERIAL: MILD STEEL
② BUSH @ OD 24, ID 22, DEPTH 9
OD PRESS FIT, WITH ID TOL H7-e8 (REF SHEET 2)
③ Ø@ TOLERANCE H11 - LIMITS -L' 42.00 U' 42.16
④ HOLE ⑤ TO FIT Ø4 LOCATING DOWELS
⑤ SURFACE ⑥ AND ⑦ TO BE ABSOLUTELY PARALLEL
⑥ PLEASE REMOVE ALL BURRS AND SHARP EDGES

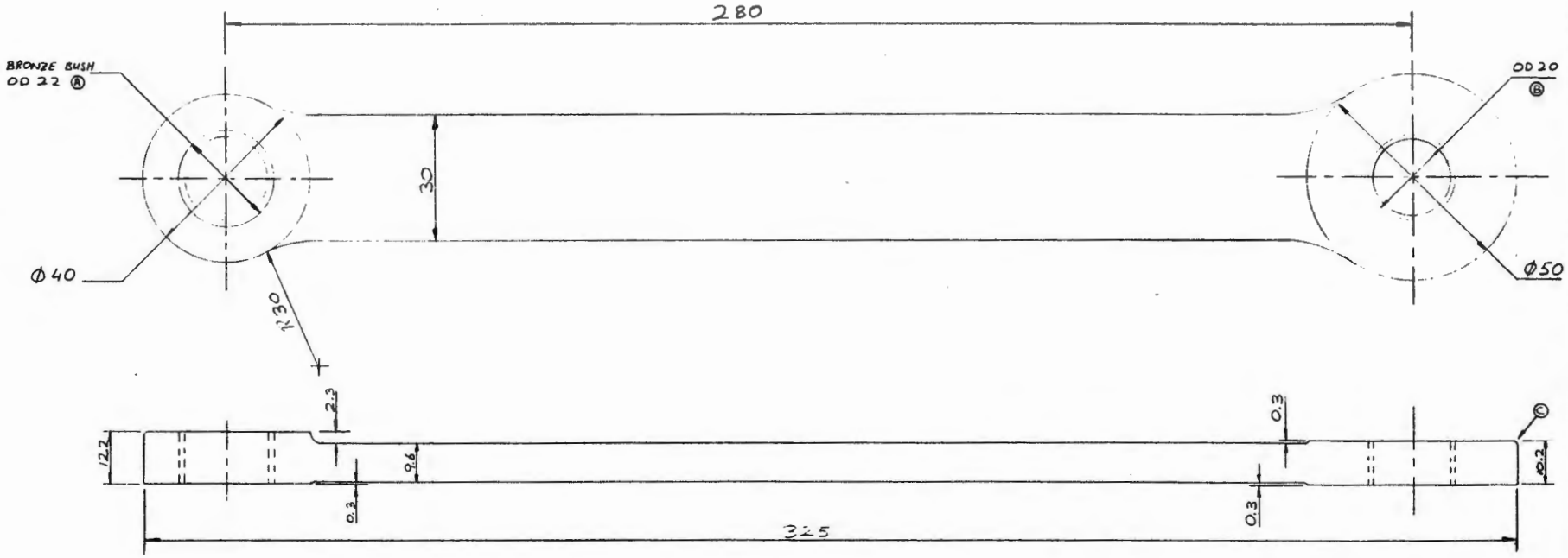

NOTES: ① MATERIAL - 7075 ALUMINIUM ALLOY
② BUSH Ⓐ - OD 22 PRESS FIT
ID 20 RUNNING FIT WITH ADJUSTER
Ⓑ - OD 20 PRESS FIT
ID 18 CLOSE RUNNING FIT
WITH GUDGEON PIN ③
③ GEN. TOLERANCE 0.05
④ PLEASE REMOVE BURRS AND SHARP EDGES
* RADIUS ALL CORNERS Ⓒ
⑤ SEE DRWN ⑤ FOR LOCUS OF CNC CUTTER
⑥ PLEASE MAKE 2 OFF

CONTROL ARMS	
SCALE 1:1	DRAWING 4.6
DATE APRIL 91	
DRAWN BY: P J VAN BINSBERGEN	

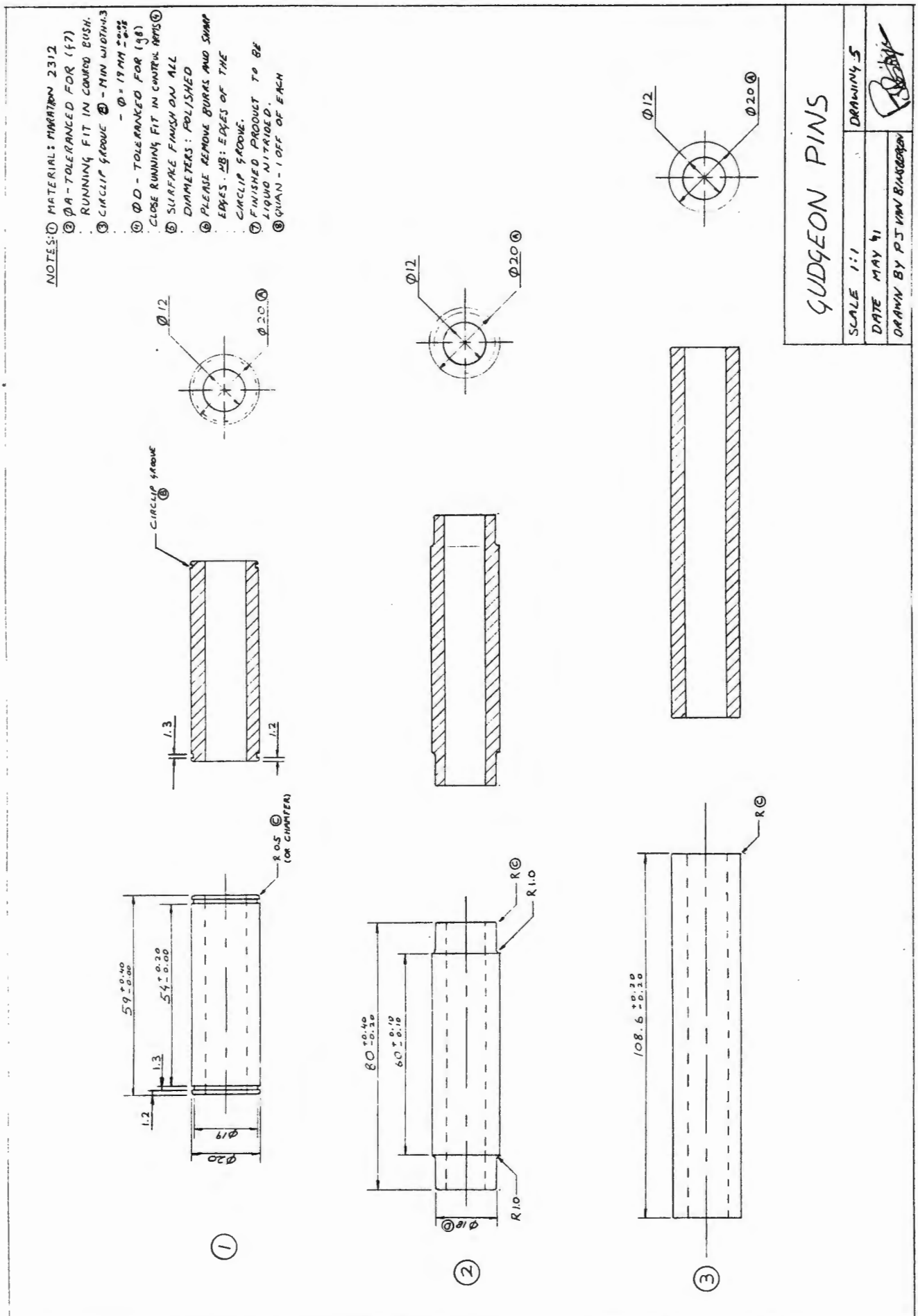
NOTES: ① MATERIAL: MARATHON 2312
② ØA - TOLERANCED FOR (F7) RUNNING FIT IN CONROD BUSH.
③ CIRCLIP GROOVE Ⓑ - MIN WIDTH 1.3
④ ØD - TOLERANCED FOR (g6) CLOSE RUNNING FIT IN CONTROL RODS
⑤ SURFACE FINISH ON ALL DIAMETERS: POLISHED
⑥ PLEASE REMOVE BURRS AND SHARP EDGES. NB: EDGES OF THE CIRCLIP GROOVE.
⑦ FINISHED PRODUCT TO BE LIQUID NITRIDED.
⑧ QUAN - 1 OFF OF EACH
GUDGEON PINS
SCALE 1:1
DRAWING 5
DATE MAY 91
DRAWN BY PETER BJERGSEN
CIRCLIP GROOVE Ⓑ
Ø12
Ø20 Ⓐ
1.3
1.2
R 0.5 Ⓒ (OR CHAMFER)
59 +0.40 -0.00
54 +0.20 -0.00
Ø19
Ø20
R Ⓒ
R1.0
80 +0.40 -0.20
60 +0.12 -0.10
Ø18
108.6 +0.20 -0.20
①
②
③

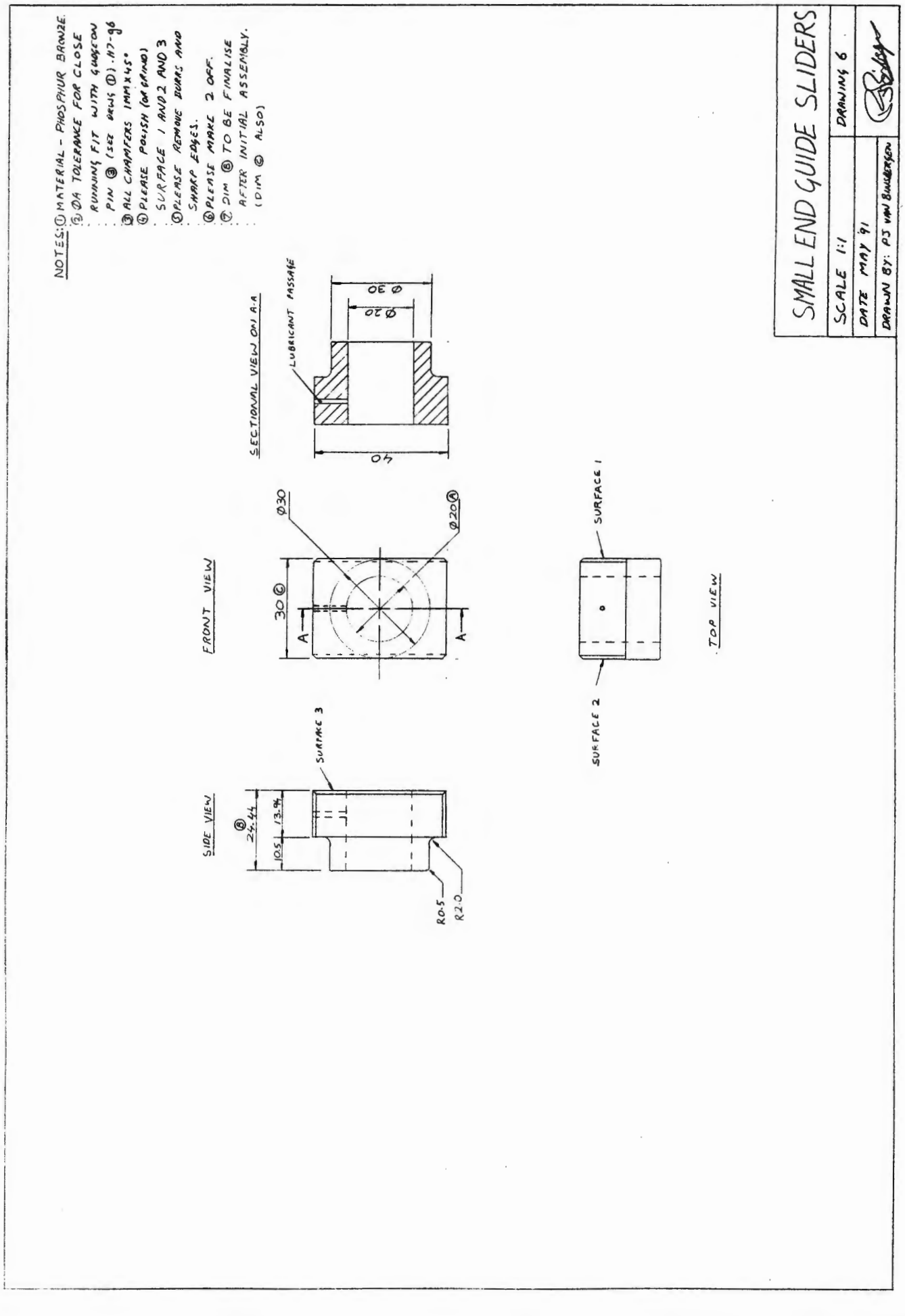
NOTES: ① MATERIAL - PHOSPHUR BRONZE.
② ØA TOLERANCE FOR CLOSE RUNNING FIT WITH GUDGEON PIN ③ (SEE DRWG ①). H7-g6
③ ALL CHAMFERS 1MM x 45°
④ PLEASE POLISH (OR GRIND) SURFACE 1 AND 2 AND 3
⑤ PLEASE REMOVE BURRS AND SHARP EDGES.
⑥ PLEASE MAKE 2 OFF.
⑦ DIM ⑥ TO BE FINALISE AFTER INITIAL ASSEMBLY. (DIM ⑥ ALSO)
SMALL END GUIDE SLIDERS
SCALE 1:1
DRAWING 6
DATE MAY '91
DRAWN BY: PJ VAN BUUREN
SECTIONAL VIEW ON A-A
LUBRICANT PASSAGE
Ø30
Ø20
40
FRONT VIEW
Ø30
30 ⑥
Ø20 ⑧
A
A
SIDE VIEW
SURFACE 3
24.44
13.94
10.5
R0.5
R2.0
SURFACE 1
SURFACE 2
TOP VIEW

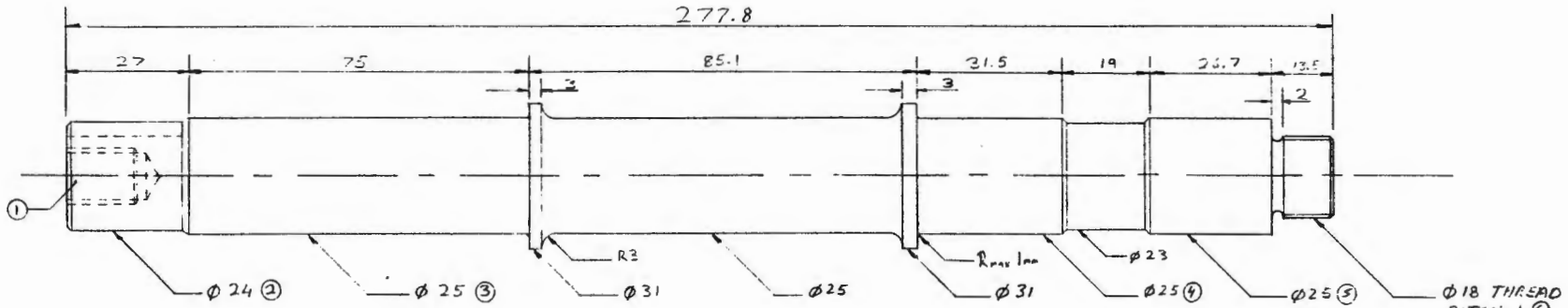

SCRAP VIEW OF KEYWAY

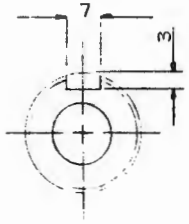

NOTES: ① MATERIAL : Vi55 (BOHLER)
② HOLE ① : THREAD M12 X20 DEEP
③Ø ② : Ø24 TOL J6 WITH HUB
④Ø ③ : Ø25 TOL J6 - BEARING
⑤Ø ④ : Ø25 TOL J6 - BEARING
⑥Ø ⑤ : Ø24 SPLINED AS PER SAMPLE
⑦THREAD ⑥ : Ø18 X PITCH 1 (CHECK SAMPLE)
⑧ALL CHAMFERS 45°
⑨TOLERANCE ON KEYWAY 7.0 $^{+0.03}_{-0.00}$ 3.0 $^{+0.025}_{-0.025}$
⑩ PLEASE REMOVE ALL BURR AND SHARP EDGES
GENERAL TOLERANCE ± 0.1

POWER-OUT SHAFT	
SCALE 1:1	DRAWING 7
DATE MAR 4 '91	
DRAWN BY: P J VAN BINSBERGEN	

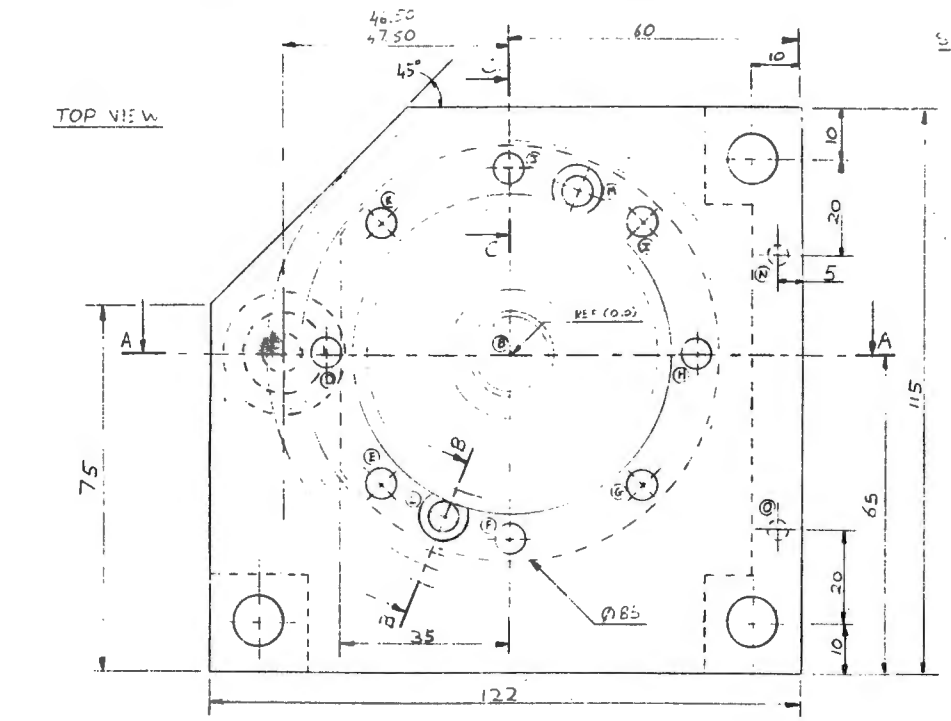

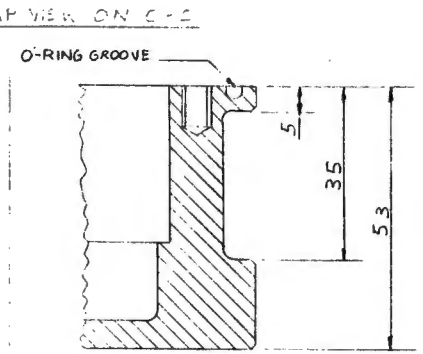

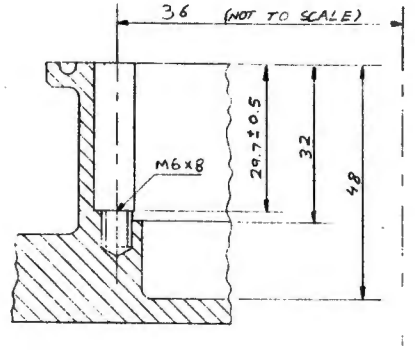

SCRAP VIEW ON B-B

NOTES:
1. MATERIAL - MILD STEEL.
2. ALL RADII 2 MM
   ALL CHAMFERS 1MM X 45°
3. O-RING GROOVE TO FIT 3 MM Ø O-RING.
4. BRONZE BUSH ⑧ - SHRINK FIT IN CASING TOL (H7-s6)
   ID RUNNING FIT (H7-f7) WITH SHAFT - 15 MM.
5. THREAD M6 X 8MM DEEP
   RECORD: ⑩ (-38.0, 0.0)
   ⑪ (-26.87, -26.87)
   ⑫ (0.0, -38.0)
   ⑬ (26.87, -26.87)
   ⑭ (38.0, 0.0)
   ⑮ (26.87, 26.87)
   ⑯ (0.0, 38.0)
   ⑰ (-26.87, 26.87)
6. OTHER POINTS: ⑱ REF (0,0)
   ⑲ (-47.07, 0.0)
7. ⑨ AND ⑱ - STEPPED HOLE Ø10 x 29.7 DEEP, M6 THRED x 8MM DEEP. (SEE SCRAP VIEW B-B)
   ⑨ (-13.28, -33.26)
   ⑱ (13.78, 33.26)
8. ⑱ AND ⑲ - Ø4 MM HOLES, 8 MM DEEP (FROM SURFACE ⑱)
9. PSE REMOVE BURRS AND SHARP EDGES

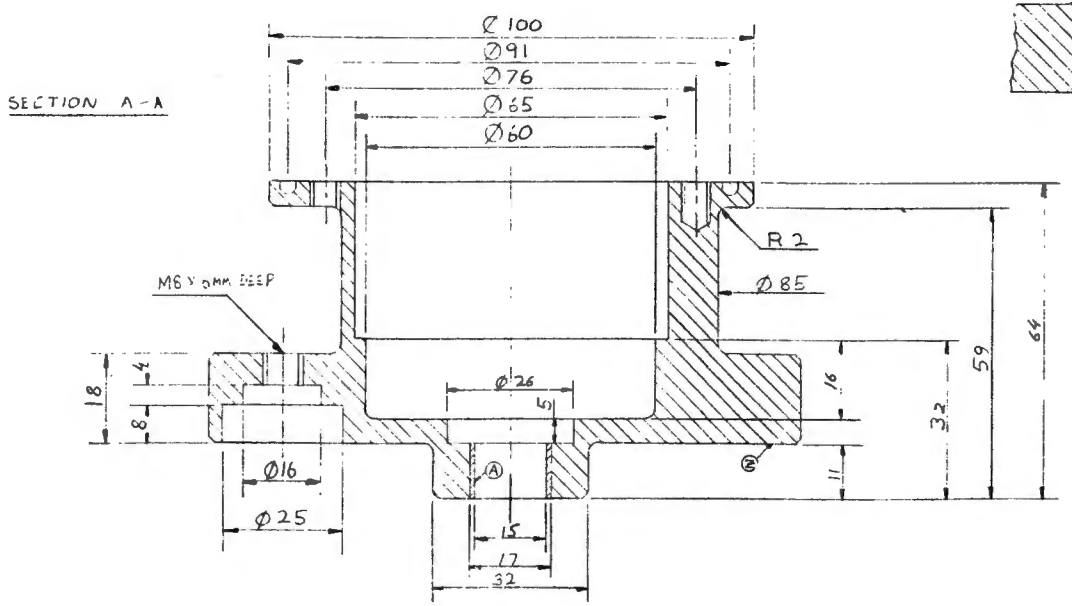

UNIVERSITY OF CAPE TOWN
DEPARTMENT OF MECHANICAL ENGINEERING

POINTS CASING

SCALE 1:1	DRAWING 8
DATE 26/01/91	
DRAWN BY P J VAN BINSBERGEN	

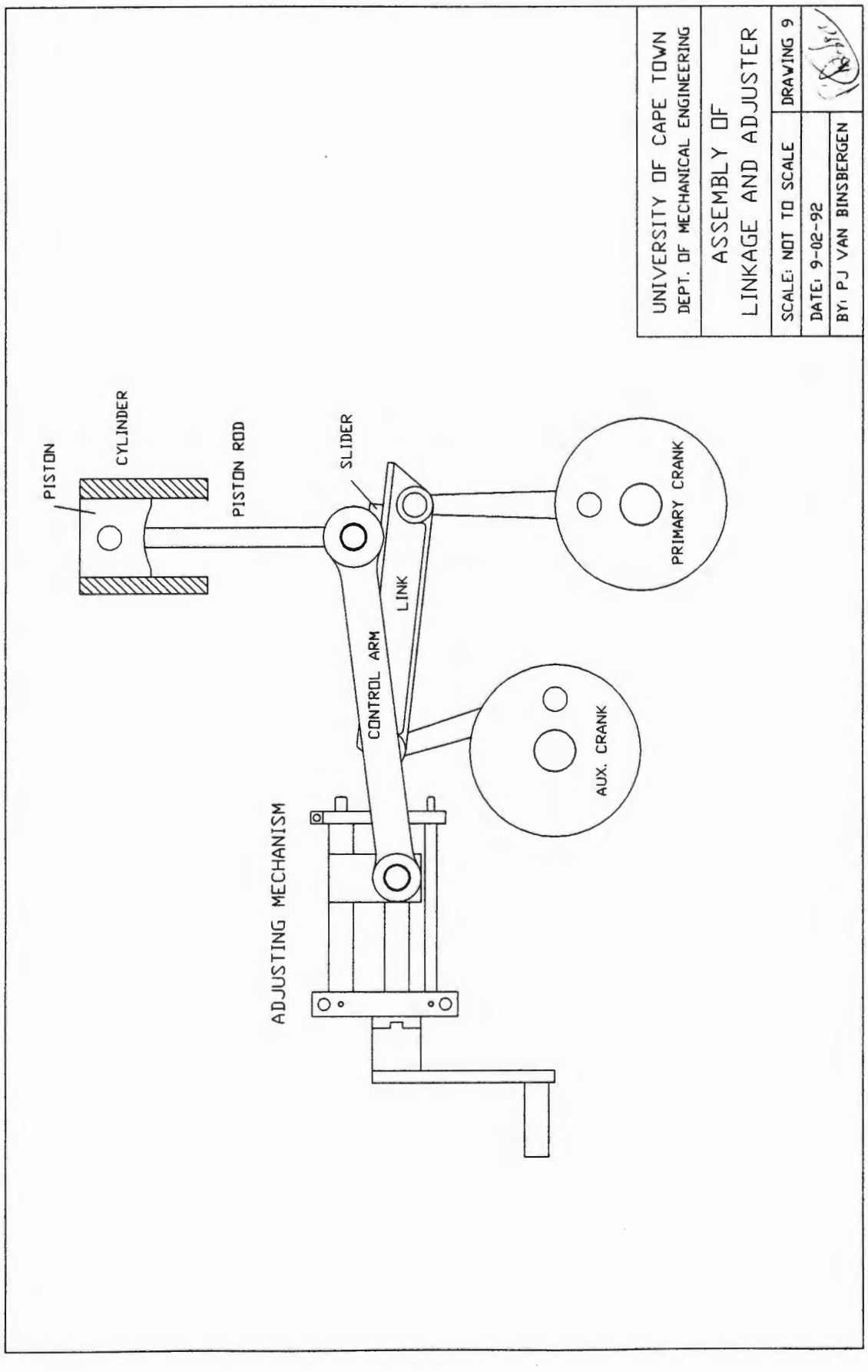
UNIVERSITY OF CAPE TOWN
DEPT. OF MECHANICAL ENGINEERING
ASSEMBLY OF
LINKAGE AND ADJUSTER
SCALE: NOT TO SCALE
DRAWING 9
DATE: 9-02-92
BY: PJ VAN BINSBERGEN
PISTON
CYLINDER
PISTON ROD
SLIDER
PRIMARY CRANK
LINK
CONTROL ARM
AUX. CRANK
ADJUSTING MECHANISM

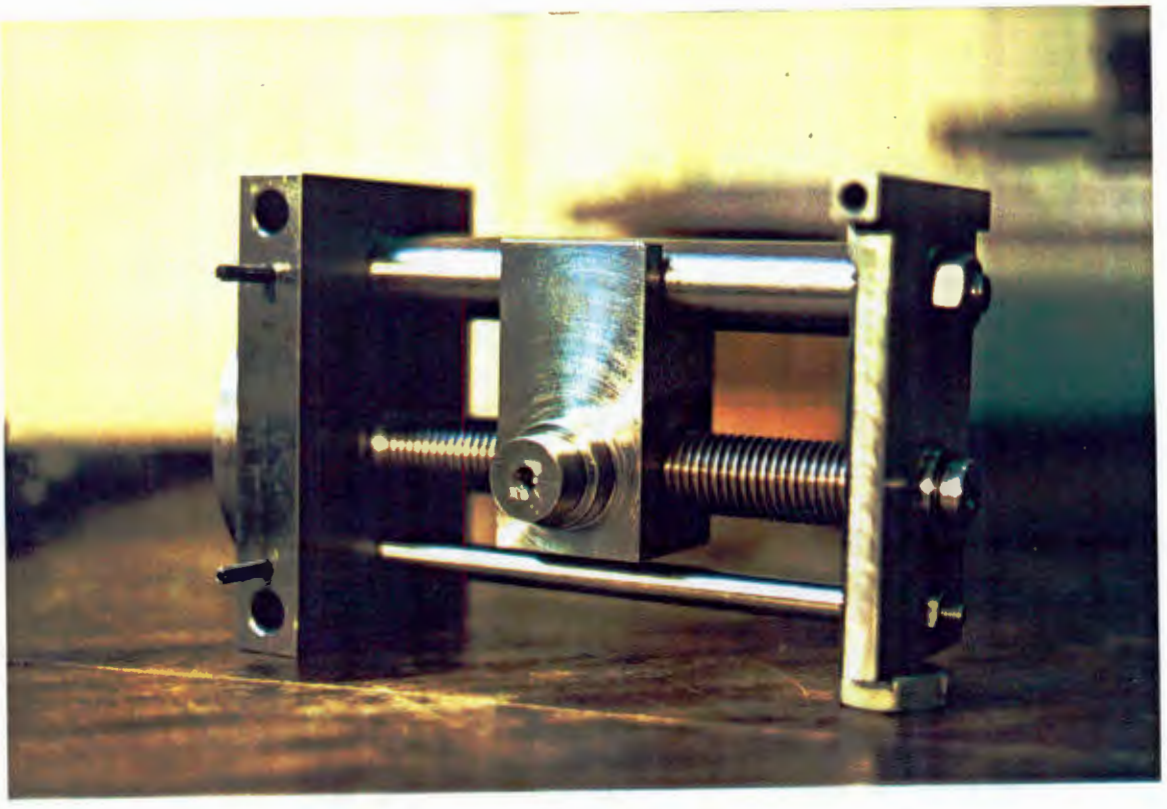

Photo 1. Adjusting mechanism.

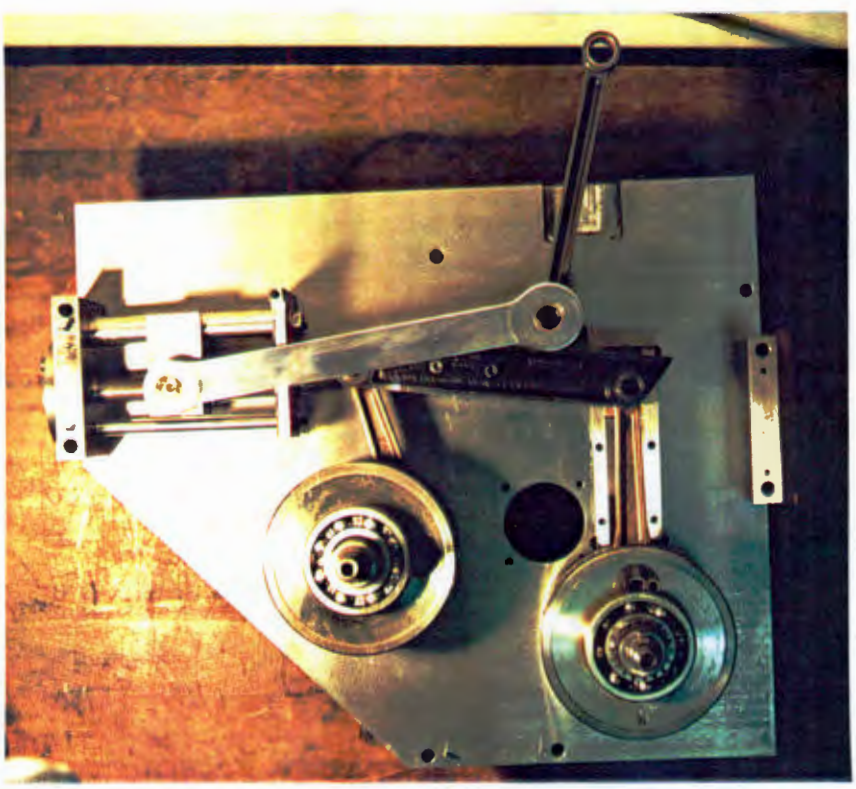

Photo 2. Assembly of the Otto-Atkinson linkage.

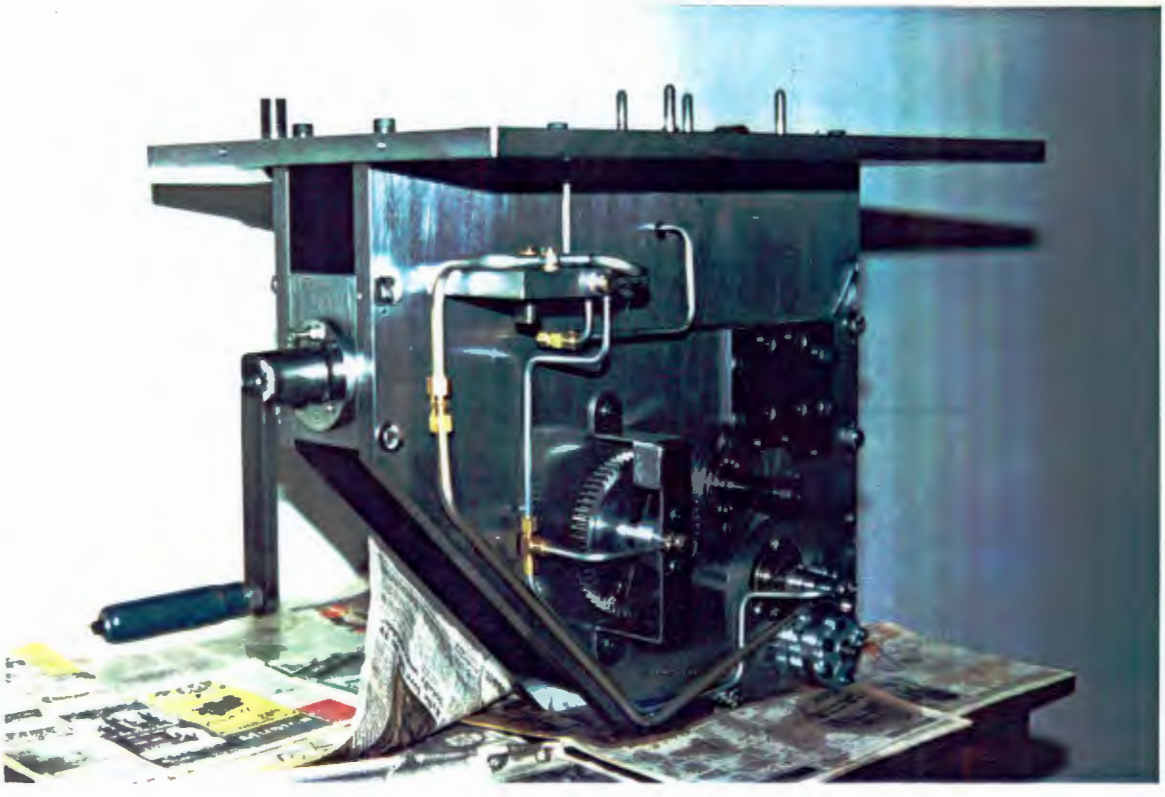

Photo 3. Assembly of the crank-case.

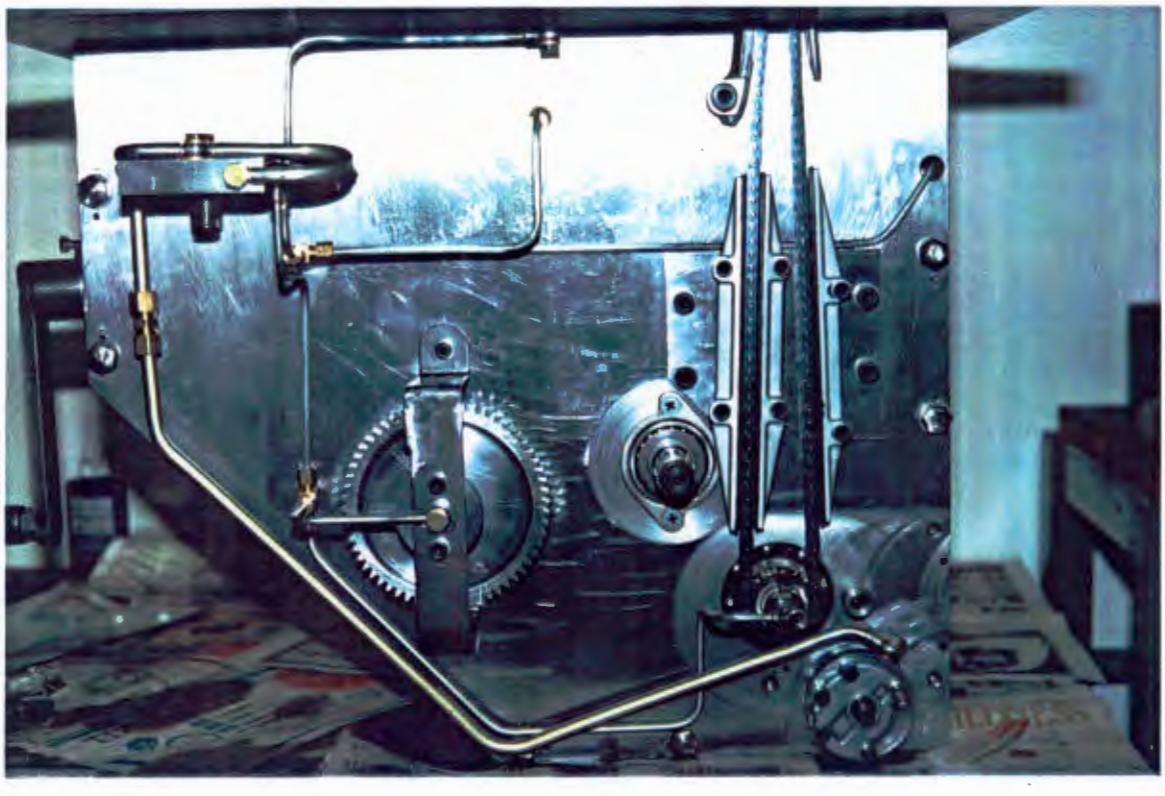

Photo 4. Lubrication system and valve timing drive.

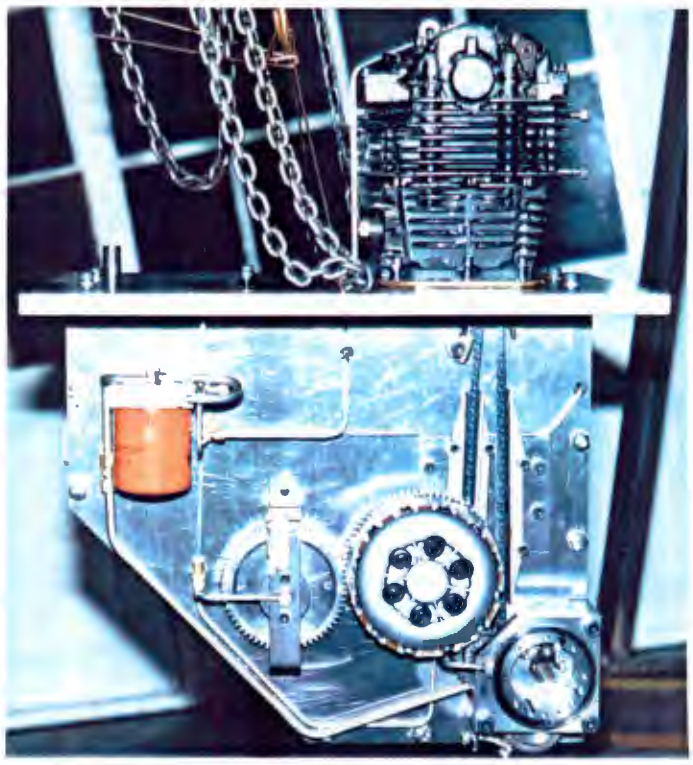

Photo 5. Assembly ready to fit sump.

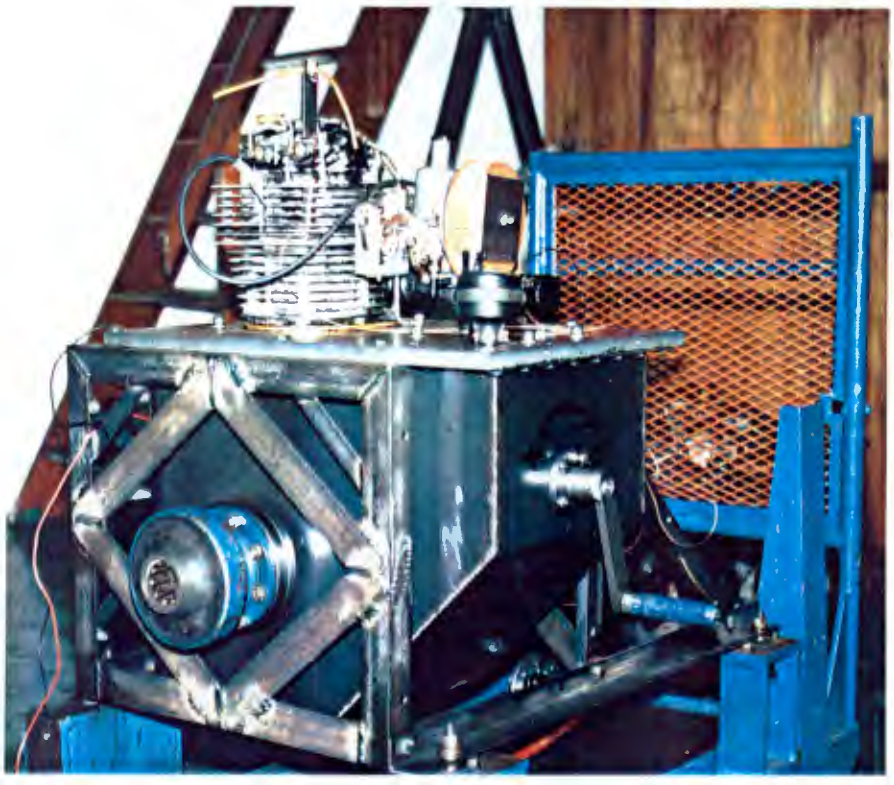

Photo 6. Complete engine assembly.

NOTES: ① MATERIAL: MILD STEEL 525 X 405 X 19
② HOLE (A) STEPPED HOLE 14mm CLEARANCE FOR M10, 30 mm x M10.
(B) STEPPED HOLE 21mm CLEARANCE FOR M8, 32 mm x M8.
(C) CLEARANCE FOR M10 - FULL DEPTH
(D) M10 - FULL DEPTH
(E) Ø10 - FULL DEPTH. TOL: LIGHT PRESS FIT-P6 (REF TO PART)
(F) M8 - FULL DEPTH
(G) CLEARANCE FOR M6 - FULL DEPTH
(H) M6 X 10 DEEP
(J) Ø4 X 10 DEEP - TOLERANCED FOR LOCATING DOWELS
(K) Ø4 X 10 DEEP NO MACHINED FROM OTHER SIDE! (SIDE B)
(L) STEPPED HOLE - Ø16 X 4 DEEP, Ø11 BY 12 DEEP
TOL +0.01 mm (SEE SCRAP VIEW K)
(M)-(P) LOCATION FOR CRANK BEARING - SEE SCRAP VIEW L
(N) STEPPED HOLE - SEE SCRAP VIEW M
③ PLEASE REMOVE ALL BURRS AND SHARP EDGES
④ ALL DIMENSIONS TOLERANCED TO 0.05 FOR CENTERS
⑤ ALL SCRAP VIEWS SECTIONED ALONG THE VERTICAL AXIS.

SCRAP VIEW FOR HOLE (B) AND (A)

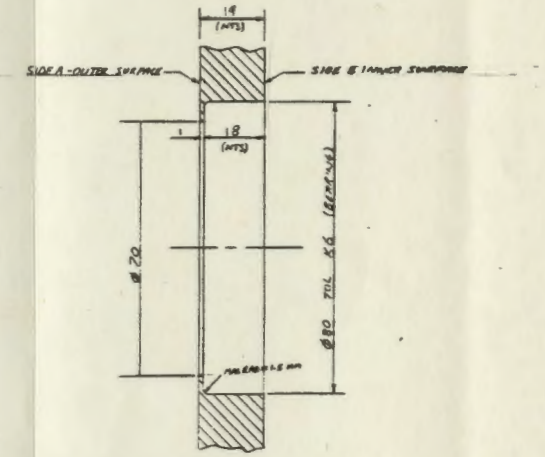

SCRAP VIEW FOR HOLE (K) (NOT TO SCALE - MTS)

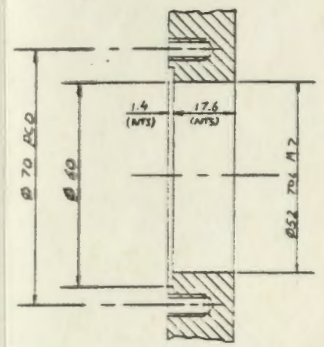

SCRAP VIEW FOR HOLE (G)

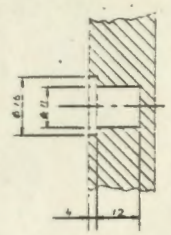

PLATE 1 - E.W.A

CRANKCASE 1(a)

CRANK CASE PLATE 1 - SIDE A (OUTER SURFACE)
SCALE 1:1
DRAWING 9
DRAWN BY F VAN BENSBERSEN

TOP VIEW

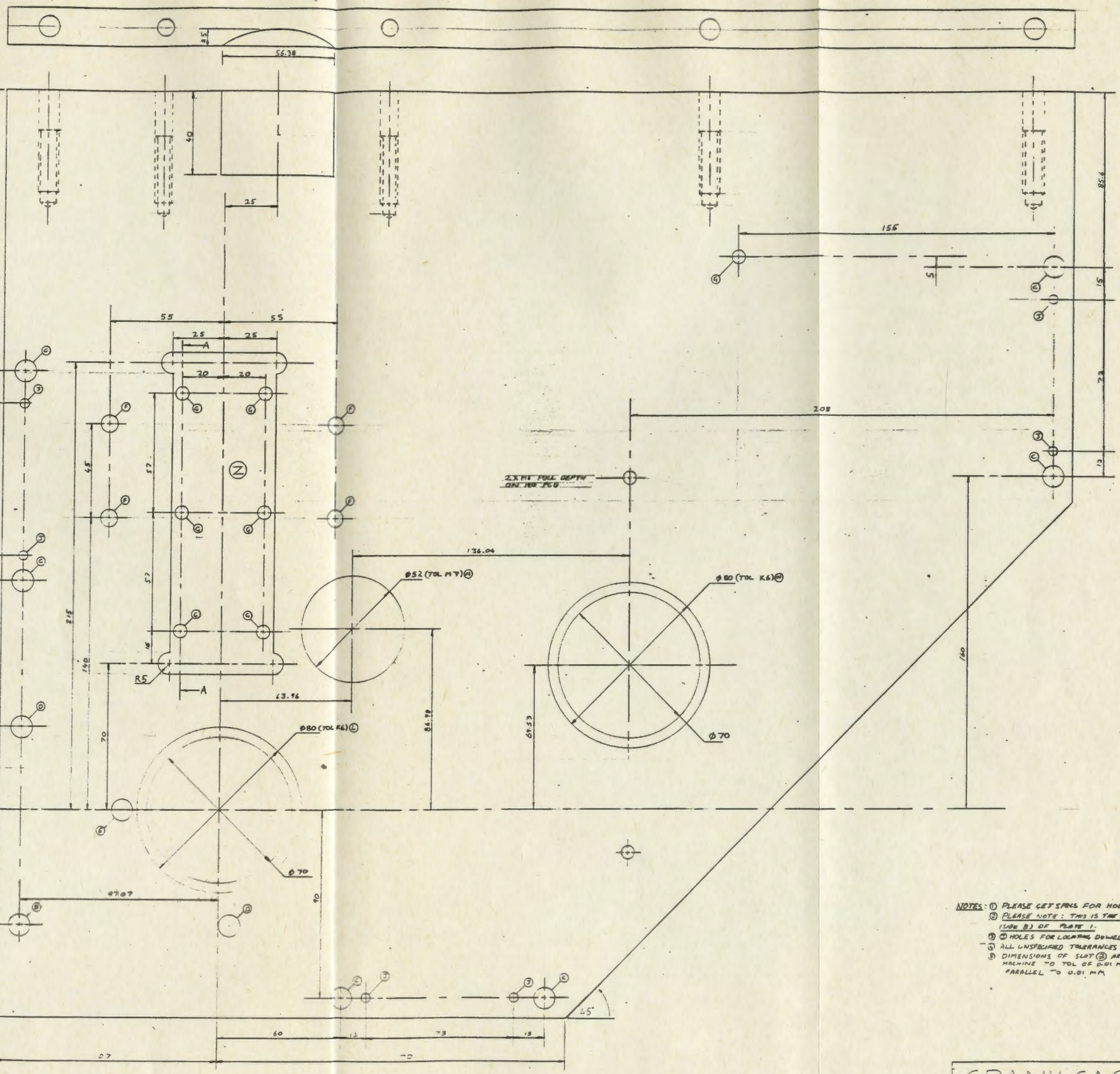

SCRAP VIEW ON A-A

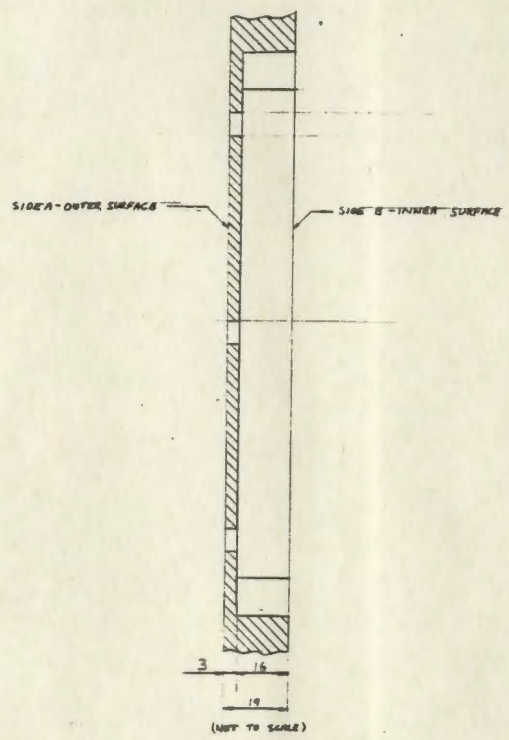

PLATE 1 - VIEW B

NOTES: ① PLEASE GET SPECS FOR HOLES FROM SHEET 1
② PLEASE NOTE: THIS IS THE INSIDE SURFACE (SIDE B) OF PLATE 1.
③ ⑦ HOLES FOR LOCATING DOWELS - 10MM DEEP
④ ALL UNSPECIFIED TOLERANCES - 0.05 FOR CENTERS
⑤ DIMENSIONS OF SLOT ② ARE CRITICAL PLEASE MACHINE TO TOL OF 0.01 MM VERTICAL SURFACES PARALLEL TO 0.01 MM

CRANKCASE (1)(6)

CRANKCASE PLATE 1 - SIDE B (INNER SURFACE)
SCALE 1:1
DRAWN BY P VAN TIMMEREN
DRAWING 10

NOTES: ① MATERIAL: MILD STEEL 525 X 445.6 X 19
② HOLES: ① STEPPED - 19 X CLEARANCE FOR M10, 30 X M10
② STEPPED - 21 X CLEARANCE FOR M8, 32 X M8
③ CLEARANCE FOR M10 - FULL DEPTH
④ CLEARANCE FOR M6 - FULL DEPTH
⑤ Ø6 X 10 DEEP (DOWELS) - 1/8" MACHINE FROM INNER SURFACE
⑥ ① + ⑧ STEPPED Ø 72 X 16, Ø64 X 3
⑦ Ø62 FULL DEPTH
FOR DETAILS ON ⑤, ⑦ AND ⑨ SEE SCRAP VIEW ON SHEET
③ PLEASE REMOVE ALL BURRS AND SHARP EDGES
④ TOLERANCES: HOLES: ① AND ② - K6
③ —— J7
ALL OTHER DIMENSIONS: 0.05 FOR CENTERS
PLEASE NOTE THIS IS THE VIEW OF SIDE A (THE OUTER SURFACE OF PLATE NO 2.

SCRAP VIEW ON SECTION A-A

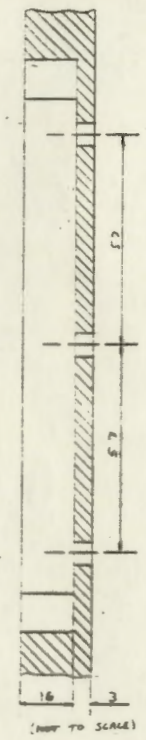

PLATE 2 - VIEW A

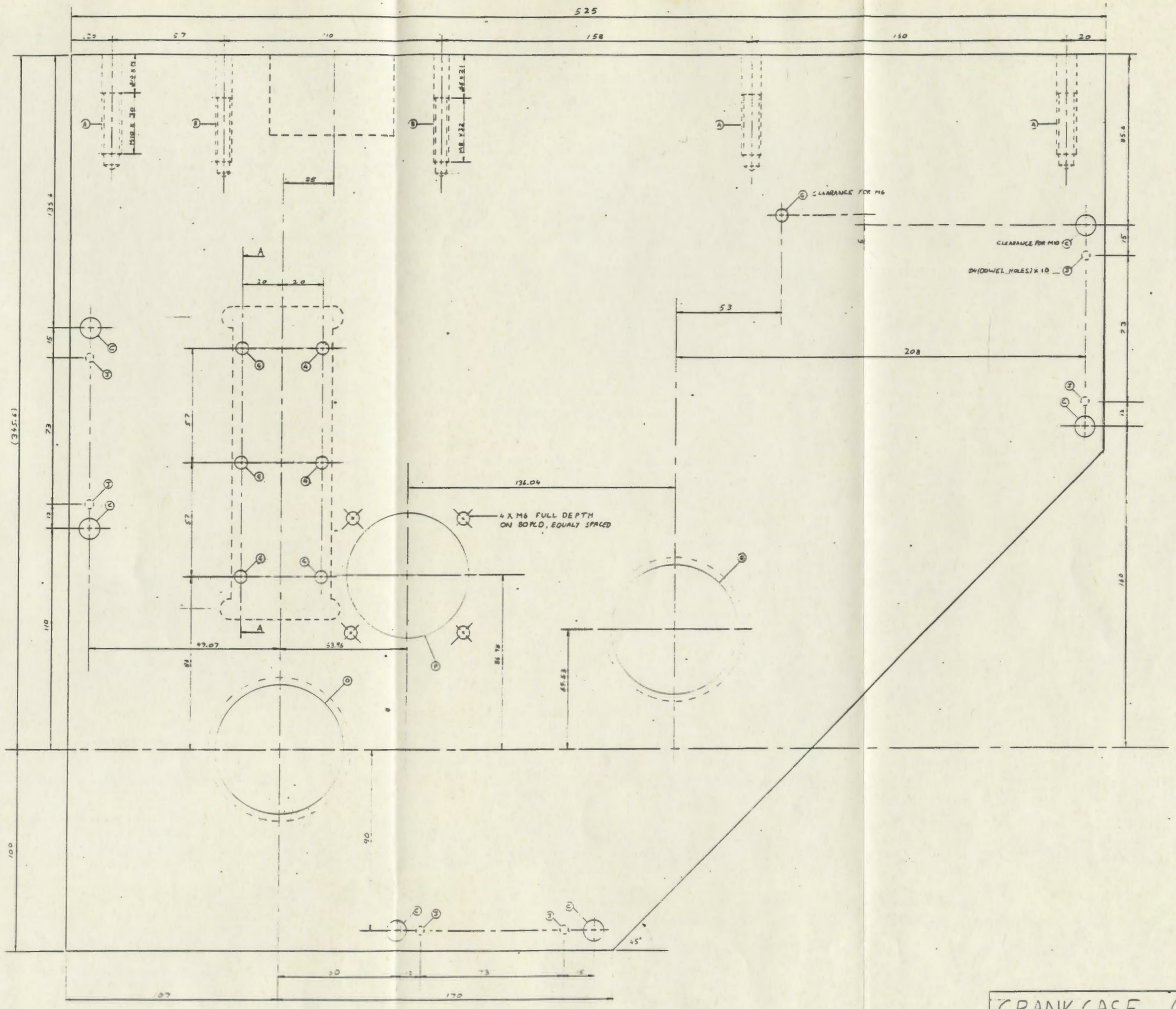

CRANK CASE (2)(a)

CRANK CASE PLATE 2 - SIDE A (OUTER SURFACE)
SCALE 1:1
DRAWING 11
DRAWN BY P. VAN BINSBERGEN

NOTES: ① MATERIAL: MILD STEEL 538 x 449.6 x 19
② HOLE: ⑧ STEPPED Ø72 x 16, Ø44 x 3 DEEP - SEE SCRAP VIEW ⑤-⑧
⑦ Ø62 - FULL DEPTH - SEE SCRAP VIEW ⑦
⑨ SEE ⑧
⑦ Ø4 x 10 DEEP - FOR LOCATING DOWELS
ALL OTHERS SEE SHEET 1 FOR SIZES
③ PLEASE REMOVE ALL BURRS AND SHARP EDGES
④ ALL DIMENSIONS TOLERANCED TO 0.05 FOR CENTERS.
⑤ ALL SCRAP VIEWS SECTIONED ON THE VERTICLE AXIS.
⑥ PLEASE NOTE: THIS VIEW IS THE INSIDE SURFACE (SIDE B) OF PLATE 2.
① SLOT ⑫: PLEASE SEE SHEET 2 ⑥① FOR TOLERANCES (NOTE 6)

SCRAP VIEW FOR HOLE ⑦

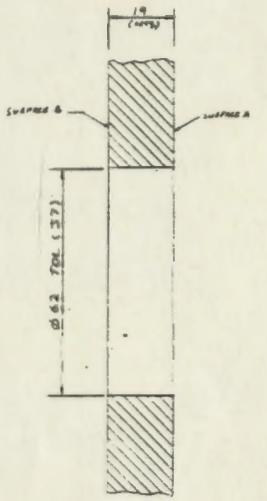

SCRAP VIEW FOR HOLE ⑧ AND ⑨

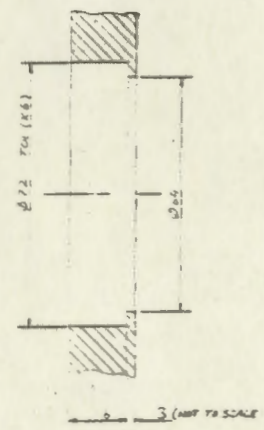

PLATE 2 - SIDE 3

CR-NK CASE (2)(6)

CRANKCASE PLATE 2 -SIDE 3 -INSIDE SURFACE)
SCALE 1:1
DRAWN BY P VAN BINSBERGEN
DRAWING 12

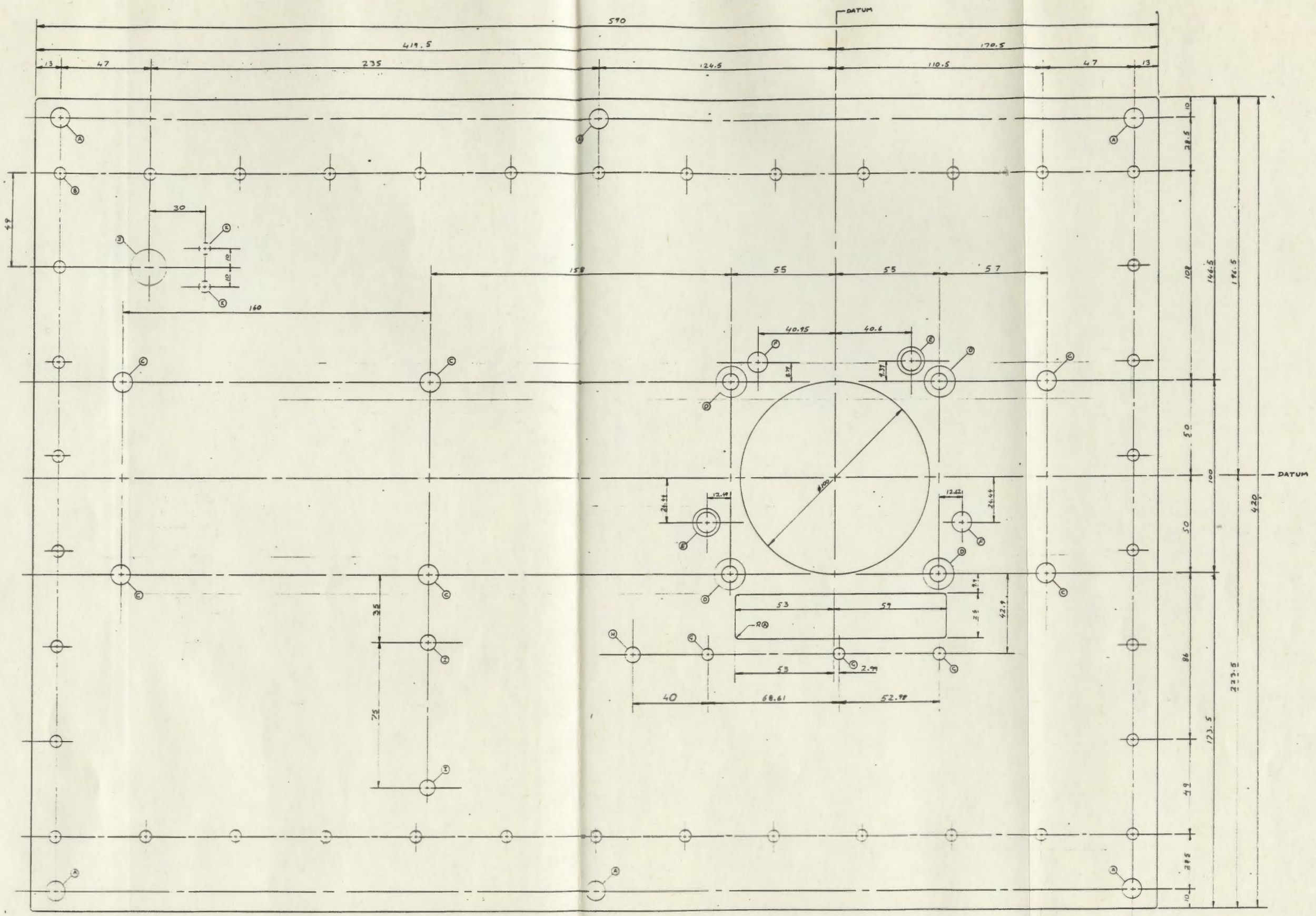

NOTE: ① MATERIAL : MILD STEEL 510 x 420 x 18
② PLEASE SEE SHEET ② FOR DETAIL ON HOLES.
③ PLEASE REMOVE BURRS AND SHARP EDGES

CRANK CASE - TOP DECK	
SCALE 1:1	DRAWING 13
DATE JUNE '92	
DRAWN BY: P J VAN BREDERODE	